12-2010

DESIGN AND REGIOSELECTIVE SYNTHESIS OF TWO AND THREE-PRONGED C_{60} FULLERENE DERIVATIVES AND THEIR APPLICATIONS IN MOLECULAR ELECTRONICS

Angy Ortiz-hernandez
Clemson University, angyloor@gmail.com

DESIGN AND REGIOSELECTIVE SYNTHESIS OF TWO AND THREE-PRONGED C_{60} FULLERENE DERIVATIVES AND THEIR APPLICATIONS IN MOLECULAR ELECTRONICS

A Dissertation
Presented to
the Graduate School of
Clemson University

In Partial Fulfillment
of the Requirements for the Degree
Doctor of Philosophy
Chemistry

---

by
Angy L. Ortiz-Hernandez
December 2010

Accepted by:
Dr. Steve Creager, Committee Chair
Dr. Luis Echegoyen, advisor
Dr. Julia Brumaghim
Dr. George Chumanov
Dr. Rhett Smith

ABSTRACT

Since the introduction of semiconductors in the second half of the 20th century, advancements in electronics and technology have been tremendous. In particular, the rapid development of silicon-based computer chip technology and miniaturization of electronic components has been tremendous. Since silicon-based materials have a limit in terms of size, scientists proposed that individual molecules could behave as single electronic components for high degree of miniaturization.

Given that the molecules of interest must have dimensions on the nanometer scale, be able to bind to the electrode surface and have electron donor-acceptor properties, C_{60} fullerene has been a prime candidate for these studies. It has also been found that a covalent bond between a C_{60} derivative and the surface of a metal substrate enhances the electron tunneling conductance upon accepting electrons, demonstrating the importance of the design and regioselective synthesis of C_{60} fullerene derivatives. However, regiochemical control is very challenging given its high symmetry.

The work presented here explores the synthesis, characterization and electrochemical properties of *pentakis*-, *hexakis*- and *heptakis*-adducts of C_{60} and some of its Fe-complexes under a regio-controlled protection-deprotection protocol. Derivatives were synthesized using two known reactions: cyclopropanation and 1,3-dipolar cycloaddition reactions, better known as: as the Bingel-Hirsch and Prato reactions, respectively.

This approach allowed us to introduce the addends in specific positions over the sphere. For example, two pyrrolidine groups were bonded in a *trans-1* relationship with respect to each other. These adducts were characterized by means of ^{1}H, ^{13}C, and 2D-NMR, UV-*vis*, MALDI-TOF MS and ESI-MS. Their electrochemical properties were analyzed by Cyclic Voltammetry (CV) and Differential Pulse Voltammetry (DPV) experiments.

DEDICATION

To Mateo Santiago and Angel, you guys are the reason of my existence. My heart belongs to you.

ACKNOWLEDGMENTS

I sincerely thank my advisor, Dr. Luis Echegoyen, for his continuous support and guidance throughout my journey in obtaining my PhD degree. The time that I spent doing research under Dr. Echegoyen's guidance, has prepared me as a competent professional and fruitful researcher. I am also grateful to the current and former post-docs of Dr. Echegoyen's research group for all their help during my research, especially to Dr. Claudia Cardona, who was my mentor during my first years of my PhD and Dr. Amit Palkar for his unconditional help, friendship and guidance through all these years.

I would also like to thank all of Prof Echegoyen's current and former graduate students: Bevan, Olena, Manuel, and Julio for their help, especially Adrian, for those uncountable laughs and scientific discussions that I really enjoyed and miss. I would like to show appreciation tothe SURPs students: Danisha, Amanda and Bettina for their important contribution to my research project.

I would also like to extend a special thank you to everyone at the chemistry staff, but in particular to Robin and Russell, for their help and great work during these five years. Also, I want to extent my gratitude to my committee members Prof. Julia Brumaghim, Prof. George Chumanov, Prof. Rhett C. Smith and prof. Steve Creager for their time and help during the completion of this dissertation.

I want to express my gratefulness to my brother, mom and dad for their unconditional support. Finally, I want to give my deepest gratitude to my family in law (David, Marlene, Emma and Don Luis) for your help and love.

TABLE OF CONTENTS

Page

Table of Contents (Continued)

Page

LIST OF SCHEMES

List of Schemes (Continued)

Scheme Page

LIST OF TABLES

Table Page

LIST OF FIGURES

List of Figures (Continued)

Figure Page

List of Figures (Continued)

Figure Page

List of Figures (Continued)

Figure Page

List of Figures (Continued)

Figure Page

List of Figures (Continued)

Figure Page

List of Figures (Continued)

Figure Page

CHAPTER ONE

INTRODUCTION

Molecular-based electronic devices

Miniaturization of electronic components has been an essential and challenging task since the development of the vacuum tube, from the transistor to the current integrated circuits (see Figure 1.1).[1] The first transistor, a point-contact transistor that consisted of a slab of germanium in contact with three gold wires, was invented in 1947 by John Bardeen and Walter Brattain at Bell Labs. Shortly after, in 1948, William Shockley developed the bipolar junction transistor (BJ), which controlled current flow through alternating layers of p-type (positive charge or holes as the majority carrier) and n-type (negative charge or electrons as the majority carrier) germanium. It was not until 1954 that silicon based transistors were introduced in BJ at Texas Instruments and it was used in the development of the first integrated circuit in 1958 by physics Nobel Prize winner Jack Kilby at Texas Instruments. Later on in 1961, BJs were replaced by field-effect transistors (FETs). FETs are commonly used for weak-signal amplification by controlling the migration of electrons or holes into conduction channels between a source and drain electrode.[2]

Despite the reduction in size of electronic components (including wires, resistors, capacitors, and transistors) over the last five decades, integrated silicon-based circuits can be produced with a resolution greater than 100 nm,[1] but these materials are facing natural limits that prevent them from following Moore's law[3] (which states that chip

densities would double every 2 years) because of their size constraints on the nanometer scale.[2]

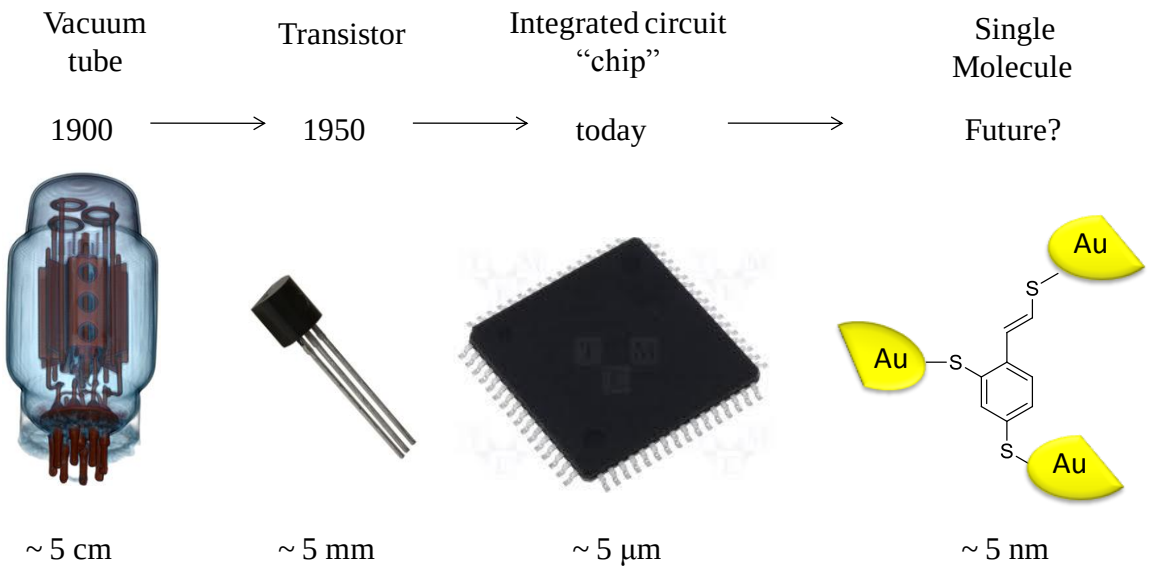

Figure 1.1. Miniaturization of amplification devices used in electronic circuits over the last century. [1]

Molecular electronics (technology using single molecules) is a promising approach to overcome this limitation since it would be low cost, flexible and yield small weight and low power devices.[4] For instance, an organic field-effect transistor (OFET) consists of an organic semiconductor, a dielectric layer and at least three conducting electrodes (Figure 1.2). Two of them, the source and drain, are in contact with the semiconductor and they inject or extract charge carriers from it. If the Fermi level of the source/drain metal is close to the band gap (HOMO-LUMO) level of the organic semiconductor; the third electrode could be separated from the semiconductor by a

dielectric layer. A voltage is applied between the source and the gate to modify the resistance of the semiconductor, which amplifies or switches the electric signal.[4]

Complex physical setups are currently available to investigate the correlation between the structural features and electronic transport properties of single molecules or clusters of molecules sandwiched between metal or semiconductor electrodes. These methods include mechanically controlled break junctions (MCBs),[5-8] scanning probe microscope (SPM) based molecular junctions,[9-11] crossed wire junctions[12-13] and others.[13-14] A nanopore, crossed-wire junction, and nanowire junction contain a few hundred to a thousand molecules. On the other hand, MCBs and SPM have a small lateral junction area and can access a small number of molecules, down to a single molecule. An SPM system has advantages over a mechanical break-junction system because it can image the surface morphology and at the same time study properties and the measurements can be done in various environments including an electrolyte solution with controlled potentials of the probe and substrate against a reference electrode.[9-11]

Tao and co-workers[11] were the first to measure the conductance of a single molecule using scanning tunnelling microscopy (STM) break junctions. This was achieved by moving the STM tip in and out of contact with a gold substrate in a solution containing 4,4'-bipyridine (BPY) repeatedly forming thousands of gold-molecule-gold junctions at different gate potentials (V_{gate}) (Figure 1.3).[11]

The measurement of this system recorded a current between the electrodes due to an applied voltage V_{gate}, with a conductance *g* defined as:[15]

$$g(V) = \partial I(V)/ \partial V$$

I (current) and V (sample voltage), in units of the quantum conductance $G_0 = 2e^2/h = (12.9\ k\Omega)^{-1}$ (where *e* and *h* are the electron charge and Planck's constant, respectively).[11]

Figures 1.3A-B show the stepwise decrease in the conductance during the initial stage of pulling the STM tip out of contact with the substrate, with each step being an integer multiple of the conductance quantum G_0. After breaking the gold nanowire contact, the BPY molecules are able to form stable molecular junctions with conductance peaks at 1 X, 2 X, and 3 X 0.01 G_0 corresponding to one, two, and three molecules, respectively, in the junctions (Figures 1.3C-D). This SPM break-junction method is a feasible way to assess the conductance of single molecules.[11]

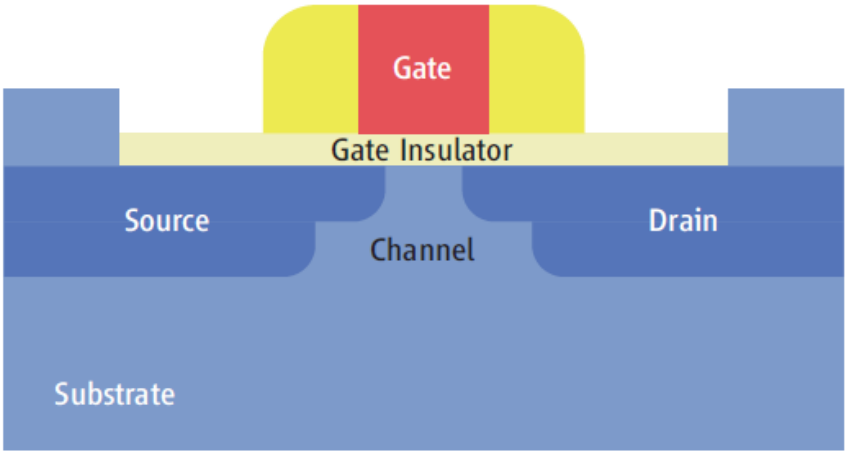

Figure 1.2. Schematic illustration of OFET configurations. [4]

Suitable organic compounds for molecular electronic require optimal charge carrier ability,[16] air stability and high mobility (μ).[4] There are many proposed examples of OFETs based on quantum effects such as single molecules, carbon nanotubes, and quantum dots or nanoparticles. For example, Park and co-workers studied the Coulomb blockade and the Kondo effect of a single-molecule transistor using a Co ion complexed to polypyridyl ligands and attached to insulating tethers of different lengths (Figure 1.4A). The Co ion acts as an island whose charge state (2+ or 3+) can be controlled using the V_{gate}.[17] Coulomb blockade is the increased resistance at small V_{gate}, a consequence of the transference of one electron onto the metal that blocks the flow of electrons due to electrostatic repulsion.[2] This switching behavior was observed for the Co complex with longer linkers and weaker coupling, proving that the device functioned as an OFET (Figure 1.4B).[17] The shorter linker with stronger coupling showed a peak with logarithmic temperature dependence and magnetic-field splitting, indicating a Kondo-assisted tunneling. The Kondo effect is the formation of a bound state between a local spin on an island and the electrical resistivity in the electrodes, which enhances the conductance at low biases and changes with temperature.[17]

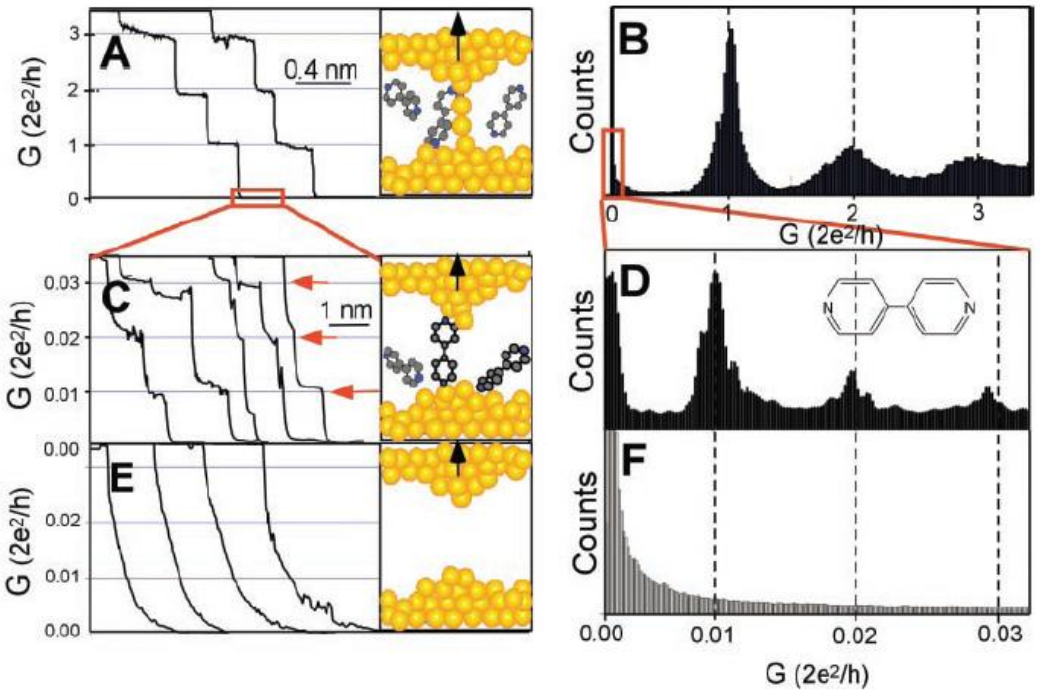

Figure 1.3. (**A**) Conductance of a gold contact formed between a gold STM tip and a gold substrate decreases in quantum steps at multiples of G_0 ($2e^2/h$) as the tip is pulled away from the substrate. (**B**) A corresponding conductance histogram constructed from 1000 conductance curves. (**C**) When the contact shown in (A) is completely broken, corresponding to the collapse of the last quantum step, a new series of conductance steps appears if molecules such as 4,4-bipyridine are present in the solution. (**D**) A conductance histogram obtained from 1000 measurements as shown in (C) shows peaks near 1 x, 2 x, and 3 x 0.01 G_0 that are ascribed to one, two, and three molecules in the gap, respectively. (**E**) and (**F**) in the absence of molecules, no steps or peaks are observed within the same conductance range. [11]

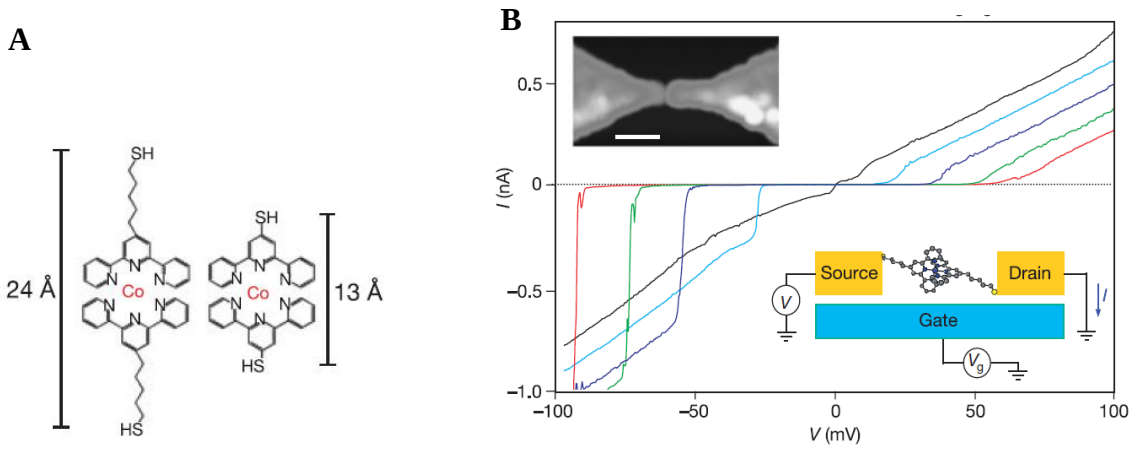

Figure 1.4 (**A**) Structure of Cobalt complexes. (**B**) *I* –V curves of a $[Co(tpy\text{-}(CH_2)_5\text{-}SH)_2]^{2+}$. Single-electron transistor at different gate voltage (V_{gate}) from 20.4 V (red) to 21.0 V (black) with $\Delta V_{gate} \approx$ -0.15 V. Upper inset, a topographic atomic force microscope image of the electrodes with a gap (scale bar, 100 nm). Lower inset, a schematic diagram of the device. [17]

Viologen, a dialkyl pyridinium with two terminal sulfur anchor groups at the end of the alkyl chains, is a redox-active molecule that was studied by Schiffrin and co-workers using STM, Figure 1.5. The molecule was self-assembled on a gold surface and gold nanoclusters were placed on top of the sulfur functionalized molecules. The STM tip was positioned on top of a nanoparticle to measure the tunnelling current, while the redox state of the viologen subunits in the linking molecules was controlled electrochemically without affecting the bias between the STM and the substrate. Increased conductivity was observed for the reduced viologen linkers ($V^{\bullet+}$) compared to their dicationic state (V^{2+}) by these measurements.[18]

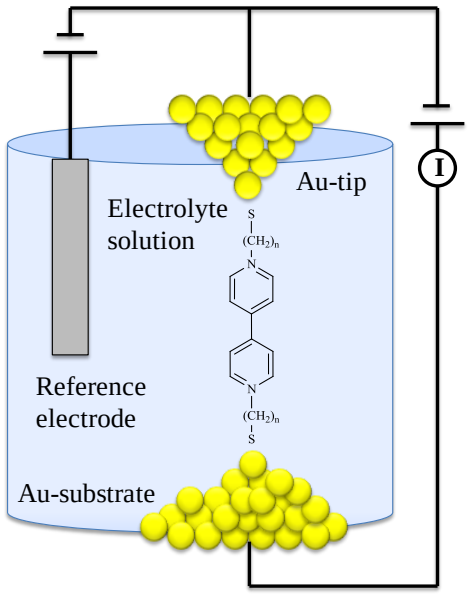

Figure 1.5. Viologen derivative (*n* = 6) diagram in an electrochemical scanning tunnelling microscopy (STM) setup. [18]

Dekker and co-workers found OFETs based properties using a carbon nanotube at room temperature. The electronic characteristics of the device were measured by sweeping the bias between the two electrodes at various applied V_{gate}.[19] Later, Rao and co-wokers demonstrated electrical switching behavior in a Y-junction multiwalled carbon-nanotube (Y-MWNT) system doped with a nanoparticle which was grown by a modified chemical vapor deposition (CVD) process.[20] The modulation of the current from an on- to an off-state between of the source–drain channel in one branch was achieved by applying a voltage to the third terminal presumably mediated by defects and the topology of the junction. An advantage of this approach over conventional OFETs is that the current is only switched between two outputs rather than completely turned on/off, which leads to higher speed and efficiency of operation.[20] Multiwalled Y-

junctions are difficult to use as transistors with a high gain and high frequency modulation at room temperature. Therefore, Choi and co-workers[21] studied the electrical properties of the branches and stem of pseudo Y-junction single wall nanotube Y-SWNTs (i.e., metallic or semiconducting) and found ambipolar characteristics for the Y-MWNTs at room temperature (Figure 1.6).

Even though it has been proved that single molecules can behave as transistors with two[17] and three[20-21] legs, the performance of OFETs not only relies on their nature but also on the electrodes and gate dielectrics, and eventually on other factors such as device architecture and deposition methods, among others.[22] When a molecule is coupled to macroscopic electrodes, three important problems arise: 1) how to fabricate electrodes with a controllable gap size adequate for the molecule size of interest; 2) arranging the molecules of interest between the electrodes with precise location and orientation control; and 3) achieving robust contacts between the molecules and the electrodes.[22] C_{60} promises to be an excellent candidate to solve the last two problems because of its rich electrochemical properties and 3D structure. In the following section the work that has been done in molecular electronics using C_{60} will be discussed.

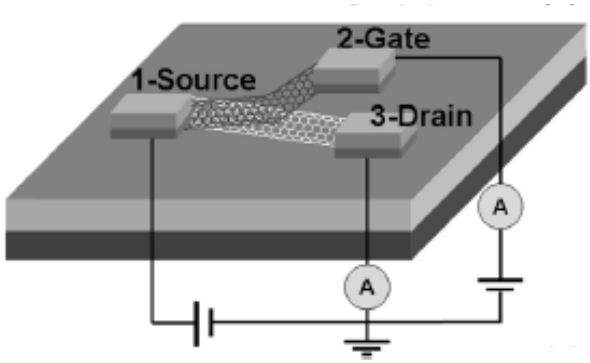

Figure 1.6. The device schematic for a pseudo Y-junction transistor. Rather than using a back gate (or top gate) electrode, the metallic branch of the Y-SWNTs is used as the gate electrode. [21]

C_{60} as a single molecule transistor

Since the molecules of interest for OFETs applications must have dimensions on the nanometer scale as well as electron donor-acceptor properties and degenerate highest-occupied (HOMO) and lowest-unoccupied molecular orbital (LUMO) manifolds, C_{60} is excellently suited for these studies.[23] Additional key features of C_{60} is that its ruggedness and elasticity permits multiple cycles of operation,[24] and its eight reasonably accessible redox states [1+ to 6-] provide the possibility of more states than simply on and off.[25] In addition, C_{60} can handle electron currents of up to several nanoamperes using SPM techniques.[26] The conductance of C_{60} has been studied in an electromechanical amplifier design by Joachim and *et al*.,[26] in which a single C_{60} molecule was deposited on clean Cu (111) and it was distorted by the STM tip when a signal (V_{in}) was applied to the piezoelectric tube (Figure 1.7). The conductance of the junction was increased by two orders of magnitude. This phenomenon was attributed to the shift and broadening of the HOMO-LUMO band gap upon distortion, which leads to

a greater conductance through the molecule.[26] Later, Wang and co-workers[27] reported an *ab initio* model of the charge transfer, electron conduction and molecular switching of the physically distorted C_{60} molecular electromechanical amplifier. Charge transfer from the electrodes to the molecular region was found to play a crucial role in aligning the LUMO orbital of the C_{60} to the Fermi level of the electrodes. This alignment induced a device conductance of $2.2G_0$. The end result is that a gate potential can inhibit charge transfer, thereby producing a field-effect molecular current switch.[27]

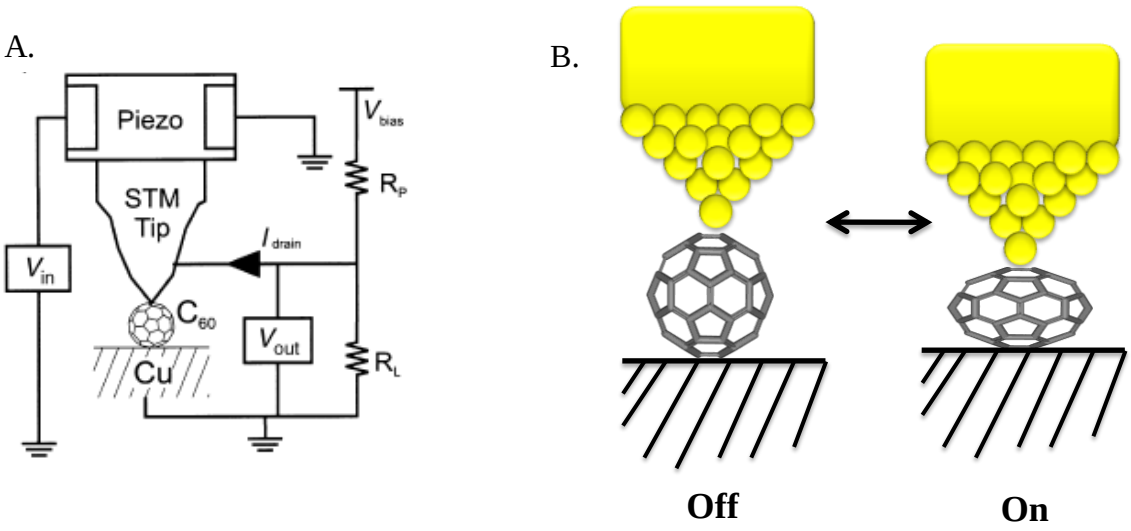

Figure 1.7. (**A**) Circuit diagram of a single-molecule electromechanical amplifier based on the interaction of an STM tip with a C_{60} molecule. (**B**) Schematic representation of the off/on states of the electromechanical amplifier. [26]

Another electromechanical amplifier based on C_{60} was reported by Park and *et al.*[28] This single-molecule transistor works by inducing nanomechanical quantized oscillations of C_{60} between two gold electrodes with a frequency near 1.2 THz (Figure

1.8). The conduction mechanism involves a coupling between the centre-of-mass motion of the C_{60} molecules and single-electron hopping according to the transport measurements. In other words, the single-C_{60} transistor behaves as a high-frequency nanomechanical oscillator by single-electron-tunnelling which can excite and probe the motion of the cage.[28]

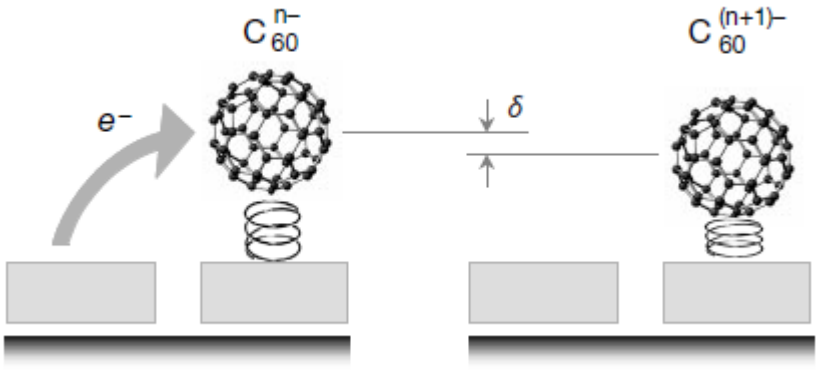

Figure 1.8 Diagram of the centre-of-mass oscillation of C_{60}. When an electron jumps on to C_{60}^{n-}, the attractive interaction between the additional electron and its image charge on gold pulls the C_{60} ion closer to the gold surface by a distance δ. This electrostatic interaction results in the mechanical motion of C_{60}.[28]

Kubozono and co-workers[29] reported an OFETs of a thin film of C_{60} using Eu electrodes with a $\mu = 0.5\ cm^2\ V^{-1}\ s^{-1}$. This high μ value was obtained because the electrons could be smoothly injected into the thin film of C_{60}, since its LUMO (E_{LUMO} = -3.6 eV) was lower than the Fermi level (E_F = -2.5 eV) of Eu. Consequently, the control of the electronic structure near the interface between the metal electrodes and the organic semiconductor is crucial for the performance control of the organic device.[29] Later,

Kubozono and co-workers[30] fabricated C_{60} OFET devices with Au electrodes modified by various types of 1-alkanethiols and studied the electronic structure produced by the contact thin films of C_{60} and the electrodes. Large carrier-injection barriers were observed for the C_{60} OFET devices with the Au electrodes modified by 1-alkanethiols with long alkyl chains.[30]

MCB junctions (Figure 1.9A) were also used to study of the C_{60} derivative (4-bis(fullero[*c*]pyrrolidin-1-yl)benzene, BDC_{60}) (low-bias conductance and junction stabilities), which possesses fullerenes that acts a the contact groups (Figure 1.9B).[31] The linear and rigid $BDAC_{60}$-capped molecule led to a lower spread in the low-bias conductance compared to thiols because the fullerenes provide larger junction stabilities and minimize fluctuations. In addition, junctions of fullerene-anchored benzenes exhibited an increased stretching length before breaking.[31]

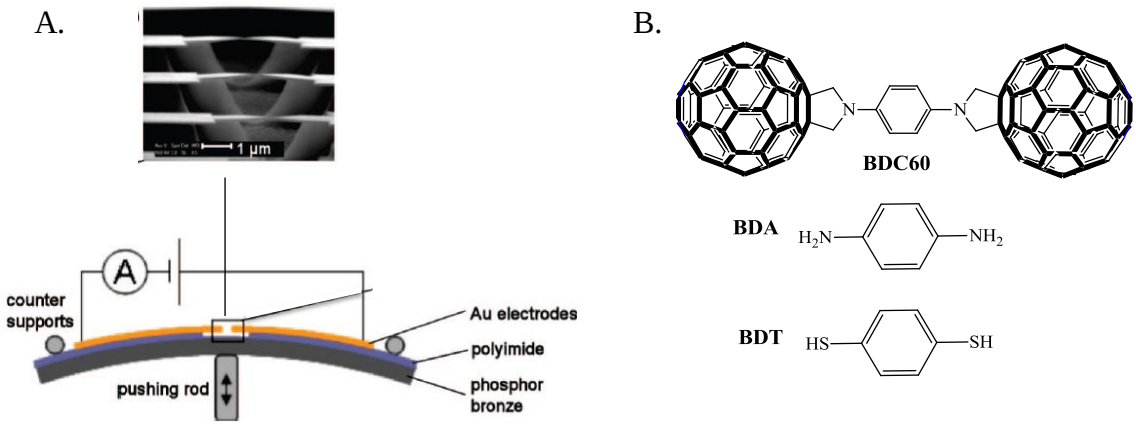

Figure 1.9. (**A**) Schematic of a mechanically controllable break junction. (**B**) Molecular structures of the benzene derivatives studied. [31]

Other C_{60} derivatives have also been used to build OFETs. Morita and Lindsay[32] reported the first example of a bis-adduct of C_{60} acting as single-molecule transistors. They demonstrated a two-step switching process of the C_{60} derivatives in an STM break junction in water and in dimethylformamide (DMF) (Figure 1.10). The *bis*-adducts, *trans-2* and *trans-3*, pyrrolidine rings with amino-terminated linkers exhibited enhanced electron tunneling conductance upon accepting electrons, with the dianion being the highest conductor and the neutral species the lowest. These observations clearly demonstrate that the electron tunneling through the junction is significantly enhanced upon the reductions of the C_{60} moiety.[32]

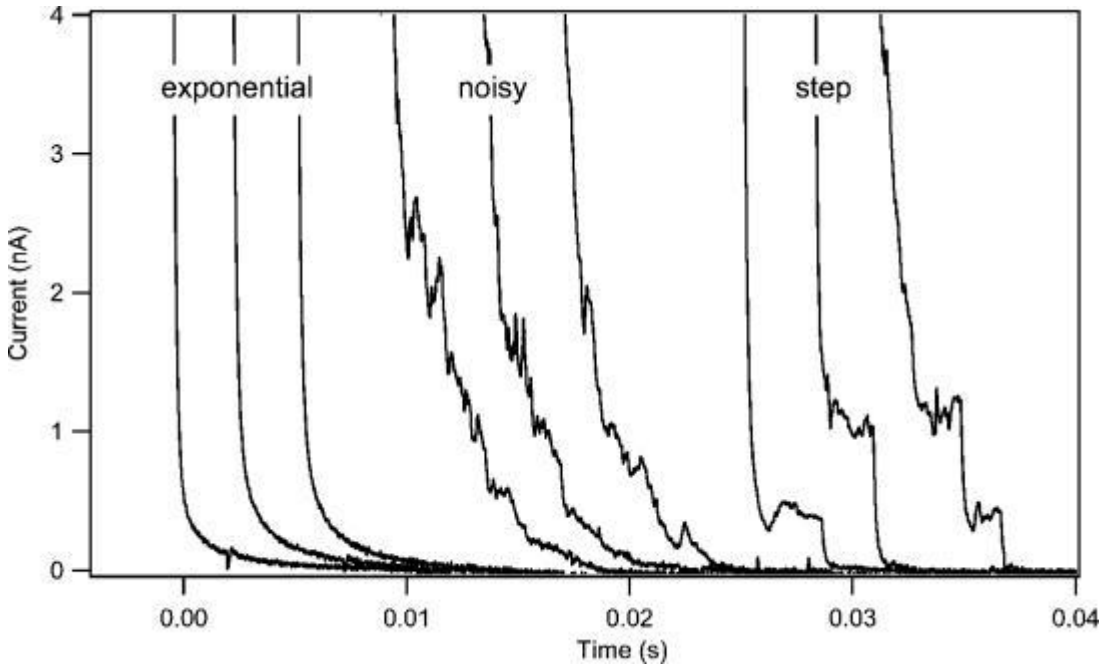

Figure 1.10 Representative current-time curves in the STM break-junction measurement on *trans*-2-C_{60} in a 0.1 M $TBAPF_6$ DMF solution at a tip bias of +0.1 V. [32]

Two main problems of this approach are: 1) even though it was evident that the C_{60} derivatives were immobilized on the gold surface, the gold surface-amino group interactions are rather weak. It is well known that C_{60} fullerene can be self-assembled on gold with an energy of 30-60 kcal:mol^{-1} (vide infra) which is similar to the Au-S bond strength;[33] 2) another shortcoming of this report is that the amino linker is a saturated chain that can not promote direct electron coupling of the substrate with the cage. The use of a specific covalent binding between a functional group and a metal surface is preferred, such as SH-Au, but the functional group should be electronically coupled with the fullerene. For example, *N*-(*p*-pyridyl)-3,4-fulleropyrrolidine (Figure 1.11), with a zinc porphyrin complexed to the pyridyl nitrogen shows efficient photoinduced charge transfer between the porphyrin and the C_{60}.[34]

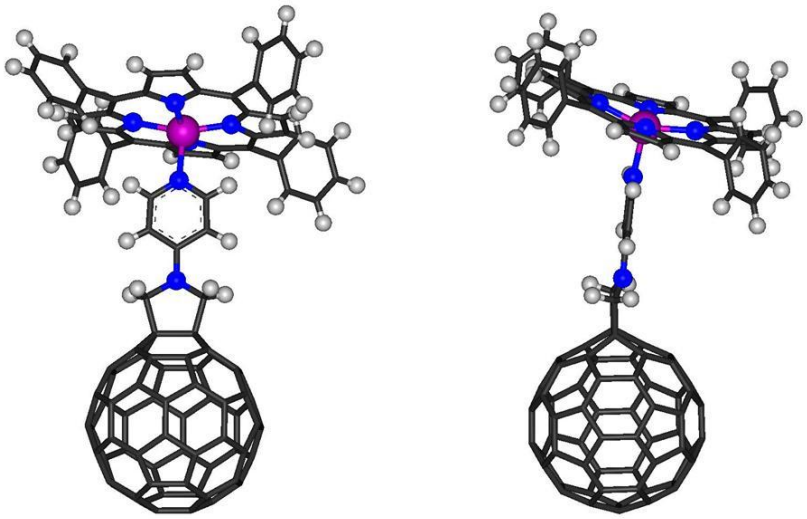

Figure 1.11. X-Ray structure of a complex of N-pyridyl pyrrolidino C_{60} fullerene and ZnTPP. [34]

The work reported here addresses the design, syntheses and characterization of C_{60} derivatives that could be good candidates in molecular electronic applications. For the construction of a fullerene-based molecular junction, we suggest anchoring the C_{60} sphere via two or three linkers with pyrrolidine addends, since these linkers exhibit good electronic coupling with the cage, thus enabling tunneling through the two electrodes.

Also, the linker must have functional groups that can selectively self-assemble on different metals in order to form an addressable transistor. The functional groups selected here fulfill these requirements since pyridyl groups are known to self-assemble on Au (6-10 kcal:mol^{-1}), Pd or Pt,[35] while terpyridyl groups are known to form stable complexes with Ru(II), Co(II), Fe(II) and Os(II).[36] SCN groups can interact with Cu(II), Ag, Pt and Au but it cleaves upon self-assembly on Au, thus releasing CN to result in an identical bond as that formed by thiol groups on Au.[37]

We targeted *bis*-adducts of C_{60} that are expected to self-assemble on break junctions to create OFETs that can be gated by potential control in a solvent:electrolyte medium (Figure 1.12A). Also, *tris*-adducts were designed that can self-assemble through three different leads to form addressable OFETs, where one of the linkers can be used to gate the response, without the need for an intervening electrolyte solution (Figure 1.12B). These would be three terminal single molecule transistors such as the Y-SWNTs previously mentioned.[21] If the compounds reported here can be made to self-assemble as planned, they would constitute the smallest three terminal molecular OFETs known with the advantage that the core fullerene could exist in multiple redox states thus yielding more flexibility than a simple "on-off" switch.

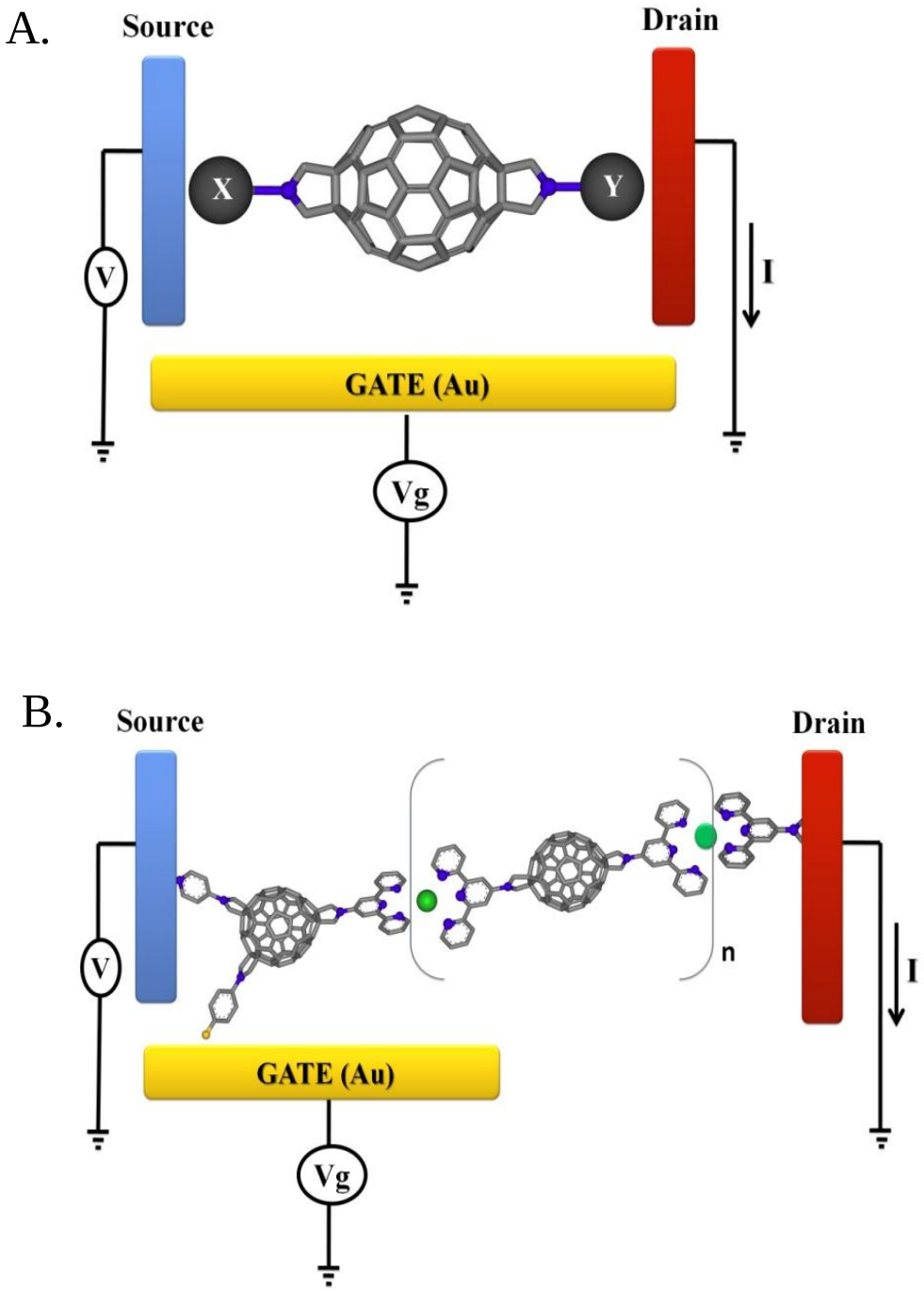

Figure 1.12. A) two terminal single molecule transistors, OFET. **B)** Three terminal single molecule transistors.

Regiochemistry of C_{60} Addition Reactions

Since Krätschmer, Huffman, and co-workers discovered a bulk fullerene preparation method in 1990,[38] C_{60} reactivity has been studied worldwide. C_{60} fullerene has low regioselectivity and poor stereocontrol because its framework has 30 equivalent reactive double bonds in [6,6] ring junctions, which makes regio-selective chemical modification a real challenge.[39] After the formation of the mono-adduct, successive additions of one, two, and three symmetrical addends yield 8, 46, and 262 possible regioisomers, respectively. Additionally, the isolation of pure *bis*-adduct isomers is challenging because *bis*- and *tris*-adducts co-elute chromatographically due to their similar polarities.[40] After the eight regioisomers of (ethoxycarbonyl)methylene-C_{60} bisadducts were isolated and characterized, a general nomenclature for positional relationships of the two addends was established (Figure 1.13a),[41] which divided the C_{60} core into two hemispheres. If the two addends are in the same hemisphere they are in a *cis* relationship with respect to each other and if the two addends are in opposite hemispheres they are in a *trans* relationship with respect to each other. Finally, if the two addends are positioned on the equator belt they are equatorial (*e*) to each other (Figure 1.13b).[41] This nomenclature has been adopted by people in the field and it will be used through out this work.

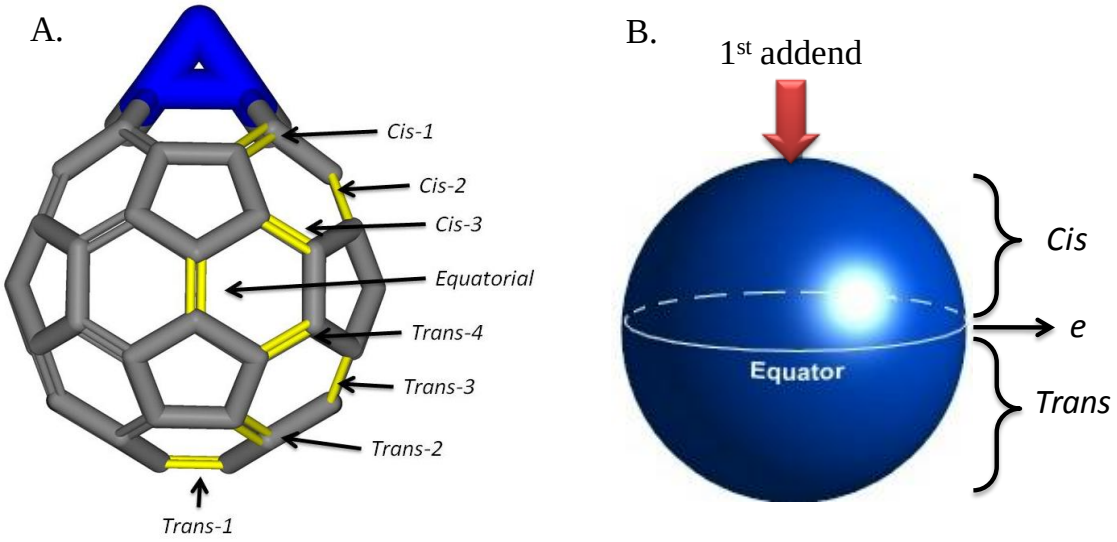

Figure 1.13 (**A**) Hirsch nomenclature for the eight regioisomers (yellow) for C_{60} *bis*-adducts with respect to the first addend (blue). (**B**) Schematic representation of the Hirsch nomenclature. [41]

Among the different reactions possible on C_{60}, we were interested on three types of cycloadditions: [2+1] cyclopropanations (known as the Bingel-Hirsch reaction),[42] [3+2] 1,3-dipolar cycloadditions (known as the Prato reaction),[43] and [4+2] *Diels-Alder* reactions.[44] The addition-elimination Bingel-Hirsch reaction was reported in 1994, where the deprotonation of an α-halomalonate **1.1** (Scheme 1.1) leads to a nucleophilic anion which attacks the fullerene core (**1.2**, Scheme 1.1), followed by an intramolecular displacement of the halide by cyclization with the anionic center formed in the core (Scheme 1.1).[41] The most favorable positions for nucleophilic addition are the equatorial and *trans*-3 positions (Figure 1.13a).[45] The cyclopropane ring is unstable under reduction conditions and it can undergo *retro*-cyclopropanations (known as retro-Bingel reaction) and isomerization under reduction conditions.[46]

In 1993, Prato and co-workers first reported the 1,3-dipolar cycloaddition of azomethine ylides to C_{60}, which yields a pyrrolidine ring addend (Scheme 1.2). Azomethine ylides are reactive intermediates that can be generated in several ways, although the decarboxylation of imminium salts derived from condensation of α-amino acids with aldehydes or ketones, is the easiest and most commonly followed procedure.[43] In 1996, Wilson and co-workers found that 1,3-dipolar cycloadditions to C_{60} are less chemoselective than cyclopropanations.[47] *Diels-Alder* reactions are an effective reaction because fullerenes are excellent dienophiles, they can react with different dienes such as anthracene, furan and cyclopentadiene. This reaction is controlled by the properties of the dienes and can proceed at room temperature, at reflux or under microwave conditions.[48]

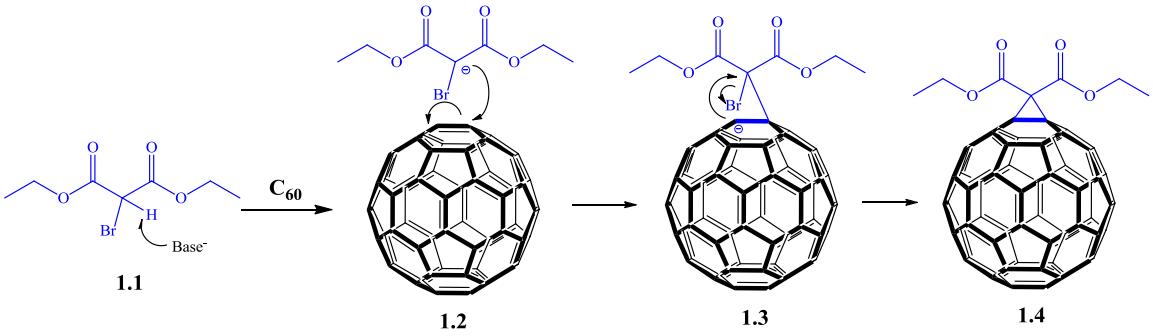

Scheme 1.1. Addition-elimination mechanism of Bingel-Hirsch reaction. [41]

Unusual regiochemical addition patterns have been prepared using ingenious schemes, most notable are the "tether-directed remote functionalization" method introduced by Diederich et al.,[49] and the "orthogonal transposition" method by Kräutler et al.[50] The "tether-directed remote multifunctionalization" approach was used for the

regiospecific formation of *bis*- and *tris*-adducts of C_{60}. The fullerene is functionalized by a cyclopropanation as a covalent template and it is followed by a [4+2] cycloaddition, where the regioselectivity depends on the length, geometry and rigidity of the tether. In some examples *equatorial*, *cis-2*,[51] *trans-2*[52] or *trans-1*,[53] structures could be obtained almost exclusively. An extension of this approach is the efficient synthesis of *hexakis*-C_{60}-adducts by stepwise "*mer*-3+3" done by Rubin and co-workers. After the protection of *trans*-1 positions by *Dies-Alder* reactions with a functionalized tether, two pairs of addend (A_2 and B_2) groups were attached in the four bonds of the equatorial belt. The tether was removed and finally the last pair of groups (C_2) were added, resulting in topologies similar to those of octahedral transition metal complexes.[54] Also in 2006, Rubin and co-workers reported the regioselective cyclopropanation of C_{60} at the [*trans-4*, *trans-4*, *trans-4*] positions. Initially, the *cis-1 bis*-adduct position was temporarily blocked by a tethered 1,3-diene, followed by cyclopropanation at these three bonds for which the LUMO orbital coefficients were activated by the blockage. Finally, the tether was removed thermally.[55]

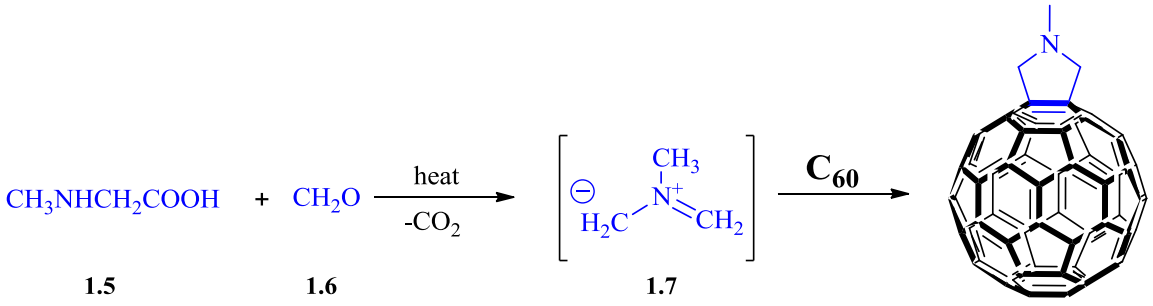

Scheme 1.2. 1,3-dipolar reaction or Prato reaction on C_{60}. [43]

The crux of the "orthogonal transposition" approach involves a protection-deprotection scheme in order to prepare an equatorially protected C_{60} compound containing four addends which leave the antipodal hemispheres of the fullerene available for further reaction.[50] C_{60} was protected with two thermally labile anthracene groups in the *trans-1* position followed by symmetric addition of four malonate groups to the equatorial belt of C_{60}. The anthracene moieties were then removed via a thermal retro-*Diels-Alder* reaction (Scheme 1.3).[50]

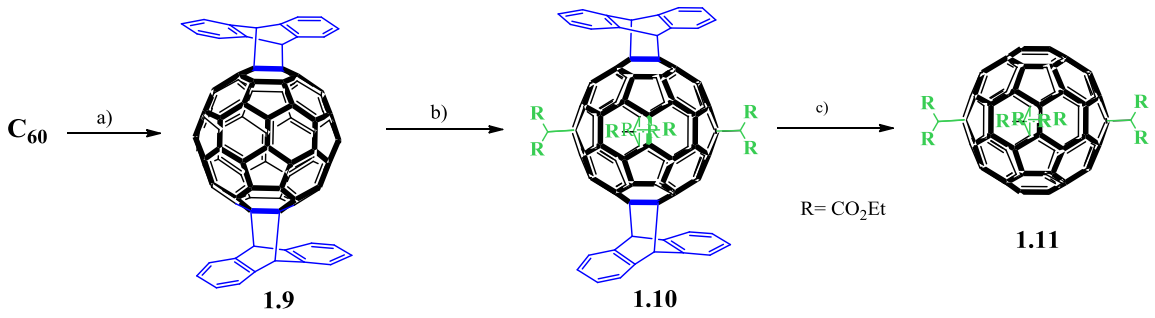

a) anthracene, 240 °C; b) diethyl bromomalonate, DBU, 48 hrs, Ar; c) 190 °C, vacuum, or refluxing *o*-DCB

Scheme 1.3. Synthesis of *e,e,e,e-tetra*-(ethoxycarbonyl)methylene-C_{60} **1.11**. [50]

We reported a "protection-deprotection" strategy derived from Kräutler's "orthogonal transposition" approach for the regioselective synthesis of hexakis-adducts of C_{60} [56] with two types of addends (cyclopropane and pyrrolidine rings) (Figure 1.14). Based on results obtained in that report,[56] further studies to develop this strategy for the regioselective synthesis of *pentakis*-, *hexakis*-, and *heptakis*-adducts of C_{60} were designed, and the results are presented in the present work as follows: Chapter II will

discuss the design and synthesis of these *pentakis*-, *hexakis*-, and *heptakis*-adducts of C_{60}. Chapter III will discuss the electrolytic retro-cyclopropanation of these derivatives by controlled potential electrolysis (CPE). Chapter IV will discuss the role of *hexakis*-adduct derivatives in supramolecular chemistry for potential applications on molecular electronics. Finally, Chapter VI will propose future directions of this research. Chapter V is an independent study of the electrochemical properties of supramolecular structures: phthalocyanines and porphyrins derivatives.

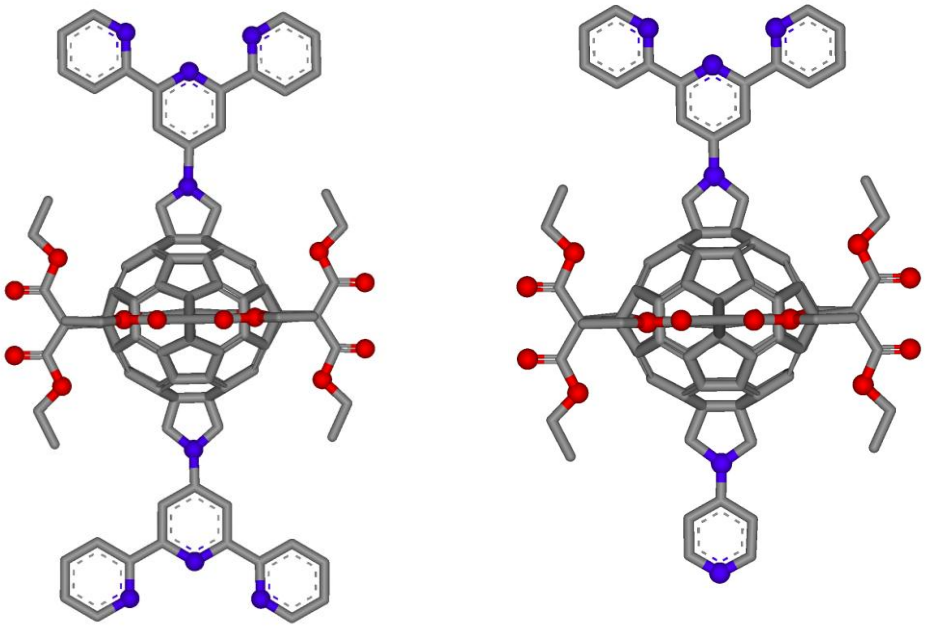

1.12 **1.13**

Figure 1.14. Structures of *hexakis*-adducts of C_{60}. [56]

References

[1] N. Weibel, S. Grunder and M. Mayor, *Org. Biomol. Chem.*, **2007**, *5*, 2343-2353.

[2] R. L. Carroll and C. B. Gorman, *Angew. Chem. Int. Ed.*, **2002**, *41*, 4378-4400.

[3] G. E. Moore in Digest of the 1975 International Electron Devices Meeting, IEEE, New York, **1975**, 1113.

[4] (a) R. F. Service, *Science,* **2009**, *323*, 1000-1002; (b) L. Miozzo, A. Yassar and G. Horowitz, *J. Mater. Chem.*, **2010**, *20*, 2513–2538.

[5] M. A. Reed, C. Zhou, C. J. Muller, T. P. Burgin and J.M. Tour, *Science*, **1997**, *278*, 252–254.

[6] C. Kergueris, J. P. Bourgoin, S. Palacin, D. Esteve, C. Urbina, M. Magoga and C. Joachim, *Phys. Rev. B: Condens. Matter Mater. Phys.*, **1999**, *59*, 12505–12513.

[7] R. H. M. Smit, Y. Noat, C. Untiedt, N. D. Lang, M. C. van Hemert and J. M. van Ruitenbeek, *Nature*, **2002**, *419*, 906–909.

[8] J. Reichert, R. Ochs,D. Beckmann, H. B.Weber,M.Mayor and H. von Lohneysen, *Phys.Rev. Lett.*, **2002**, *88*, 176804/1–176804/4.

[9] L. A. Bumm, J. J. Arnold, M. T. Cygan, T. D. Dunbar, T. P. Burgin, L. Jones, II, D. L. Allara, J. M. Tour and P. S. Weiss, *Science*, **1996**, *271*,1705–1707.

[10] X.D. Cui, A. Primak,X. Zarate, J. Tomfohr,O. F. Sankey, A. L. Moore, T. A. Moore, D. Gust,G. Harris and S. M. Lindsay, *Science*, **2001**, *294*, 571–574.

[11] B. Xu and N. J. Tao, *Science*, **2003**, *301*, 1221–1223.

[12] J. G. Kushmerick, D. B. Holt, J. C. Yang, J. Naciri, M. H. Moore and R. Shashidhar, *Phys. Rev. Lett.*, **2002**, *89*, 086802/1–086802/4.

[13] J. G. Kushmerick, A. S. Blum and D. P. Long, *Anal. Chim. Acta*, **2006**, *568*, 20–27.

[14] (a) R. E. Holmlin, R. F. Ismagilov, R. Haag, V. Mujica, M. A. Ratner, M. A. Rampi and G.M.Whitesides, *Angew. Chem., Int. Ed.,* **2001**, *40,* 2316–2320.; (b) D. J. Wold and C. D. Frisbie, *J. Am. Chem. Soc.*, **2000**, *122*, 2970–2971.; (c) B. Q. Xu, X. L. Li, X. Y. Xiao, H. Sakaguchi and N. J. Tao, *Nano Lett.*, **2005**, *5*, 1491–1495.

[15] A. Nitzan and M. A. Ratner, *Science*, **2003**, *300*, 1384-1389.

[16] W. Wu, Y. Liu and D. Zhu, *Chem. Soc. Rev.*, **2010**, *39*, 1489–1502.

[17] J. Park, A. N. Pasupathy, J. I. Goldsmith, C. Chang, Y. Yaish, J. R. Petta, M. Rinkoski, J. P. Sethna, H. D. Abruña, P. L. McEuen and D. C. Ralph, *Nature*, **2002**, *417*, 722-725.

[18] (a) D. I. Gittins, D. Bethell, D. J. Schiffrin and R. J. Nichols, *Nature*, **2000**, *408*, 67–69.; (b) W. Haiss, H. van Zalinge, S. J. Higgins, D. Bethell, H. Höbenreich, D. J. Schiffrin and R. J. Nichols, *J. Am. Chem. Soc.*, **2003**, *125*, 15294-15295.

[19] (a) S. J. Tans, A. R. M. Verschueren and C. Dekker, *Nature*, **1998**, *393*, 49-52; (b) C. Dekker, *Phys. Today*, **1999**, 22-28.

[20] P. R. Bandaru, C. Daraio, S. Jin and A. M. Rao, Nature mat., **2005**, *4*, 663-666.

[21] D-H Kim, J. Huang, B. K. Rao and W. Choi, *IEEE Trans. Nanotechnol*., **2006**, *5*, 731-736.

[22] L. Cao, S. Chen, D. Wei, Y. Liu, L. Fu, G. Yu, H. Liu, X. Liu and D. Wu, *J. Mater. Chem.*, **2010**, *20*, 2305-2309.

[23] C. Joachim, J. K. Gimzewski and H. Tang, *Phys. Rev. B*, **1998**, *58*, 16407-16417.

[24] C. Joachim, J.K. Gimzewski, R.R. Schlittler and C. Chary, *Phys. Rev. Lett*., **1995**, *74*, 2102-2105.

[25] Q. S. Xie, E. Pérez-Cordero, and L. Echegoyen, *J. Am. Chem. Soc.* **1992**, *114*, 3978-3980.

[26] C. Joachim and J.K. Gimzewski, *Chem. Phys. Lett*., **1997**, *265*, 353-357.

[27] J. Taylor, H. Guo and J. Wang, *Phys. Rev. B*, **2001**, *63*, 121104-1/-4 ®.

[28] H. Park, J. Park, A. K. L Lim, E. H. Anderson, A. P. Alivisatos and P.L. McEuen, *Nature*, **2000**, *407*, 57-60.

[29] K. Ochi, T. Nagano, T. Ohta, R. Nouchi, Y. Kubozono, Y. Matsuoka, E. Shikoh and A. Fujiwara, *Appl. Phys. Lett.* **2006**, *89*, 83511-83514.

[30] T. Nagano, M. Tsutsui, R. Nouchi, N. Kawasaki, Y. Ohta, Y. Kubozono, N. Takahashi and A. Fujiwara, *J. Phys. Chem. C*, **2007**, *111*, 7211-7217

[31] C. A. Martin, D. Ding, J. K. Sørensen, T. Bjørnholm, J. M. van Ruitenbeek and H. S. J. van der Zant, *J. Am. Chem. Soc.*, **2008**, *130*, 13198-13199.

[32] T. Morita and S. Lindsay, *J. Phys. Chem. B.* **2008,** *112*, 10563-10572.

[33] Y. Shirai, L. Cheng, B. Chen and J. Tour, *J. Am. Chem. Soc.*, **2006**, *128*, 13479-13489.

[34] F. T. Tat, Z. G. Zhou, S. MacMahon, F. Y. Song, A. L. Rheingold, L. Echegoyen, D. I. Schuster and S. R. Wilson, *J. Org. Chem.*, **2004**, *69*, 4602-4606.

[35] (a) S. Zhang, D. Dong, L. Gan, Z. Liu, C. Huang, *New J. Chem.*, **2001**, *25*, 606-610; (b) S. Lan Jeon, D. Loveless, W. Yount and S. Craig. *Inorg. Chem.***, 2006**, *45*, 11060-11068; (c) M. M. Gómez, J. M. Vara, J. C. Hernández, R. C. Salvarezza and A. J.

Arvia, *J. Electroanaly. Chem*., **1999**, *474*, 74–81; (d) P. Zelenay, L. M. Rice-Jackson and A. Wieckowski, *Langmuir***, 1990**, *6***,** 974-979.

[36] J-P. Sauvage, J-P. Collin, J-C. Chambron, S. Guillerez and C. Coudret, *Chem. Rev*. **1994,** *94*, 993-1019.

[37] (a) M. Kabešová, B. Boča, M. Melník, D. Valigura and M. Dunaj-Jurčo, *Coord. Chem. Rev.*, **1995**, *140*, 115. (b) J. Ciszek, and J. Tour, *Chem. Mater.* **2005,** *17*, 5684. (c) J. Ciszek, Z. Keane, L. Cheng, M. Stewart, L. Yu, D. Natelson, and J. Tour, *J. Am. Chem. Soc.* **2006**, *128*, 3179-3189.

[38] W. Krätschmer, L. D. Lamb, K. Fostiropoulos and D. R. Huffman, *Nature*, **1990**, *347*, 354-358.

[39] L. Pasimeni, A. Hirsch, I. Lamparth, A. Herzog, M. Maggini, M. Prato, C. Corvaja and G. Scorrano, *J. Am. Chem. Soc.* **1997**, *119*, 12896-12901.

[40] S. Marchesan, T. Da Ros and M. Prato, *J. Org. Chem.* **2005**, *70*, 4706-4713.

[41] A. Hirsch, I. Lamparth and H. R. Karfunkel, *Angew. Chem. Int. Ed. Eng.*, **1994**, *33*, 437-438.

[42] I. Lamparth and A.Hirsch, *J. Chem. Soc., Chem. Commun.* **1994**, *116*, 1727-1728.

[43] M. Maggini G. Scorrano and M. Prato, *J. Am. Chem. Soc.* **1993,** *115*, 9798-9799.

[44] R. Schwenninger, T. Müller and B. Kräutler, *J. Am. Chem. Soc*. **1997**, *119*, 9317-9318.

[45] A. Hirsch, I. Lamparth and H. R. Karfunkel, *Angew. Chem. Int. Ed. Eng.*, **1994**, *33*, 437-438.

[46] L. Echegoyen, F. Djojo, A. Hirsch, and L. Echegoyen, *J. Org. Chem*., **2000**, *65*, 4994-5000.

[47] Q. Lu, D. I. Schuster and S. R. Wilson, *J. Org. Chem.* **1996**, *61*, 4764-4768.

[48] M. Manoharan, F. de Proft and P. Geerlings, *J. Org. Chem*., **2000**, *65*, 6132-6137.

[49] L. Isaacs, R. F. Haldimann and F. Diederich, *Angew. Chem., Int. Ed. Engl.* **1994**, *33*, 2339-2342.

[50] R. Schwenninger, T. Müller and B. Kräutler, *J. Am. Chem. Soc*. **1997**, *119*, 9317-9318.

[51] F. Diederich and R. Kessinger, *Acc. Chem. Res.* **1999**, *32*, 537-545.

[52] E. Dietel, A. Hirsch, E. Eichhom, A. Rieker, S. Hackbarth and B. Röder, *Chem. Commun.* **1998**, 1981-1982.

[53] (a) J.-P. Bourgeois, L. Echegoyen, M. Fibbioli, E. Pretsch and F. Diederich, *Angew. Chem., Int. Ed.* **1998**, *37*, 2118-2121. (b) W. Qian and Y. Rubin, *Angew. Chem., Int. Ed. Engl.* **1999**, *38*, 2356-2360.

[54] W. Qian and Y. Rubin, *Angew. Chem., Int. Ed. Engl.* **2000**, *39*, 3133-3137.

[55] S-C. Chuang, S. Khan and Rubin, Y. *Org. Lett*. **2006**, *8*, 6075-6078.

[56] S. Zhang, O. Lukoyanova, and L. Echegoyen, *Chem. Eur. J*. **2006**, *12*, 2846-2853.

CHAPTER TWO

DESIGN AND SYNTHESIS OF NEW PYRROLIDINO C_{60} DERIVATIVES

Choosing the most appropriate addend

It was previously discussed that if the C_{60} cage is anchored by two and three pyrrolidine addends, these could become the smallest single molecule transistors. The pyrrolidine addends must fulfill two requirements: 1) they should have functional groups that can selectively self-assemble to different metals, for example pyridyl (Py) to Pd or Pt,[1] terpyridyl (Tpy) to Ru(II) and Fe(II),[2] thiolphenyl(PhSH) and thiocyanatephenyl (PhSCN) to Au;[3] 2) the functional group should be bonded through the N of the pyrrolidine (Pyrr) ring in order to have effective electronic coupling between the functional groups and the cage. Hence, only one type of glycine is needed:

$$X{-}NH{-}CH_2{-}COOH \qquad (X = Tpy, Py, PhSCN, SH\text{-}Ph)$$

Tpy-,[4] Py-,[5] and SH-Ph-,[6] glycines have been reported. However, the synthesis of the SH-Ph-glycine **2.5** was not possible using the reported procedure[6] (Scheme 2.1), probably due to the chemical reactivity of the SH group. The low yield of **2.4** (10%) was a problem; thus, different XCH_2CO_2Et (where X= I, Br) and several solvents (e.g. triethylamine, dioxane and ethanol:water) were tried. The yield was increased from 10% to 30%. The last chemical step (**2.4** → **2.5**) was not reproducible even with different reaction conditions. Nevertheless, compound **2.6** was obtained in reasonable yields and used in the 1,3-dipolar cycloaddition reaction with C_{60}. *Mono-*, *bis*, *tris*-additions and the loss of the protecting group (-CBz, Scheme 2.1) were detected by

means of matrix-assisted laser desorption ionization time-of-flight (MALDI-TOF) mass spectrometry. The cleavage of the CBz group during the reaction is a disadvantage because other products could be generated.[7] CH_3SPh-glycine was also pursued, it was synthesized with an overall yield of 20% using the same conditions from **2.2** to **2.6**. *Mono*, *bis* and *tris* additions were achieved on C_{60} by 1,3-dipolar cycloaddition reactions but the presence of oxidation products (S=O) was detected by means of MALDI-TOF MS. This indicated the oxidation of sulfur during the cycloaddition reaction. Sulfur oxides are not able to self-assemble on gold surfaces, thus this glycine was not suitable for the project.[8]

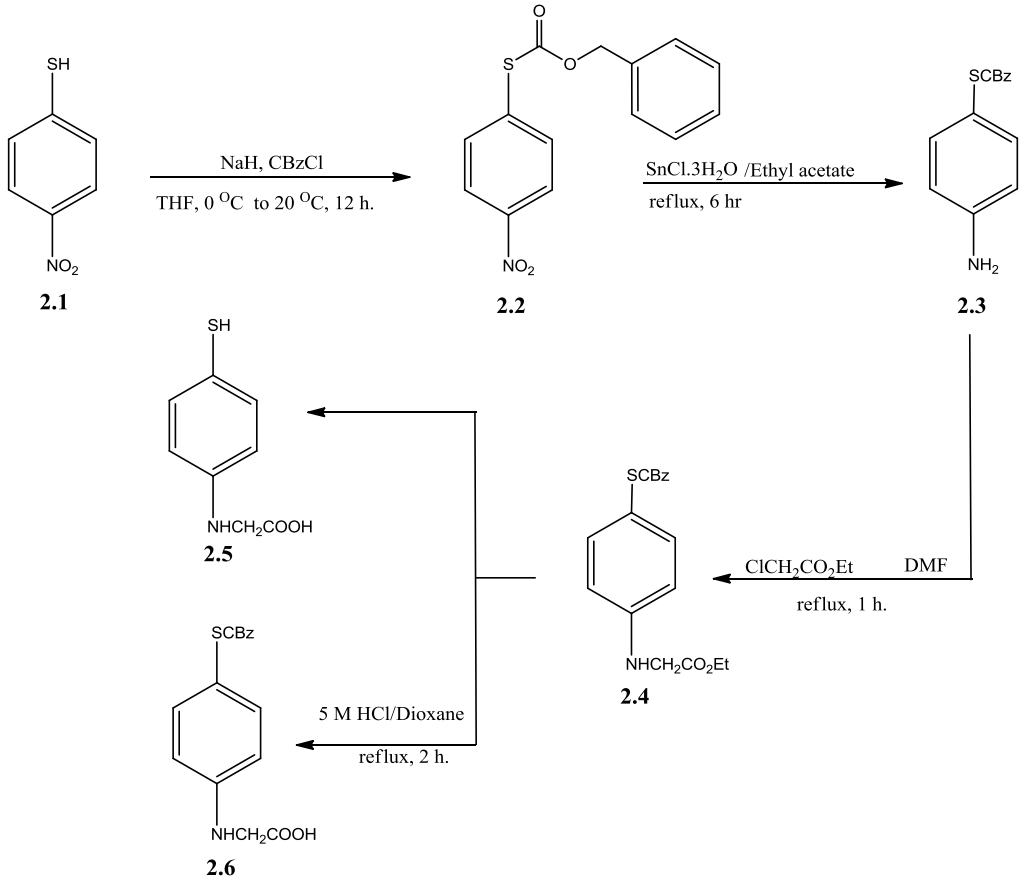

Scheme 2.1. Synthesis of the SH-Ph-glycine.

PhSCN-glycine was also synthesized (Scheme 2.2). As far as we know, this compound has not been reported. The effective and convenient conditions used to prepare PhSMe were used for this thio-glycine. The addends formed by this glycine are less polar than the previously reported ones, making its purification and characterization easier. Another advantage of the SCN group is its ability to self-assemble on Au by S-CN bond cleavage to form the thiolate bond (S-Au) and $-Au(CN)_2^-$.[9]

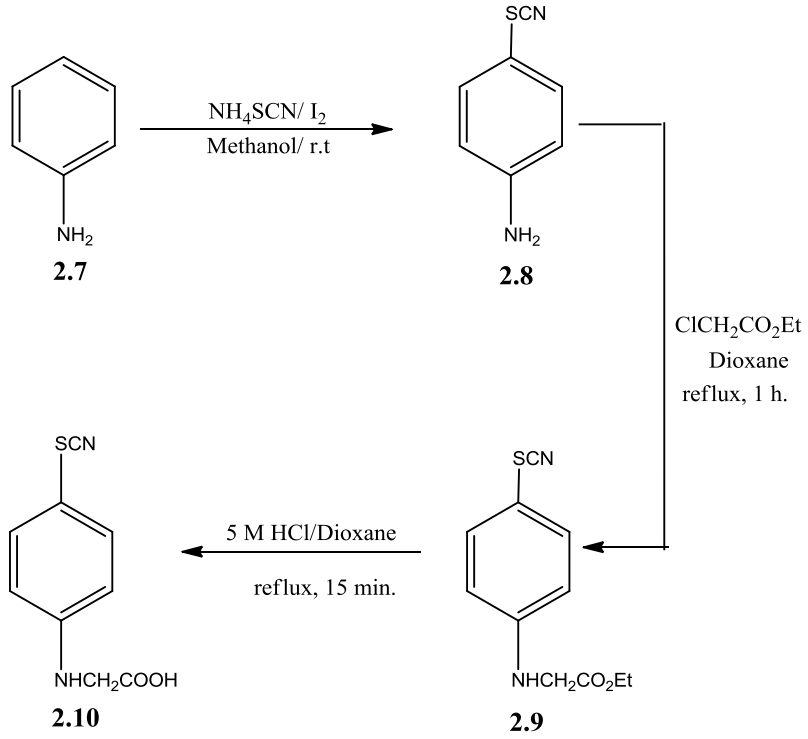

Scheme 2.2. Synthesis of the PhSCN-glycine.

Regioselective addition of *N*-(4-Thiocyanatophenyl)pyrrolidine addends to C_{60}

Our design of the bis- (**2.12** and **2.13**) and tris-adducts (**2.14** and **2.15**) of C_{60} (Figure 2.1) with different addends based on their potential applications in molecular electronics presents a synthetic challenge. This was addressed by a "protection-

deprotection" strategy[4] derived from Kräutler's "orthogonal transposition"[10] approach, which was discussed in Chapter I. The (*e,e,e,e-tetra*-(ethoxycarbonyl)methylene-C_{60}[10] adduct **2.16**) template was reacted with PhSCN-glycine and paraformaldehyde for 30 minutes to give *pentakis*-adducts (**2.17** and **2.18**) and *hexakis*-adducts (**2.19** and **2.20**) in a single step (Scheme 2.3).[11] Six different fractions were recovered by column chromatography using CH_2Cl_2 (DCM) as eluant, the first two fractions corresponding to the *pentakis*-adducts, the subsequent three fractions to *hexakis*-adducts and the last one to *heptakis*-adducts as assessed by means of MALDI-TOF mass spectrometry.

It is worth mentioning that the ethyl malonate groups in **2.16** separate the two hemispheres each of which has two types of double bonds, defined as symmetrical and unsymmetrical bonds, of the fullerene sphere available for reactions to occur (Figure 2.2). Each hemisphere has a total of five non-hindered double bonds available for cycloaddition reactions, one unique, called symmetrical, and four equivalents ones, called unsymmetrical, (Figure 2.2). Therefore, two regiosomers were expected for the *pentakis*-adducts, one corresponding addition on the symmetric bond and one corresponding addition in one of the four equivalent unsymmetric bonds. If the addition reaction occurred statistically the product ratio should be 1:4 in favor of the unsymmetrical product **2.18** *vs* **2.17**.[11] Since the observed ratio was 1:1, the reaction at the symmetric double bond is favored four-fold, probably due to steric hindrance of the malonates around the unsymmetric bonds and also to electronic effects.[12-13] The symmetrical

double bond (Figure 2.2) will be favored due to its equatorial position with respect to all cyclopropane rings by electronic factors.[12-13]

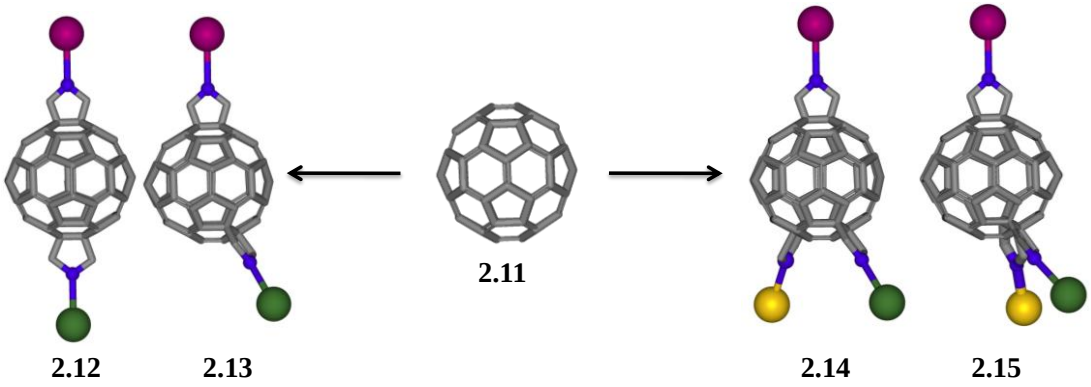

Figure 2.1 Structures of compounds **2.12**, **2.13**, **2.14** and **2.15**.

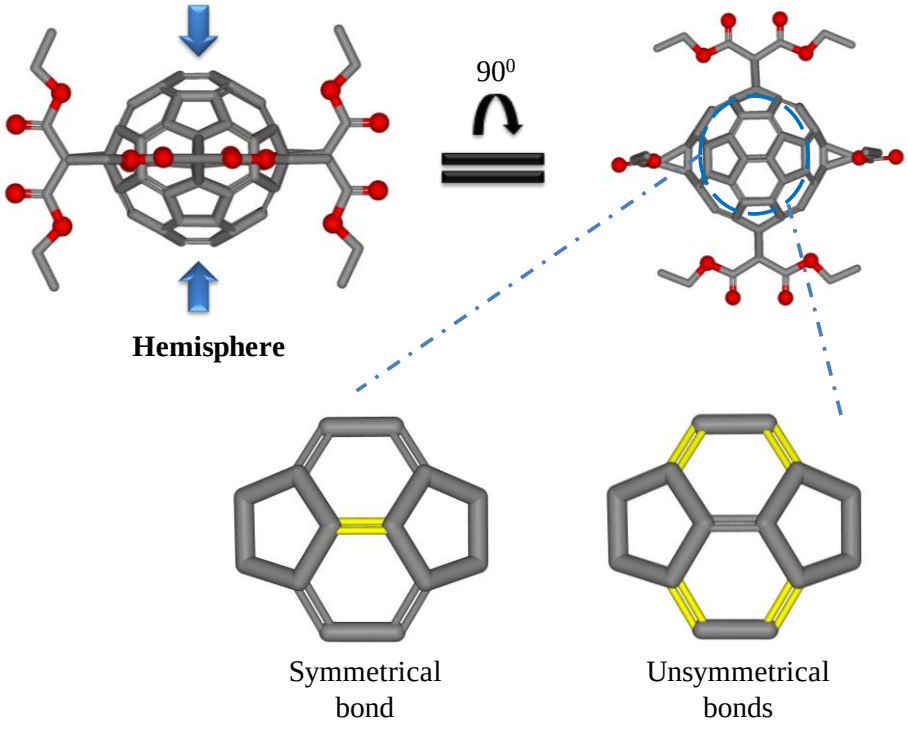

Figure 2.2 Symmetrical and unsymmetrical bonds of compound **2.16**.

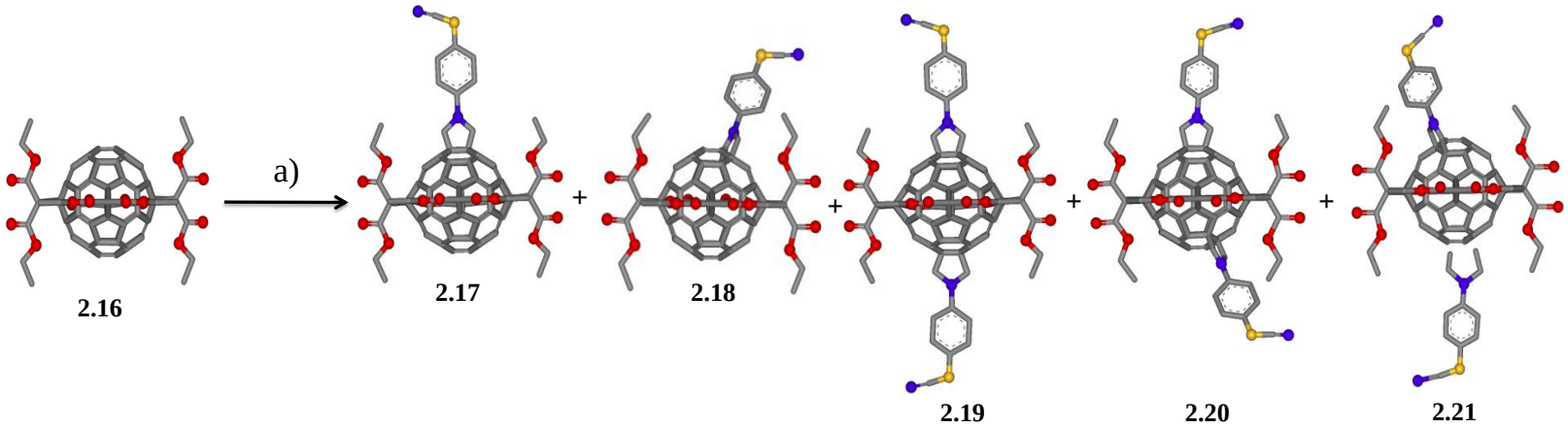

Scheme 2.3 Synthesis of fullerene derivatives with phenylthiocyanate groups.
a) PhSCN-glycine, HCHO, *o*-DCB, Ar, 175 °C, 10 min.[11]

The symmetries of the *pentakis*-adducts **2.17** and **2.18** were determined by NMR spectroscopy as follows: Figure 2.3a shows the ^{1}H NMR spectrum of **2.17** with three sets of triplets for CH_3 protons of the malonate groups, with integration ratios of 1:1:2, between δ = 1.40 – 1.30. The signals of the methylene protons from the malonate groups overlapped with those of the protons from the pyrrolidine ring in two multiplets between δ = 4.46 – 4.30 with an integration ratio of 1:4, respectively. Two doublets integrating for two protons each were observed for the four aromatic protons.

Figure 2.3b shows the ^{13}C NMR spectrum of **2.17** with three signals for carbonyl groups and three for methyl groups of the malonate addends indicating that two malonate groups were in different chemical environments and two were equivalent.[11] Twelve sp^2-C signals of the fullerene cage were observed between δ = 154 – 117. Seven sp^3-C signals were also observed between δ = 69.85 – 61.40, three of them assigned to the sp^3-fullerene carbon atoms: one was from the two sp^3-fullerene carbon atoms of the pyrrolidine ring, and the other two were from the two different sp^3-fullerene carbon atoms of the four cyclopropane rings. The remaining four sp^3-C signals left in this region were assigned to methylene groups: one signal was assigned to the methylene carbon atoms of the pyrrolidine ring and three were assigned to the methylene carbon atoms of the four malonate groups. C_{2v} symmetry was determined for compound **2.17** based upon NMR analysis.[11]

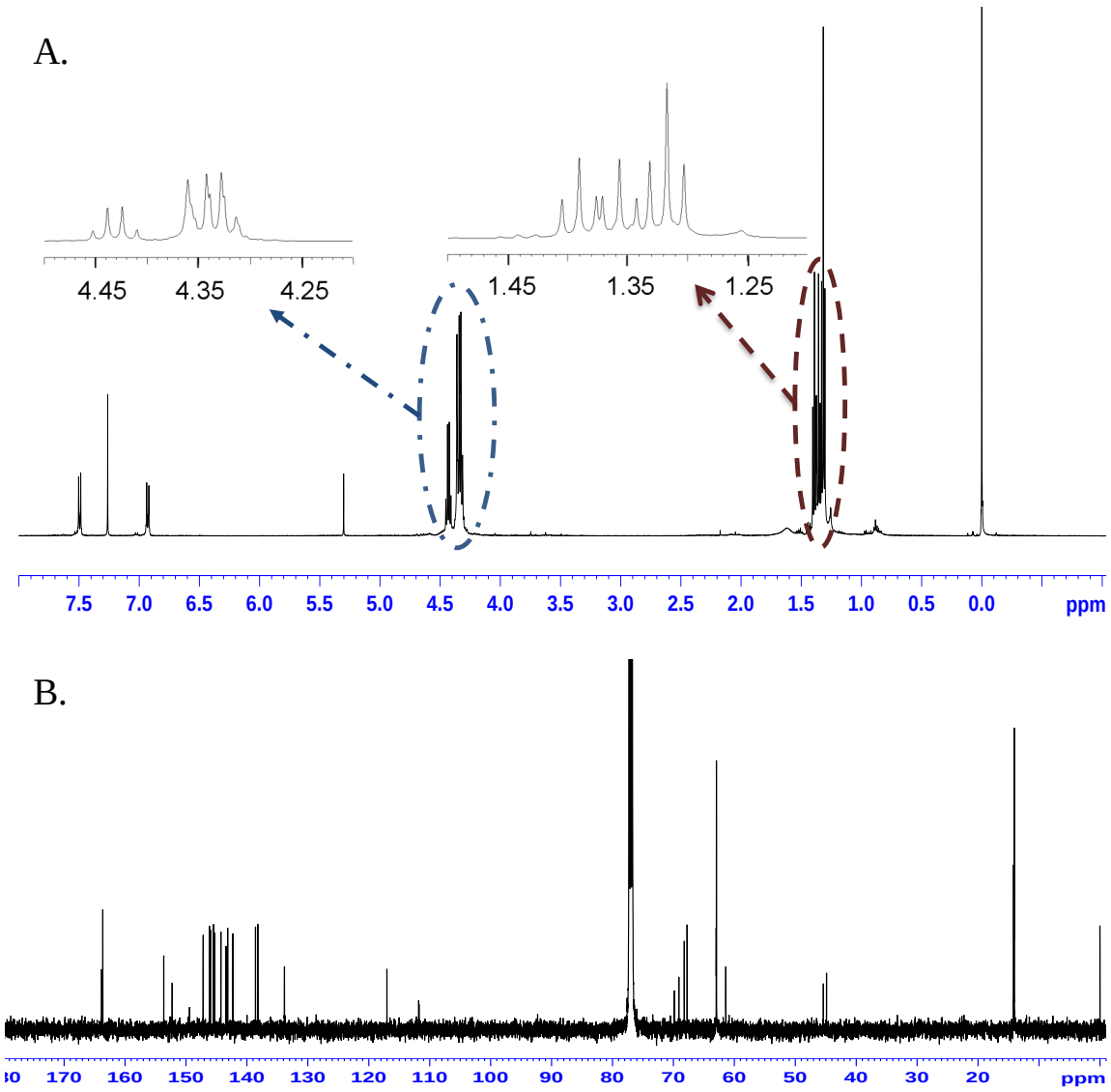

Figure 2.3 (A) ^{1}H NMR spectrum of symmetric *pentakis*-adduct **2.17** and expanded parts from 4.5 ppm to 4.2 ppm (left inset) and 1.5 ppm to 1.2 ppm (right inset); (B) ^{13}C NMR spectrum of symmetric *pentakis*-adduct **2.17.** (500 MHz, $CDCl_3$).[11]

Figure 2.4A shows the ^{1}H NMR spectrum of **2.18** with the expected lower symmetry relative to **2.17**. The aromatic proton signals were shifted downfield when compared to those of **2.17**. Seven triplets were observed between δ = 1.52 – 1.31 due to

eight different methyl groups (one triplet had twice the intensity of the others) and multiplets for the methylene protons indicate NMR non-equivalency.[11] Figure 2.4 B shows the ^{13}C NMR spectrum of **2.18** with 49 sp^2-C signals from the fullerene cage appearing between δ = 151 – 111, 7 signals for carbonyl groups and seven for methyl groups corresponding to the malonate addends. Nine signals between δ = 72.22 – 62.00 were assigned to the sp^3-C atoms of the fullerene cage, whereas seven signals were assigned to fullerene carbon atoms of the cyclopropane rings, and two were assigned to fullerene carbon atoms of the pyrrolidine ring. Finally, nine signals were assigned to the methylene moieties of the malonate groups. C_1 symmetry was assigned to compound **2.18** based upon NMR analysis.[11]

The next three fractions of *hexakis*-adducts (**a**, **b**, and **c**), with a mass ratio of 1:2.2:1.3, were purified by preparative TLC on silica gel using DCM as eluant. The plate was dried multiple times and new eluant used until a satisfactory separation was obtained. Then each fraction was removed from the plate and the derivatives were extracted from the silica gel with DCM. Fraction **a** (1st fraction eluted) was identified as *hexakis*-adduct **2.19** by means of NMR spectroscopy and MALDI-TOF. The ^1H NMR spectrum of *hexakis*-adduct **2.19** (Figure 2.5, A) exhibited two triplets at δ = 1.35 – 1.32 and 1.28 – 1.25 with a corresponding integration ratio of 1:1. They were assigned to the two different methyl groups from the malonate groups. Two quartets at δ = 4.35 – 4.30 and 4.30 – 4.26 integrating for eight protons each were assigned to the two sets of methylene moieties in the malonate groups. A sharp peak at δ = 4.59 was assigned to the eight equivalent pyrrolidine protons and two doublets integrating for four protons each to the

aromatic protons.[11] The ^{13}C NMR spectrum of **2.19** showed two peaks for carbonyl groups, two peaks for methyl groups, and six sp^2-C peaks for the fullerene cage. Finally, four signals between δ =66.87 – 61.00 for the sp^3-C atoms of the fullerene cage and methylene groups were observed. The NMR spectrum of **2.19** indicated D_{2h} symmetry because all of the addends are located at the pseudooctahedral positions on the fullerene.[11]

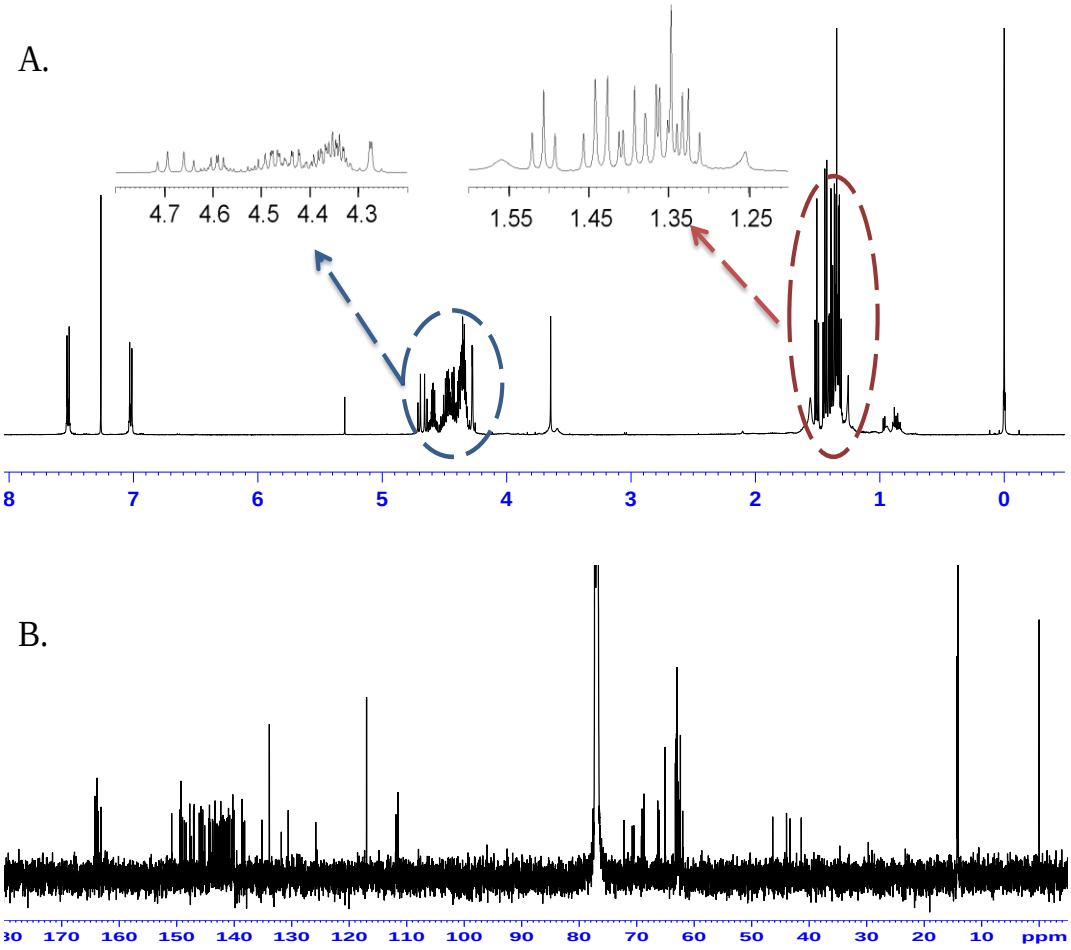

Figure 2.4 (A) ^1H NMR spectrum of unsymmetric *pentakis*-adduct **2.18** and expanded parts from 4.8 ppm to 4.2 ppm (left inset) and 1.6 ppm to 1.2 ppm (right inset); (B) ^{13}C NMR spectrum of unsymmetric *pentakis*-adduct **2.18.** (500 MHz, $CDCl_3$). [11]

The structures of the other two *hexakis*-adducts from fractions **b** and **c** were difficult to assign by NMR spectroscopy because of their structural complexity and lack of symmetry. Hence, their structures were elucidated by analyzing the regiochemistry of compounds **2.17** and **2.18** and designing an alternate synthetic route, discussed below.

Analysis of compound **2.17**: the hemisphere that has the pyrrolidine addend is hindered enough to prevent another azomethine attack. Consequently, further reactions can occur only on the unhindered hemisphere where there are 5 possible addition sites (Figure 2.6A). Addition to the symmetric double bond will lead to *hexakis*-adduct **2.19** and addition to one of the four unsymmetric double bonds leads to *hexakis*-adduct **2.20**.[11,14]

Analysis of compound **2.18**: in this case the addend is on one of the four unsymmetric double bonds, which allows the next addition to be on either of the two hemispheres. This addition could lead up to 7 regioisomers where *hexakis*-adduct **2.20** is one possibility (Figure 2.6B).

After the analysis of compounds of **2.17** and **2.18**, we proceeded to treat them with the PhSCN-glycine separately in order to identify compounds **2.20** and **2.21**. The reaction between **2.17**, PhSCN-glycine, and paraformaldehyde during 15 min (Scheme 2.4) formed two *hexakis*-adducts and one *heptakis*-adduct, which were isolated by preparative TLC using DCM as eluant. The first two fractions were identified as *hexakis*-adducts **2.19** and **2.20**, respectively by means of NMR spectroscopy and TLC R_f. Not surprisingly, **2.19** and **2.20** were obtained in a ratio of 1:2.4 instead of the expected 1:4 ratio (see Figure 2.6A). The ^{1}H NMR spectrum of *hexakis*-adduct **2.20** (Figure 2.5, B)

exhibited a multiplet from δ = 1.34 - 1.26 corresponding to 24 protons, which were assigned to the methyl groups from the malonate groups. Two multiplets at δ = 4.64 - 4.51 and 4.47 - 4.21 ppm integrating for 20 and 4 protons respectively, were assigned to the methylene groups in the malonates and on the pyrrolidine ring. Two sets of doublets were observed for each ring and two of them overlapped and corresponded to four protons. The other doublets correspond to two protons each, for a total of four different aromatic protons.[11] The controlled synthesis of the *hexakis*-adducts **2.19** and **2.20** by using **2.17** as the starting material confirmed the hypothesis (Figure 2.6A) that an addition in the same hemisphere at the first addend was not feasible and does not occur.

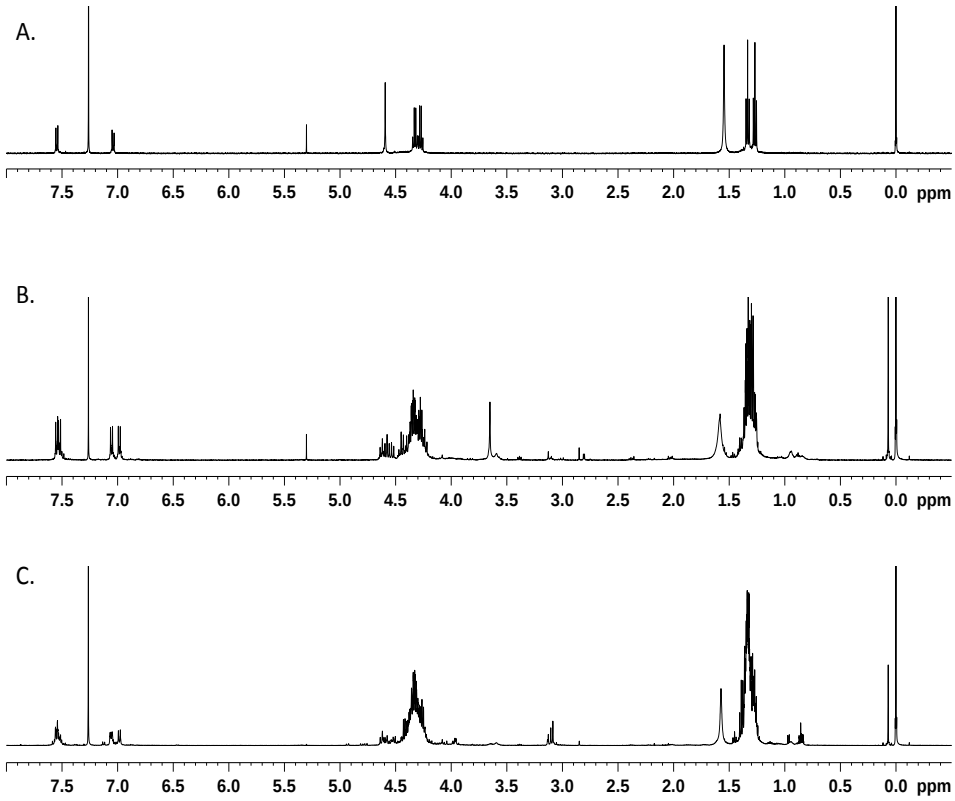

Figure 2.5. ^{1}H NMR spectrum of (A) compound **2.19**, (B) compound **2.20,** and (C) compound **2.21**. (500 MHz, $CDCl_3$). [11]

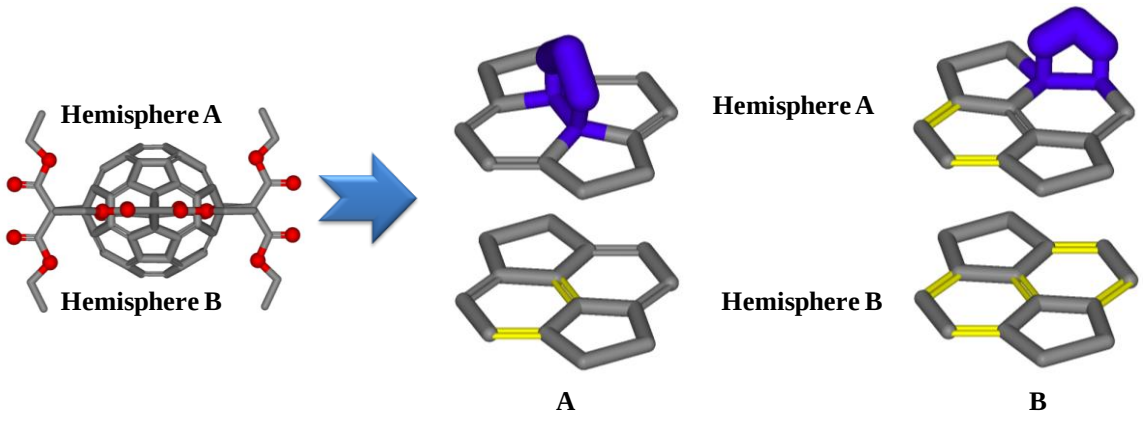

Figure 2.6. (A) Schematic representation of two possible isomers for a second addition to compound **2.17** (mono symmetric-adduct). (B) Schematic representation of seven possible isomers for a second addition to compound **2.18** (mono unsymmetric-adduct). Yellow bonds represent possible addition sites and blue triangles represent adducts position.

The reaction between **2.18**, PhSCN-glycine, and paraformaldehyde (Scheme 2.5) was stopped after 10 min when *heptakis*-adducts were observed by TLC. The *hexakis*-adducts **2.20** and **2.21** were identified in the first two fractions at a mass ratio of 1:1.4, respectively. The NMR spectra and the R_f value of fraction **c** are consistent with those of **2.21**. 7 regioisomers were expected for this reaction (Figure 2.6 B), therefore **2.21** should be a mixture of regioisomers, which was verified by HLPC using toluene as the mobile phase on a Buckyprep column (Figure 2.7). Seven peaks were observed, the retention time of one of them matching that of **2.20**. Of the seven isomers, two of them had an area three times larger than that of the other five products.[11] No further purification of "compound" **2.20** was pursued. Based on the time of reaction and presence of *heptakis*-

adducts in these two reaction schemes (**2.2** and **2.3**) it was concluded that compound **2.18** is more reactive than compound **2.17**.

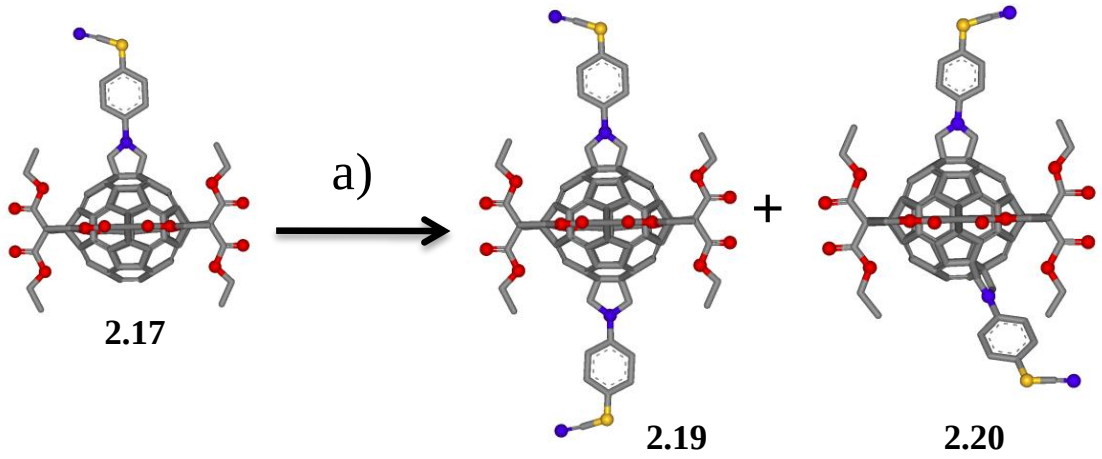

Scheme 2.4 Synthesis of [*N*-(4-thiocyanatophenyl)pyrrolidino]fullerene derivatives **2.19** and **2.20**. a) = PhSCN-glycine, HCHO, *o*-DCB, Ar, 175 °C, 10 min.[11]

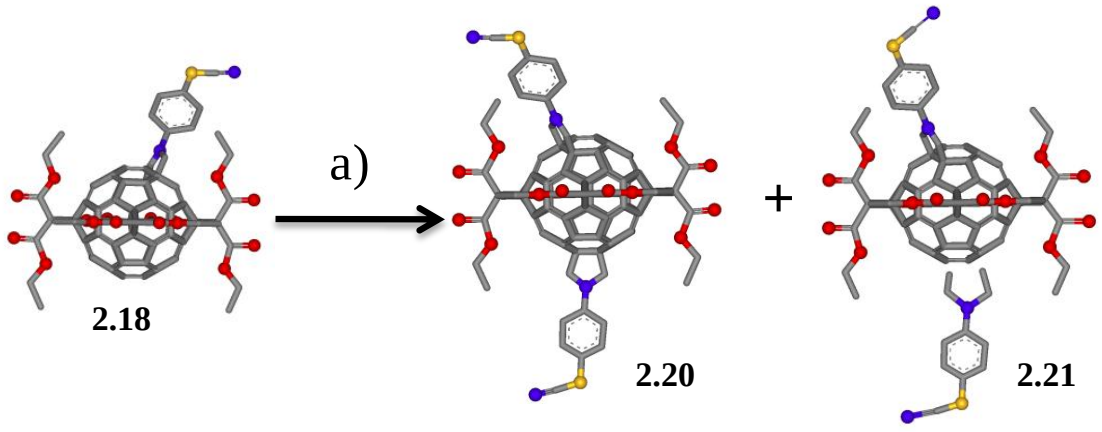

Scheme 2.5 Synthesis of [*N*-(4-thiocyanatophenyl)pyrrolidino]fullerene derivatives **2.19** and **2.20**. a) = PhSCN-glycine, HCHO, *o*-DCB, Ar, 175 °C, 15 min.[11]

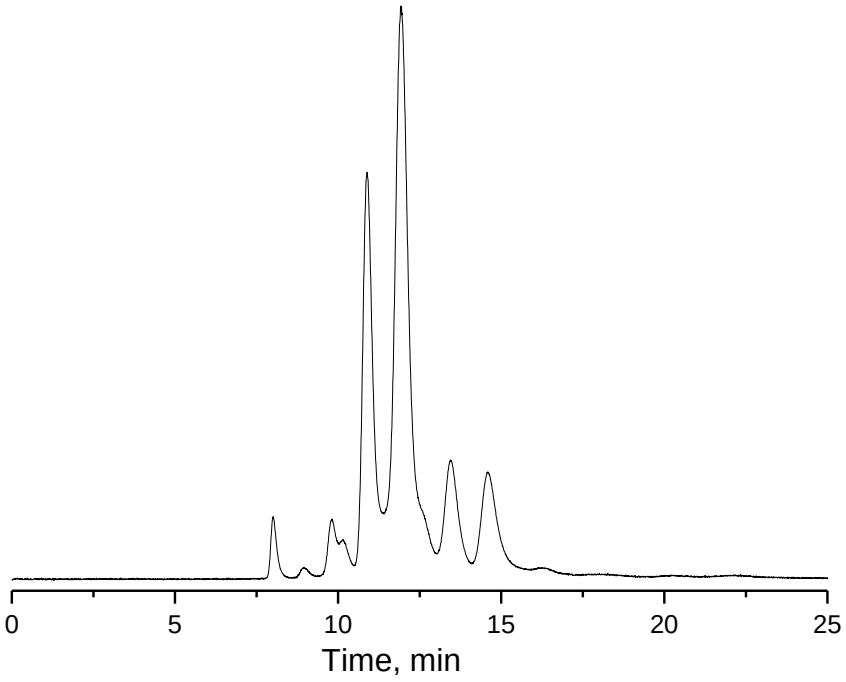

Figure 2.7. HLPC spectrum of compound **2.21**, toluene as eluent and Buckyprep column.

Up to this point we had been able to add one and two addends to compound **2.16**, where the *hexakis*-adducts **2.19** and **2.20** are the precursors for **2.12** and **2.13** (Figure 2.1). The next step was to pursue the synthesis of compounds **2.14** and **2.15** using compound **2.20** as the starting material. According to the previous results, the addition of a new group should not occur on the same six-membered ring that already has a group attached. This leads to the possibility of just the two regioisomers indicated in the Figure 2.8.

Two *heptakis*-adducts were purified by preparative TLC with DCM as eluant after 30 min of reaction of compound **2.20** with PhSCN-glycine and paraformaldehyde (Scheme 2.6). Figure 2.9A shows the ^{1}H NMR spectrum of *heptakis*-**1,** two doublets are observed in the aromatic region which integrated for two protons each, and two "triplets"

corresponding to four protons each (which were two overlapped doublets) for a total of six different aromatic protons. The ^{1}H NMR spectrum of *heptakis*-**2** shows similar chemical shifts and multiplicities to those of *heptakis*-**1** (Figure 2.9B), which makes their assignment really challenging. Hence, in an attempt to determine which *heptakis*-adducts (**2.22** or **2.23**, Scheme 2.6) are the *heptakis*-**1** and **-2,** HMBC (heteronuclear multiple bond correlation) experiments were performed.

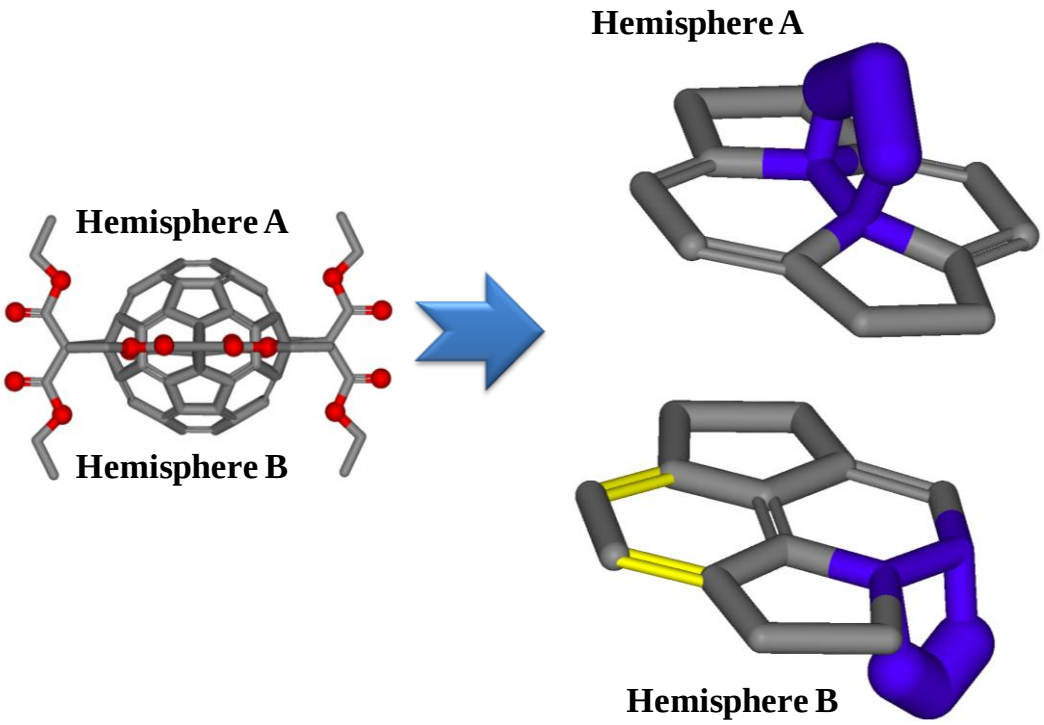

Figure 2.8. Schematic representation of two possible isomers for a third addition to compound **2.20**. Yellow bonds represent possible addition sites and blue rings represent adduct positions.

We were expecting differences between the *heptakis*-**1** and **-2** in the correlations between the pyrrolidine protons, the sp^2-hybridized carbon of the pyrrolidine ring and the sp^3 carbon atom of the fullerene. However, the two isomers did not show significant correlation differences. Although the identity of the two regioisomers cannot be established at this point, if the polarity of the molecules is considered, **2.22** should be less polar than **2.23**, since the third addend is opposite to the addends on **2.20** (Figure 9). Therefore, *heptakis*-**1** was tentatively assigned to **2.22** and *heptakis*-**2** to **2.23**.[11]

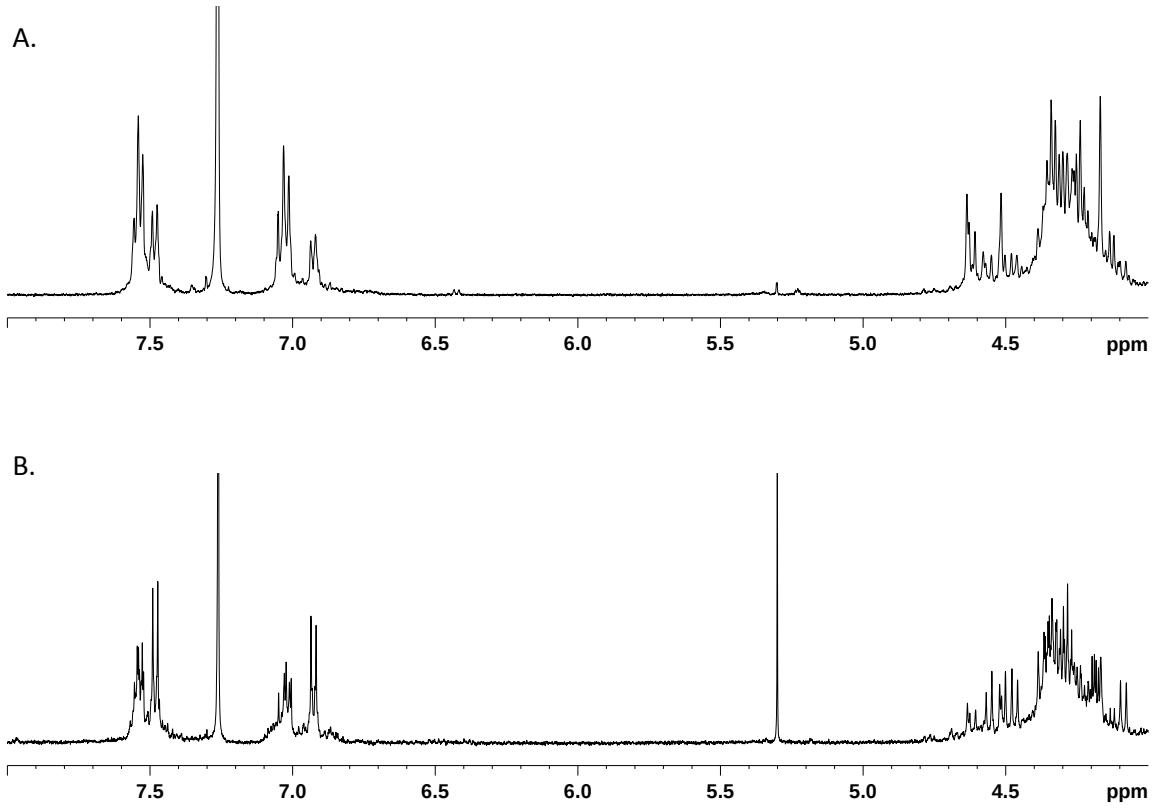

Figure 2.9. ^{1}H NMR spectrum of (A) compound *heptakis*-**1** and (B) compound *heptakis*-**2** (500 MHz, $CDCl_3$).[11]

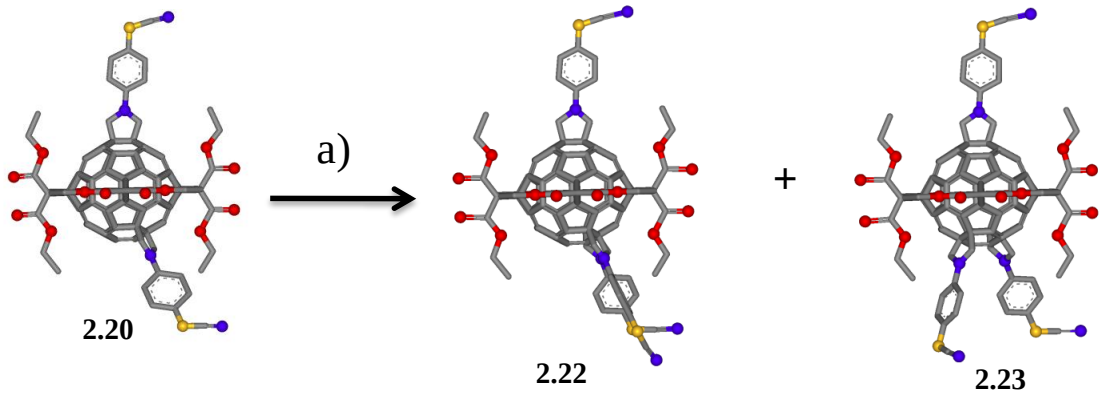

Scheme 2.6. Synthesis of *heptakis*-adducts **2.22** and **2.23**. a) = PhSCN-glycine, HCHO, *o*-DCB, Ar, 175 °C, 30 min.[11]

The principal conclusions of this study were: 1) A reactivity trend of **2.20**> **2.18**> **2.17**>>> **2.19**, with **2.20** being the most reactive; 2) The addition of a new group seems to be disfavored on the same six-membered ring that already has a group attached; and 3) The maximum number of groups that could be added to **2.16** was four (two groups per hemisphere).

Regioselective addition of two different pyrrolidine addends to C_{60}

With this examination of the regiochemistry of additions to **2.16**, and in order to pursue the plan of using these fullerene compounds in potential applications such as in molecular electronics, the next step was to synthesize compounds with different functionalities to create a library. Any reaction between **2.16** and a glycine forms two isomers: symmetrical and unsymmetrical isomers (Figure 2.2), thus *pentakis*-adducts **2.24**[4] and **2.25**[15] were synthesized (Figure 2.10). These *pentakis*-adducts **2.17**, **2.24** and **2.25** were used as precursors of *hexakis*-adducts (Figure 2.11) with different Pyrr

addends. Before beginning this discussion it is important to mention that the addition of the Tpy-Pyrr adducts occurred on the symmetric and unsymmetric double bonds (Figure 2.2) as well. This behavior was not observed previously[4] due to the small amount of material used at that time. A mixture of 1 mol of **2.16**, 20 mols of paraformaldehyde and 5 mols of Tpy-glycine was refluxed in 1,2-dichlorobenzene (*o*-DCB) under argon for 6 h. The reaction crude was filtered to remove the unreacted Tpy-glycine and purified by column chromatography on silica gel using 1–2% v/v MeOH/DCM as eluant. The fractions obtained corresponded: unsymmetrical *pentakis*-adduct, symmetrical *pentakis*-adduct **2.24** and *hexakis*-adducts including **2.30**, in that elution order.

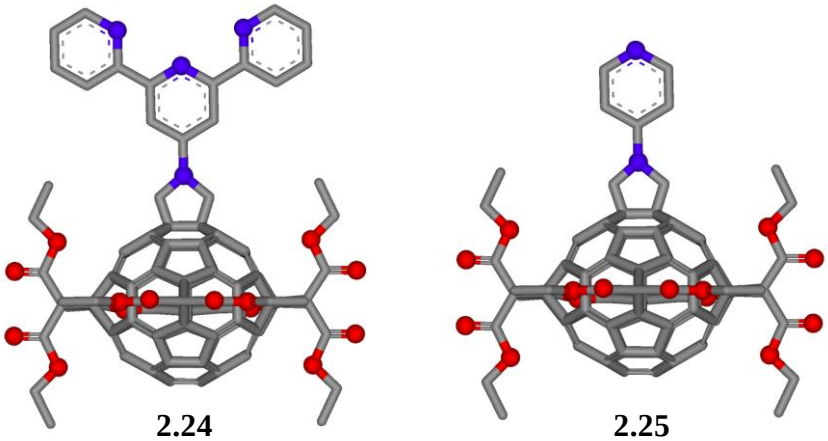

2.24 **2.25**

Figure 2.10. Structure of compounds **2.24** and **2.25**.

Figure 2.11 displays the library of C_{60} derivatives achieved by our approach. The reactivity difference of each glycine produced different yields and reaction times. All The reactions were carried out at reflux under an atmosphere of argon and *o*-DCB as solvent:

- *Hexakis*-adducts **2.26** (8%) and **2.34** (35%) were obtained from the reaction between 0.023 mmol of **2.17**, 0.23 mmol paraformaldehyde and 0.046 mmol Py-glycine after 13 hours.

- *Hexakis*-adducts **2.29** (16%) and **2.33** (10%) were prepared by the reaction between 0.020 mmol of **2.17**, 0.2 mmol paraformaldehyde and 0.040 mmol TPy-glycine after 4 hours.

- *Hexakis*-adducts **2.27** (26%) and **2.32** (21%) were obtained after 3 hours of reaction between 0.062 mmol of **2.24**, 2.48 mmol paraformaldehyde and 1.24 mmol Py-glycine.

- *Hexakis*-adducts **2.28** (8%) and **2.33** (4%) were obtained after 4 hours of reaction of 0.18 mmol of **2.24**, 1.8 mmol paraformaldehyde and 0.9 mmol PhSCN-glycine at 175 °C.

Table 2.1 summarizes the different combinations of *hexakis*-adducts of fullerenes synthesized under this strategy and their respectively yields. The reactivity trend of the glycines was as follows: PhSCN-glycine > Tpy-glycine > Py-glycine, PhSCN-glycine being the most reactive. The corresponding trend of the yields was: Tpy-glycine > Py-glycine > PhSCN-glycine, Tpy-glycine being the glycine that produces the highest yields. Also, the *pentakis*-adduct **2.24** is more reactive than the *pentakis*-adduct **2.17**.

At this point we had achieved the synthesis of *hexakis*-adducts with two different or equal Pyrr addends (Figure 2.11), these C_{60} fullerene derivatives can be the precursors of the *trans-1* **2.12** and *trans-2* **2.13** compounds (Figure 2.1) which are some of the candidates for molecular electronics applications.

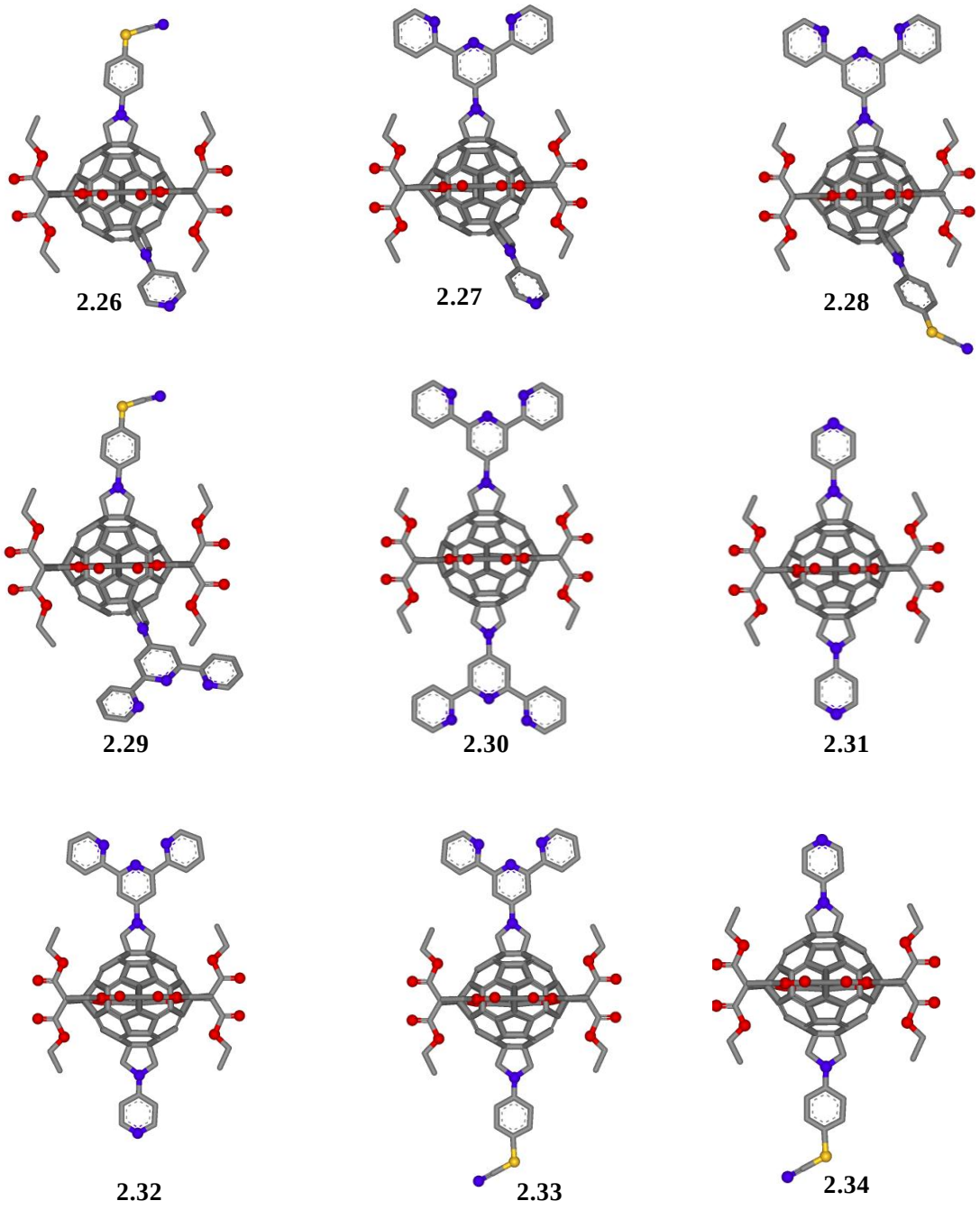

Figure 2.11. Library of C_{60} derivatives.

Table 2.1. Percentage yield of the 1,3-dipolar reaction between **2.16**, **2.17**, **2.24** and PhSCN-, Tpy-, Py-glycines

C_{60} derivatives	**Glycines**		
	PhSCN	**Tpy**	**Py**
2.16	2.17 (6.2%) 2.18 (6.3%)	2.24 (35%) Unsym (22%)	2.25 (29%) Unsym (21%)
2.17	2.19 (2.2%) 2.20 (4.6%)	2.29 (16%) 2.33 (10%)	2.26 (8%) 2.34 (35%)
2.24	2.28 (8%) 2.33 (4%)	2.30(40%) *Trans-2*-p (20%)	2.27 (26%) 2.32 (21%)

Regioselective addition of three different pyrrolidine addends to C_{60}

The information acquired up to this point allowed us to pursue the synthesis of **2.14** and **2.15**. One special feature of these compounds is the possibility to self-assemble on different metal surfaces. One of the main problems in molecular electronics is that the molecules must be arranged between the electrodes with precise location and orientation control, which can be overcome via directed self-assembly.[16] The synthesis of *heptakis*-adducts such as **2.22** and **2.23** (Scheme 2.6) with the same or different addends are the perfect precursors of *tris*-adducts **2.14** and **2.15**. We discussed in the previous sections that the addition of a Pyrr addend to **2.20** will generate only two isomers, **2.22** and **2.23** (Scheme 2.6), because two addends cannot be bonded on the same six membered ring. Also, we reported a library of *hexakis*-adducts with different or equal Pyrr addends (Figure 2.11) that can be used the same way as **2.20** to synthesize different

heptakis-adducts. For instance, 0.0151 mmol of the *hexakis*-adduct **2.35** reacted with 0.302 mmol of Py-glycine and 0.91 mmol of paraformaldehyde during 9 hours at reflux in *o*-DCB to produce the *heptakis*-adducts **2.36** and **2.37** (Scheme 2.7). The assignment of the structures for compounds **2.36** and **2.37** was based on their polarity, the same as proposed to assign compounds **2.22** and **2.23**. Figure 2.12 shows the ^{1}H NMR spectrum of compounds **2.36** and **2.37**. Broad signals are observed for the methylenes of the Pyrr rings and malonate groups between δ = 4.74 – 4.12. The aromatic region displays two sets of dd at δ = 8.39 – 8.34 and 6.82 – 6.73 for **2.36** and broad signals at δ = 8.39 and 6.84 for **2.37**.

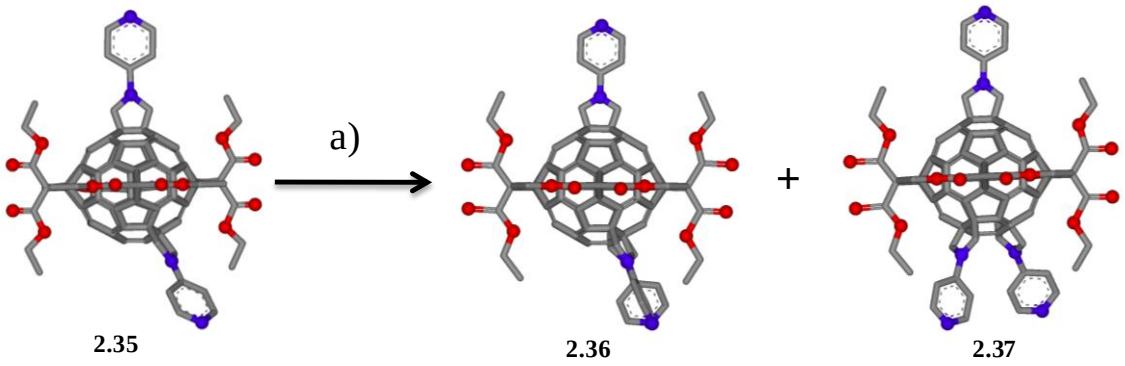

Scheme 2.7. Synthesis of compounds **2.36** and **2.37**. a) Py-glycine, paraformaldehyde, *o*-DCB, reflux, Ar, 9 h.

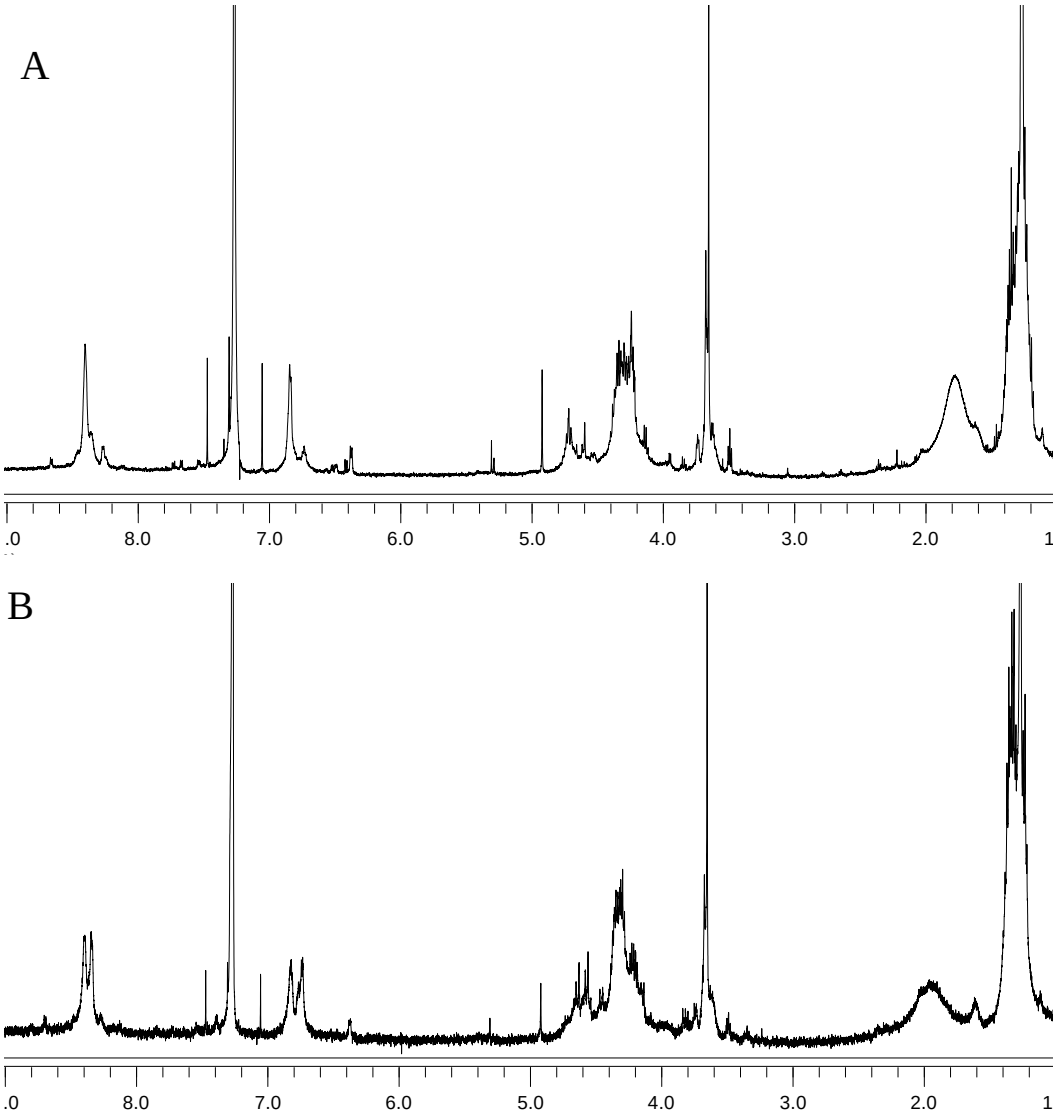

Figure 2.12 ^{1}H NMR spectrum of: a) **2.36** and b) **2.37**. (500 MHz, $CDCl_3$).

Heptakis-adducts **2.38** and **2.39** were synthesized from *hexakis*-adducts **2.27** and **2.28**, respectively. Compound **2.27** (0.0017mmol) reacted with PhSCN-glycine (0.0034 mmol) and paraformaldehyde (0.017 mmol) during 24 hours at reflux in 1 mL of *o*-DCB. After the reaction was cooled, the solvent was dryed with a N_2 stream to form a red paste,

and then it was purified using a preparative reverse TLC phase (C18) and DCM:methanol 96:4 as mobile phase.

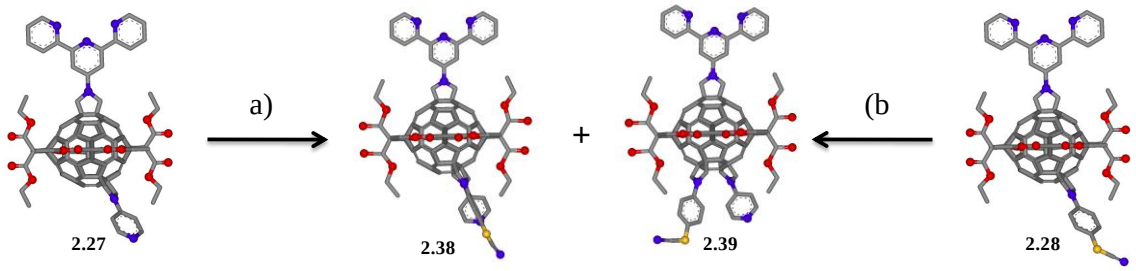

Scheme 2.8. Synthesis of compounds **2.38** and **2.39**. a) PhSCN-glycine, paraformaldehyde, *o*-DCB, reflux, Ar, 24 h; b) Py-glycine, paraformaldehyde, *o*-DCB, reflux, Ar, 13 h.

Compound **2.28** (0.006mmol) was reacted with Py-glycine (0.024 mmol) and paraformaldehyde (0.12 mmol) during 13 hours at reflux conditions in 1 mL of *o*-DCB. The crude reaction was purified using a preparative reverse phase TLC (C18) and DCM:methanol 96:4 as mobile phase. The isolation of **2.38** and **2.39** by prep-TLC was easier because the starting material (**2.28**) is less polar than **2.27**. Yields were not calculated due to the small amounts obtained (Scheme 2.8).

We were able to synthesize *heptakis*-adducts with the same type of Pyrr addends, [SCN-Ph-Pyrr (**2.22** and **2.23**) and Py-Pyrr (**2.36** and **2.37**)] and three different Pyrr addends [Tpy-Pyrr, PhSCN-Pyrr and Py-Pyrr (**2.38** and **2.39**)].

Synthesis of *N*-(4-Thiocyanatophenyl)pyrrolidino-$Sc_3N@C_{80}$

The high reactivity of the PhSCN-glycine with C_{60} and the easier purification and characterization of their derivatives encouraged us to try to add this group to the endohedral fullerene $Sc_3N@C_{80}$. Endohedral metallofullerenes (EMFs) are fullerenes hosting metals, metal clusters, or small molecules inside.[17] For example, the Sc_3N cluster is encapsulated in a cage of 80 carbon atoms and the cage exhibits two possible symmetries, I_h and D_{5h}.[17] Organic functionalization of endohedral fullerenes is necessary to build novel organo-fullerene materials for a variety of future applications such as high-relaxivity contrast agents for magnetic resonance imaging,[18] molecular electronics and electron donor/acceptor systems.[19] Their reactivity and regioselectivity are influenced by the encapsulated cluster, metal species, carbon cage size, and symmetry.[13] Therefore the amount of functionalized EMFs reported is lower when compared to results with C_{60}.

A mixture of I_h- and D_{5h}- $Sc_3N@C_{80}$ (2 mg, 0.0018 mmol) was heated up at reflux in ODCB (5 mL) with PhSCN-glycine (7.5 mg, 0.0036 mmol) and paraformaldehyde (3.15 mg, 0.104 mmol) (Scheme 2.9) and after 30 min a product was identified by TLC. The crude was purified by column chromatography on silica gel. The starting material was removed by first using CS_2 as eluant, and then three fractions were obtained with a solution of CS_2:toluene (ratio was increased progressively) as eluant. *Mono*-, *bis*- and *tris*-addition products were found in fractions one, two and three by means of MALDI-TOF, respectively.

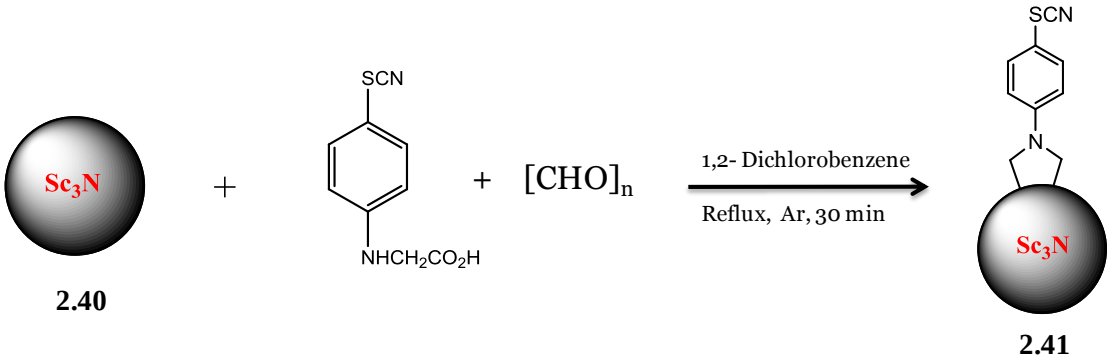

2.40 **2.41**

Scheme 2.9. Synthesis of compound **2.41.**

Figure 2.13 shows the MALDI-TOF spectrum of the *mono*-(I_h- and D_{5h}-)-PhSCN-pyrrolidine-$Sc_3N@C_{80}$ adducts **2.41**, where the peaks *m/z* = 1286 and 1109 correspond to the mono adduct and to $Sc_3N@C_{80}$, respectively. Full characterization of these mono-adducts was not pursued due to the small amount of material obtained.

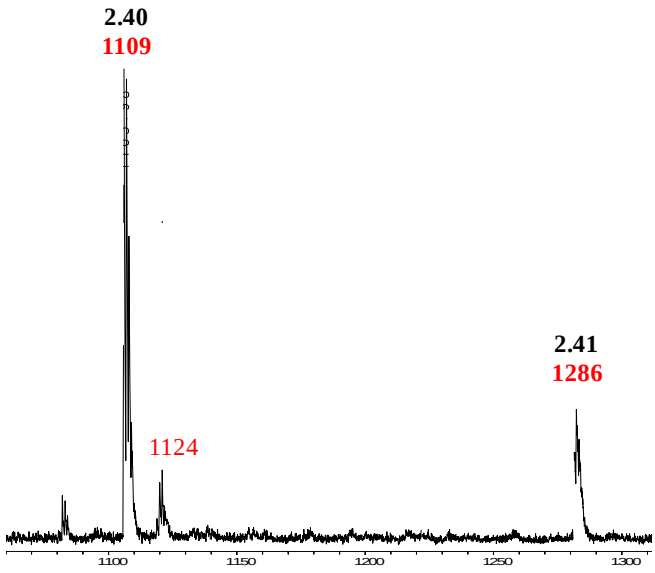

Figure 2.13 MALDI-TOF spectrum of compound **2.40**.

Conclusions

Herein we described the regioselective synthesis and characterization of *hexakis*- and *heptakis*-C_{60} adducts that are potentially useful candidates for molecular electronic applications. The synthesis was achieved by using a selective protection/deprotection strategy shown in Figure 2.14. It begins with the synthesis of the starting template, C_{60}-tetramalonate **2.16**, followed by the reaction with a glycine [Tpy-, Py-, or PhSCN-] and aldehyde to form the Pyrr ring by 1,3-dipolar cycloaddition reactions (Figure 2.14, step a). In this step, two regioisomers are obtained, one symmetrical and one unsymmetrical. Each regioisomer can react with the same glycine or a second one to form different *hexakis*-adduct regioisomers (Figure 2.14, steps b-d). After full characterization and purification a third glycine can be introduced in the system to obtain *heptakis*-adducts (Figure 2.14, step e).

The 1,3-cyclopropanation reaction reactivity trend observed was: *trans-2* precursor *hexakis*-adduct > unsymmetric-*pentakis*-adduct> symmetric-*pentakis*-adduct>>> two *heptakis*-adduct ≈ *trans-1* precursor *hexakis*-adduct, with the *trans-2* precursor *hexakis*-adduct being the most reactive.

The addition of a new group seems to be disfavored on the same six-membered ring that already has a group attached, and the maximum number of groups that could be added to **2.16** was four.

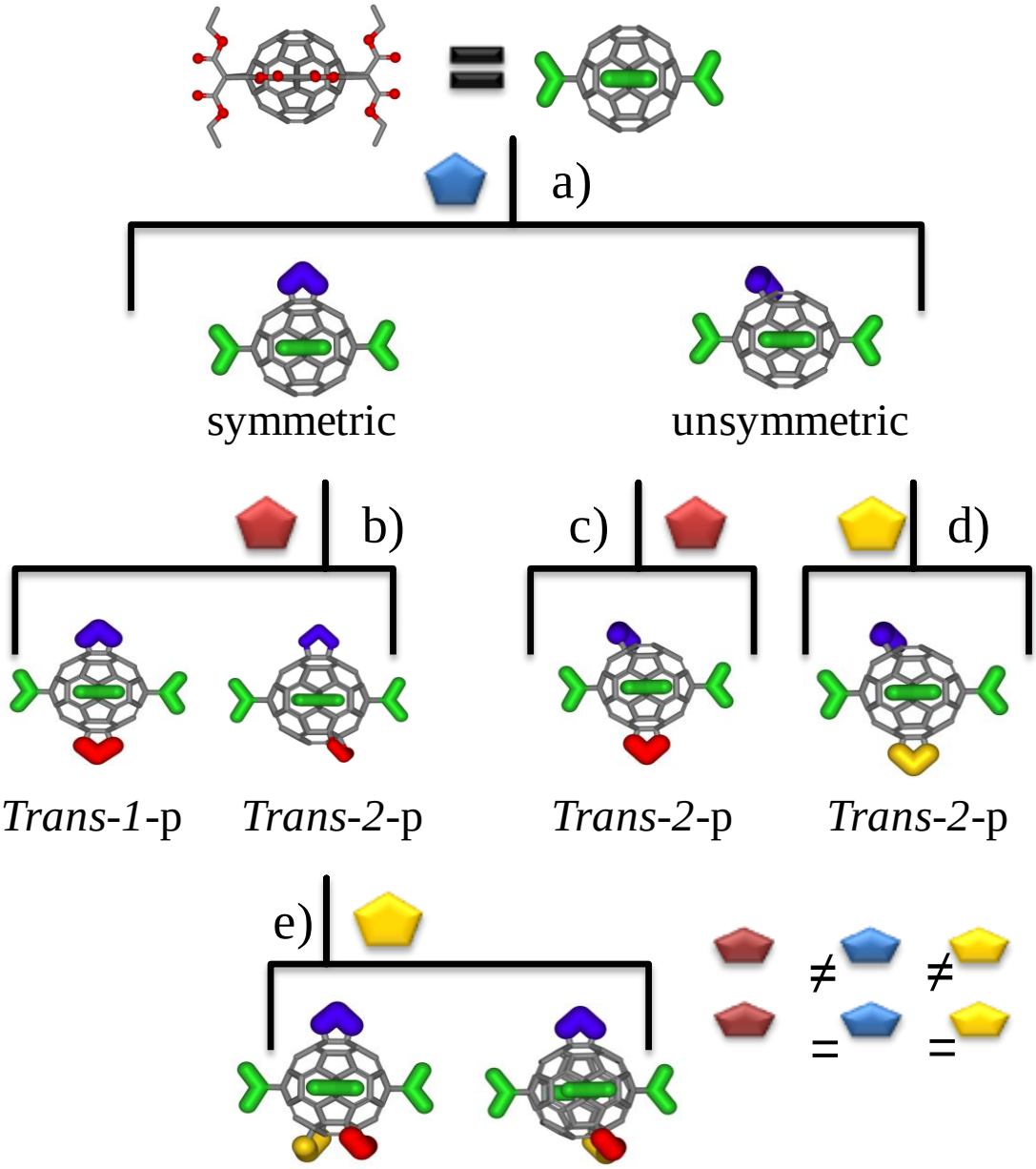

Figure 2.14. Schematic representation of the synthesis of *hexakis*- and *heptakis*-adducts of C_{60}.

Experimental Section

General: Reagents were purchased from commercial suppliers and used without further purification. Compounds **2.16**,[10] terpyridyl glycine[4] and pyridylglycine[5] were synthesized as described in the literature procedures. NMR spectra were recorded on a Bruker AC 500 MHz spectrometer. Mass spectroscopy was recorded with an Omni Flex MALDI-TOF spectrometer. HPLC was performed using a COSMOSIL® Buckyprep-M Packed Column, 10.0mm I.D.×250mm.

Synthesis of phenylthiocyanate glycine: A mixture 4-aminophenyl thiocyanate[20] (3.0 g, 19.97 mmol) and ethylbromoacetate (1.10 mL, 9.99 mmol) in anhydrous 1,4-dioxane (6 mL) was heated to reflux for 1 hour. After the solution cooled, 10 mL water was added and the mixture was extracted with chloroform. The organic layer was removed and washed twice with saturated $NaHCO_3$, then with brine, dried with $MgSO_4$, then concentrated. The resulting product was purified by column chromatography on silica gel, chloroform:acetone 9:1 as eluant, to give ethyl N-(4-thiocyano)phenylglycinate (4.0 g, 60%). ^{1}H NMR (500 MHz, $CDCl_3$, 25 °C): δ = 7.41 (m, 2H, ArH), 6.60 (m, 2H, ArH), 4.64 (b, 1H, NH), 4.26 (q, $^3J_{H,H}$ = 7.1 Hz, 2H, -$COCH_2$-), 3.90 (d, 2H, -CH_2CO-), 1.32 (t, $^3J_{H,H}$ = 7.1 Hz, 3H, -CH_3). ^{13}C NMR (500 MHz, $CDCl_3$, 25 °C): δ = 170.30 (C=O), 148.81, 134.58, 114.05, 112.28, 109.21, 61.69, 45.19, 14.19. MALDI-MS: *m*/*z* 237 (MH^+).

Ethyl N-(4-thiocyano)phenylglycinate (2.5 g, 10.6 mmol) was dissolved in 11 mL of 5M HCl/dioxane[21] and heated to reflux for 15 min under Ar. After the solution was cooled, the phenylthiocyanate glycine precipitated, was filtered and washed with dioxane

to give a white solid. (2.8 g, 76%) ^{1}H NMR (500 MHz, DMSO, 25 °C): of N-(4-thiocyano)phenylglycine: δ = 12.65 (b, 1H, CO_2H), 7.39 (m, 2H, ArH), 6.66 (m, 2H, ArH), 3.86 (s, 2H, -CH_2-), 3.50 (b, 1H, NH). ^{13}C NMR (DMSO, 500 MHz): δ 172.5 (C=O), 151.0, 135.1, 114.0, 113.0, 106.3, 44.55. MALDI-MS: *m*/*z* 209 (MH^+).

***Pentakis*-adducts 2.17, 2.18 and *Hexakis*-adducts 2.19 and 2.20:** The mixture of **2.16** (1 g, 0.74 mmol), *N*-(4-thiocyano)phenylglycine (385 mg, 1.85 mmol), and paraformaldehyde (111 mg, 3.7 mmol) in 1,2-dichlorobenzene (300 mL) was heated to 175 ℃ under Ar for 30 min. The crude reaction was cooled and evaporated with N_2. Separation of the **2.16** (200 mg, material recovered), **2.17** (71 mg, 6.3 %), **2.18** (70 mg, 6.2%), **2.19** (24.4 mg, 2.2%), and **2.20** (51.9 mg, 4.6%) was achieved by column chromatography on silica gel respectively, using dichloromethane as eluant. Better purification of **2.19** and **2.20** was achieved via preparative TLC on silica gel using dichloromethane as eluant.

2.17: ^{1}H NMR (500 MHz, $CDCl_3$, 25 °C): δ = 7.50 (d, $^{3}J_{H,H}$ = 8.9 Hz, 2H, ArH), 6.93 (d, $^{3}J_{H,H}$ = 8.9 Hz, 2H, ArH), 4.45-4.41 (q, 4H, -CH_2-), 4.36-4.31 (m, 16H, -CH_2-), 1.40-1.30 (m, 24H, -CH_3). ^{13}C NMR (500 MHz, $CDCl_3$, 25 °C): δ = 163.83, 163.73, 163.64, 153.64, 152.36, 149.41, 147.17, 146.14, 145.98, 145.47, 145.30, 144.26, 143.41, 143.15, 142.29, 138.58, 138.20, 133.83, 117.01, 111.80, 69.85, 69.11, 68.22, 67.75, 62.98, 62.94, 61.40, 45.39, 44.88, 14.17, 14.09 and 14.06. UV-vis: λ_{max} (nm) 291, 309, 339, 476, 545. MS (MALDI): *m/z*: 1527 [M^+ - 1], 1369, 1352.

2.18: ^{1}H NMR (500 MHz, $CDCl_3$, 25 °C): δ = 7.53 (d, $^{3}J_{H,H}$ = 8.9 Hz, 2H, ArH), 7.02 (d, $^{3}J_{H,H}$ = 8.9 Hz, 2H, ArH), 4.71-4.27 (m, 20H, -CH_2-), 1.52-1.31 (8t, 24H, -CH_3).

^{13}C NMR (500 MHz, $CDCl_3$, 25 °C): δ = 164.21, 164.11, 163.86, 163.70, 163.65, 163.15, 150.88, 149.45, 149.28, 149.00, 148.66, 148.34, 147.74, 147.44, 147.07, 147.02, 146.95, 146.08, 145.78, 145.47, 145.13, 144.42, 144.30, 144.23, 144.15, 143.78, 143.47, 143.32, 143.27, 142.99, 142.82, 142.74, 142.52, 142.34, 142.11, 141.95, 141.90, 141.74, 141.61, 141.30, 141.11, 140.99, 140.87, 140.79, 140.45, 140.33, 140.25, 140.07, 138.69, 138.64, 138.34, 138.19, 135.18, 133.89, 131.81, 130.60, 125.81, 116.98, 111.86, 111.51, 72.22, 70.77, 70.50, 69.17, 69.05, 68.71, 66.34, 66.07, 65.08, 63.27, 63.13, 63.05, 63.03, 62.98, 62.78, 62.65, 62.39, 62.00, 46.33, 43.94, 43.31, 41.37, 14.29, 14.25, 14.20, 14.18, 14.11, 14.09 and 14.08. UV-vis: λ_{max} (nm) 271, 330, 548. MS (MALDI): *m/z*: 1528 [M^+], 1369, 1352.

***Hexakis*-adducts 2.19 and 2.20:** A solution of **2.17** (20 mg, 0.013 mmol), N-(4-thiocyano)phenylglycine (14 mg, 0.065 mmol), and paraformaldehyde (4 mg, 0.130 mmol) in 1,2-dichlorobenzene (2 mL) was heated at 175 ℃ under Ar for 15 min. The reaction was cooled and evaporated. Separation of **2.17** (6 mg, material recovered), **2.19** (2 mg, 9%) and **2.20** (5 mg, 22%) was achieved by preparative TLC on silica gel, using dichloromethane as eluant.

2.19: ^{1}H NMR (500 MHz, $CDCl_3$, 25 °C): δ = 7.54 (d, $^3J_{H,H}$ = 9.0 Hz, 4H, ArH), 7.04 (d, $^3J_{H,H}$ = 9.0 Hz, 4H, ArH), 4.59 (s, 8H, NCH_2-), 4.35-4.30 (q, $^3J_{H,H}$ = 7.1 Hz, 8H, -CH_2-), 4.30-4.26 (q, $^3J_{H,H}$ = 7.1 Hz, 8H, -CH_2-), 1.35-1.32 (t, $^3J_{H,H}$ = 7.1 Hz, 12H, -CH_3), 1.28-1.25 (t, $^3J_{H,H}$ = 7.1 Hz, 12H, -CH_3). ^{13}C NMR (500 MHz, $CDCl_3$, 25 °C): δ = 163.87, 163.83, 152.34, 149.45, 146.11, 145.79, 145.53, 145.40, 143.88, 143.66, 143.47, 141.62, 141.13, 140.99, 140.33, 139.72, 133.89, 117.19, 111.82, 70.83, 69.38, 69.08, 66.87,

66.11, 62.85, 61.99, 61.12, 46.11, 45.44, 45.38, 44.71, 14.27, 14.06. UV-vis: λ_{max} (nm) 275, 332, 546. MS (MALDI): *m/z*: 1704 [M^+], 1669, 1596, 1511, 1352.

2.20: ^{1}H NMR (500 MHz, $CDCl_3$, 25 °C): δ = 7.55 (d, $^3J_{H,H}$ = 9.0 Hz, 2H, ArH), 7.52 (d, $^3J_{H,H}$ = 9.0 Hz, 2H, ArH), 7.06 (d, $^3J_{H,H}$ = 8.8 Hz, 2H, ArH), 6.98 (d, $^3J_{H,H}$ = 8.9 Hz, 2H, ArH), 4.64-4.51 (m, 4H, -CH_2-), 4.47-4.21 (m, 20H, -CH_2-), 1.34-1.26 (m, 24H, -CH_3). ^{13}C NMR (500 MHz, $CDCl_3$, 25 °C): δ = 164.00, 163.95, 163.86, 163.83, 163.50, 163.20, 163.03, 153.84, 153.17, 152.06, 151.60, 151.13, 149.45, 149.32, 148.66, 147.80, 146.92, 146.66, 146.61, 146.51, 146.42, 146.29, 146.21, 145.99, 145.90, 145.79, 145.71, 145.51, 145.33, 145.25, 144.37, 144.12, 143.50, 143.18, 143.00, 142.48, 142.39, 142.34, 142.25, 142.04, 141.85, 141.43, 141.32, 140.94, 140.68, 139.71, 138.82, 138.53, 136.75, 136.68, 136.59, 136.18, 136.12, 133.93, 133.88, 130.27, 125.23, 117.09, 117.02, 111.89, 111.75, 111.52, 70.55, 70.37, 70.20, 69.15, 68.89, 67.86, 67.74, 67.56, 67.37, 66.99, 64.84, 63.76, 62.98, 62.92, 62.89, 62.84, 62.80, 62.75, 62.56, 62.52, 61.85, 61.57, 61.50, 61.34, 45.55, 43.77, 43.46, 42.03, 14.14, 14.09, 14.06, 14.04. UV-vis: λ_{max} (nm) 286, 482, 525. MS (MALDI): *m/z*: 1706 [M^+ + 2], 1671, 1553 [M^+ - PhSCN group], 1354 [M^+ - 2PhSCN group].

***Heptakis*-adducts 2.22 and 2.23:** A solution of **2.20** (11 mg, 0.064 mmol), *N*-(4-thiocyano)phenylglycine (19 mg, 0.093 mmol), and paraformaldehyde (6 mg, 0.190 mmol) in 1,2-dichlorobenzene (1 mL) was heated at 175 ℃ under Ar for 30 min. The reaction was cooled and evaporated. Separation of **2.20** (4.7 mg, material recovered), **2.22** (2.2 mg, 18%) and **2.23** (1.7 mg, 14%) was achieved by preparative TLC on silica gel, using dichloromethane as eluant.

2.22: ^{1}H NMR (500 MHz, $CDCl_3$, 25 °C): δ = 7.55 (m, 4H, ArH), 7.48 (d, $^{3}J_{H,H}$ = 8.1 Hz, 2H, ArH), 7.05 (m, 4H, ArH), 6.93 (d, $^{3}J_{H,H}$ = 8.1 Hz, 2H, ArH), 4.65-4.10 (m, 28H, -CH_2-), 1.42-1.05 (m, 24H, -CH_3). UV-vis: λ_{max} (nm) 274, 520. MS (MALDI): *m/z*: 1881 [M^++1], 1723, 1705 [M^+ - PhSCN group], 1547, 1529 [M^+ - 2PhSCN group], 1371.

2.23: ^{1}H NMR (500 MHz, $CDCl_3$, 25 °C): δ = 7.54 (m, 4H, ArH), 7.48 (d, $^{3}J_{H,H}$ = 8.8 Hz, 2H, ArH), 7.03 (m, 4H, ArH), 6.93 (d, $^{3}J_{H,H}$ = 8.8 Hz, 2H, ArH), 4.64-4.10 (m, 28H, -CH_2-), 1.37-1.15 (m, 24H, -CH_3). UV-vis: λ_{max} (nm) 287, 497, 529. MS (MALDI): *m/z*: 1880 [M^+], 1722, 1704 [M^+ - PhSCN group], 1546, 1529 [M^+ - 2PhSCN group], 1367.

Mono-Terpyridylpyrrolidine-C_{60}-tetra(diethyl)malonate symmetric 2.24 and unsymmetric adducts: A mixture of **2.16** (1 g, 0.74 mmol), paraformaldehyde (222.0 mg, 7.4 mmol), and terpyridyl glycine (620 mg, 2.0 mmol) was heated to reflux in 1,2-dichlorobenzene (120 mL) under argon for 6 h. The crude product was filtered to remove the unreacted tpy-glycine, and purified by column chromatography (silica gel). 1–2% MeOH/CH_2Cl_2 eluted adducts **2.16** (300 mg recovered), unsymmetrical isomer (220 mg, 22%) and **2.24** (340 mg, 35%) as a pink-brown solid and orange solid, respectively.

Unsymmetric mono-Terpyridylpyrrolidine-C_{60}-tetra(diethyl)malonate isomer: ^{1}H NMR (500 MHz, $CDCl_3$) δ: 8.75-8.65 (m, 4H), 8.09 (s, 1H), 8.02 (s, 1H), 7.85 (m, 2H), 7.36 (m, 2H), 4.68-4.32 (b m, 20H), 1.51-1.29 (m, 24H). UV-vis: λ_{max} (nm) 235, 281, 473, 545. MALDI-TOF MS: 1626 [M^+ + 1], 1554, 1483.

2.24: ^{1}H NMR (500 MHz, $CDCl_3$) δ: 8.71 (b, 2H), 8.66 (b, 2H), 8.00 (s, 2H), 7.89 (b, 2H), 7.35 (b, 2H), 4.70-4.58 (2b, 4H), 4.46-4.27 (3q, 20H), 1.42-1.25 (8t, 24H). ^{13}C

NMR (500 MHz, $CDCl_3$) δ: 163.82, 163.57, 152.28, 148.86, 147.16, 146.21, 145.96, 145.44, 145.33, 144.25, 143.48, 143.09, 142.28, 138.67, 138.18, 121.50, 106.95, 70.58, 69.86, 69.15, 68.16, 67.78, 62.99, 62.92, 60.12, 45.39, 14.17, 14.08 and 14.06. UV-vis: λ_{max} (nm) 220, 237, 281, 477, 544. MALDI-TOF MS: 1626 [M^+ + 1], 1554, 1483.

Mono-pyridylpyrrolidine-C_{60}-tetra(diethyl)malonate symmetrical 2.25 and unsymmetrical isomers: A mixture of **2.16** (1.6 g, 1.2 mmol), (4-pyridyl)glycine (2.7g, 18 mmol), and paraformaldehyde (1.8g, 6.0 mmol) in 1,2-dichlorobenzene (400 mL) was heated to reflux under Ar for 3 hours. The resulting mixture was cooled and the solvent evaporated. The crude reaction product was purified by column chromatography (silica gel) using 1% MeOH in CH_2Cl_2 as eluant. After unreacted C_{60}-tetramalonate (1.0 g recovered) was isolated the polarity was increased to 3% MeOH, which eluted **unsymmetrical** adducts (140 mg, 21%) and **2.25** (190 mg, 29%).

Unsymmetric mono-pyridylpyrrolidine-C_{60}-tetra(diethyl)malonate isomer: ^{1}H NMR (500 MHz, $CDCl_3$) δ: 8.38 (d, 2H), 6.82 (d, 2H), 4.77-4.32 (m, 20H), 1.52-1.31 (m, 24H). ^{13}C NMR (500 MHz, $CDCl_3$) δ: 164.18, 164.10, 163.85, 163.84, 163.67, 163.64, 163.14, 152.48, 150.67, 150.24, 149.46, 149.03, 148.68, 148.38, 147.73, 147.45, 147.04, 146.96, 146.07, 145.65, 145.47, 147.17, 144.43, 144.30, 144.28, 144.24, 144.10, 143.79, 143.60, 143.48, 143.31, 143.27, 143.02, 142.82, 142.74, 142.41, 142.38, 142.14, 141.95, 141.89, 141.74, 141.57, 141.26, 141.14, 141.02, 140.88, 140.81, 140,45, 140.37, 140.26, 140.08, 138.66, 138.52, 138.31, 138.18, 131.75, 130.50, 135.13, 125.74, 109.90, 72.23, 70.78, 70.51, 69.18, 69.06, 68.66, 66.33, 66.05, 64.91, 63.28, 63.14, 63.07, 62.99, 62.80, 62.22, 61.26, 60.61, 46.35, 43.95, 43.33, 41.39, 14.28, 14.25, 14.20, 14.18, 14.11,

14.09 and 13.86. UV-vis: λ_{max} (nm) 236, 245, 329, 506, 549. MALDI-TOF MS: 1474 [M^+ + 1].

2.25: ^{1}H NMR (500 MHz, $CDCl_3$) δ: 8.36 (d, 2H), 6.73 (d, 2H), 4.46-4.39 (m, 8H), 4.38-4.28 (m, 12H), 1.41-1.29 (3t, 24H). ^{13}C NMR (500 MHz, $CDCl_3$) δ: 163.91, 163.78, 163.70, 153.61, 152.35, 147.10, 146.20, 146.01, 145.59, 145.40, 144.34, 143.28, 143.08, 142.42, 138.69, 138.28, 69.94, 69.20, 68.16, 67.84, 63.33, 63.04, 62.85, 59.96, 45.48, 31.67, 14.16 and 14.14. UV-vis: λ_{max} (nm) 218, 245, 276, 312, 476, 544. MALDI-TOF MS: 1474 [M^+ + 1]

***trans*-1 bis-pyridylpyrrolidine-C_{60}-tetra(diethyl)malonate adduct 2.31:**

A solution of **2.25** (0.0634g, 0.043 mmol), (4-pyridyl)glycine (0.130g, 0.861 mmol), and paraformaldehyde (0.026g, 0.861 mmol) in 1,2-dichlorobenzene (40 mL) was heated to reflux under Ar for 4 hours. More pyridyl glycine and paraformaldehyde were added in the same amounts as above every 4 hours until all the mono-adduct was consumed as detected by TLC (5% MeOH: CH_2Cl_2). When the reaction was complete, the mixture was cooled and the solvent evaporated. The crude was purified by column chromatography on silica gel using first 3% MeOH in CH_2Cl_2 as eluant to remove any remaining mono-adduct. Then the polarity was increased to 5% MeOH and the bis-adducts were isolated. This material was purified via preparative TLC by running the plate with 4% MeOH in CH_2Cl_2, drying, running the plate again with 5% MeOH, drying, and finally running with 6% MeOH. The resulting band had a yellow head and orange tail. The two fractions were eluted with 5% MeOH: CH_2Cl_2 on silica and the orange fraction was reapplied to a new preparative TLC plate, and subjected to the same

chromatography until no more yellow was eluting on the plate. The solvent was evaporated to give pure *trans*-1 bisadduct (0.006g) as a yellow solid.

2.31: ^{1}H NMR (500 MHz, $CDCl_3$) δ: 8.40 (br d, 4H), 6.84 (br d, 4H), 4.66 (s, 8H), 4.33 (q, 8H), 4.27 (q, 8H), 1.33 (t, 12H), 1.26 (t, 12H). ^{13}C NMR (500 MHz, $CDCl_3$) δ: 163.86, 163.44, 152.65, 152.27, 150.35, 146.13, 145.35, 143.58, 140.43, 140.33, 139.74, 110.00, 70.85, 66.88, 66.01, 62.86, 59.58, 46.13, 44.73, 14.13. MALDI-TOF MS: 1594 [M^+ + 1]

***trans*-1 bis-terpyridylpyrrolidine-C_{60}-tetra(diethyl)malonate adduct 2.30:** A solution of **2.24** (0.167g, 0.103 mmol), (4-terpyridyl)glycine (0.316g, 1.03 mmol), and paraformaldehyde (0.062g, 2.01 mmol) in 1,2-dichlorobenzene (40 mL) was heated to reflux under Ar for 2.5 hours. When the reaction was complete, the mixture was cooled and the solvent evaporated. Addition of CH_2Cl_2 (3 mL) removed starting material and other products leaving behind compound **2.30** (0.017g, 8%) as a yellow solid. It was filtered, rinsed with diethyl ether and dried.

2.30: ^{1}H NMR (500 MHz, $CDCl_3$) δ: 8.73 (dd, 4H), 8.69 (d, 4H), 8.11 (s, 4H), 7.87 (t, 4H), 7.35 (d, 4H), 4.90 (s, 8H), 4.39 (q, 8H), 4.27 (q, 8H), 1.38 (t, 12H), 1.25 (t, 12H). ^{13}C NMR (500 MHz, $CDCl_3$) δ: 163.81, 163.53, 156.49, 156.23, 154.55, 153.02, 152.42, 148.97, 146.12, 145.46, 143.60, 143.49, 140.31, 139.76, 136.79, 70.85, 66.92, 66.20, 66.05, 62.81, 62.76, 59.86, 46.08, 44.80, 14.17, 14.03. MALDI-TOF MS: 1900 [M^+], 1828, 1756.

***Hexakis*-adducts 2.34 and 2.26:** A solution of **2.17** (35 mg, 0.023 mmol), pyridyl glycine (7 mg, 0.046 mmol), and paraformaldehyde (7 mg, 0.23 mmol) in 1,2-

dichlorobenzene (15 mL) was heated to reflux under Ar for 13 hours. The resulting mixture was cooled and dried. Using a silica gel preparative TLC the separation of 3 fractions using CH_2Cl_2:MeOH 2% as eluant was obtained. Adduct **2.17** (16 mg recovered), adduct **2.34** (fraction 2, 7 mg, 35%) and adduct **2.26** (fraction 3, 1.5 mg, 8%), were thus isolated.

2.34: ^{1}H NMR (500 MHz, $CDCl_3$) δ: 8.40 (d, 2H), 7.54 (d, 2H), 7.05 (dd, 2H), 6.83 (d, 2H), 4.66 (s, 4H), 4.59 (s, 4H), 4.38-4.31 (m, 8H), 4.30-4.24 (q, 8H), 1.37-1.27 (m, 24H). MALDI-TOF MS: 1650 [M^+ + 1].

2.26: ^{1}H NMR (500 MHz, $CDCl_3$) δ: 8. 38 (dd, 2H), 7.54 (d, 2H), 7.05 (dd, 2H), 6.91 (d, 1H), 6.83 (d, 1H), 4.67-4.52 (m, 8H), 4.39-4.22 (m, 16H), 1.37-1.27 (m, 24H). MALDI-TOF MS: 1650 [M^+ + 1].

***Hexakis*-adducts 2.33 and 2.29:** A solution of **2.17** (30 mg, 0.020 mmol), terpyridyl glycine (12.3 mg, 0.040 mmol), and paraformaldehyde (6 mg, 0.2 mmol) in 1,2-dichlorobenzene (8 mL) was heated to reflux under Ar for 4 hours. The resulting mixture was cooled and evaporated. Separation of compounds **2.17** (fraction 1, 9 mg recovered), **2.33** (fraction 2, 4 mg, 16%), and **2.29** (fraction 3, 2.5 mg, 10%) was achieved via reverse phase preparative TLC using CH_2Cl_2:MeOH 1% as eluant.

2.33: ^{1}H NMR (500 MHz, $CDCl_3$) δ: 8.74 (b, 2H), 8.69 (d, 2H), 8.11 (s, 2H), 7.90 (b, 2H), 7.54 (d, 1H), 7.53 (d, 1H), 7.37 (b, 2H), 7.04 (d, 1H), 7.00 (dd, 1H), 4.93 (b, 4H), 4.60 (s, 4H), 4.41- 4.36 (q, 4H), 4.35-4.32 (q, 4H), 4.31-4.25 (q, 8H), 1.40-1.33 (m, 12H), 1.29-1.25 (t, 12H). ^{13}C NMR (500 MHz, $CDCl_3$) δ: 163.98, 163.72, 163.49, 152.32, 149.49, 148.91, 146.18, 146.07, 145.48, 145.37, 143.65, 143.61, 140.34, 140.30, 139.79,

139.70, 133.90, 117.18, 107.09, 70.86, 70.82, 70.58, 66.90, 66.11, 66.03, 62.89, 62.81, 61.13, 59.81, 46.10, 44.77, 14.17, 14.09 and 14.03. MALDI-TOF MS: 1803 [M^+ + 1], 1732, 1661.

2.29: ^{1}H NMR (500 MHz, $CDCl_3$) δ: 8.73 (d, 2H), 8.69 (d, 2H), 8.11 (s, 2H), 7.88 (dd, 2H), 7.53 (d, 1H), 7.35 (b, 2H), 7.05 (d, 1H), 6.98 (d, 2H), 5.01- 4.50 (m, 8H), 4.45-4.22 (m, 16H), 1.40-1.23 (m, 24). MALDI-TOF MS: 1803 [M^+ + 1]

***Hexakis*-adducts 2.32 and 2.27:** A solution of **2.24** (100 mg, 0.062 mmol), *N*-pyridyl glycine (188 mg, 1.24 mmol), and paraformaldehyde (74 mg, 2.48 mmol) in 1,2-dichlorobenzene (30 mL) was heated to reflux under Ar for 3 hours. The resulting mixture was cooled and evaporated. Separation of the compounds **2.24** (orange, fraction 1, 47 mg recovered), **2.32** (orange, fraction 3, 12 mg), and **2.27** (yellow, fraction 4, 15 mg) was achieved via reverse phase preparative TLC using CH_2Cl_2:MeOH 3% as eluant.

2.32: ^{1}H NMR (500 MHz, $CDCl_3$) δ: 8.72 (dd, 2H), 8.68 (d, 2H), 8.39 (d, 2H-Py), 8.10 (s, 2H), 7.87 (t, 2H), 7.34 (d, 2H), 6.83 (d, 2H-Py), 4.89 (s, 4H-Py), 4.66 (s, 4H), 4.38 (q, 4H), 4.34 (q, 4H), 4,28 (q, 8H), 1.36 (m, 12H), 1.28 (t, 12H). ^{13}C NMR (500 MHz, $CDCl_3$) δ: 163.99, 163.69, 163.49, 156.46, 156.25, 154.52, 152.66, 152.49, 152.22, 150.45, 148.96, 146.22, 146.03, 145.43, 145.38, 143.62, 143.57, 140.32, 139.78, 139.71, 136.81, 70.87, 70.82, 66.90, 66.06, 66.00, 62.87, 62.81, 59.82, 59.61, 46.10, 44.77, 14.16, 14.09, 14.03. MALDI-TOF MS: 1747 [M^+ + 1], 1676, 1605.

2.27: ^{1}H NMR (500 MHz, $CDCl_3$) δ: 8.66 (m, 4H), 8.37 (d, 2H-Py), 8.10 (s, 1H), 8.09 (s, 1H), 7.88 (m, 2H), 7.35 (m, 2H), 6.91 (dd, 2H-Py), 4.91-4.71 (m, 8H), 4.70-4.24 (m, 16H), 1.40-1.34 (m, 24H). ^{13}C NMR (500 MHz, $CDCl_3$) δ: 163.96, 163.86, 163.61,

163.45, 156.43, 156.23, 154.45, 152.60, 151.69, 148.94, 146.48, 146.37, 146.16, 145.95, 145.76, 145.36, 143.62, 143.49, 143.03, 142.30, 142.20, 141.97, 140.36, 140.31, 140.21, 139.79, 139.86, 70.89, 70.57, 66.94, 66.08, 65.57, 62.99, 62.91, 62.87, 62.71, 62.61, 60.98, 60.28, 59.77, 59.32, 44.81, 14.16, 14.09, 14.03. MALDI-TOF MS: 1747 [$M^+ + 1$], 1676, 1605.

***Heptakis*-adducts 2.36 and 2.37:** A solution of **2.35** (24 mg, 0.0151 mmol), *N*-pyridyl glycine (46 mg, 0.302 mmol), and paraformaldehyde (27 mg, 0.91 mmol) in 1,2-dichlorobenzene (5 mL) was heated to reflux under Ar for 9 hours. The resulting mixture was cooled and evaporated. Compounds **2.36** and **2.37** were purified using a preparative TLC using CH_2Cl_2:MeOH 5% as eluant.

2.36: ^{1}H NMR (500 MHz, $CDCl_3$) δ: 8.39 (dd, 8H), 6.77 (m, 4H), 4.65-4.10 (m, 28H), 1.30-1.40 (m, 24H, overlapped with grease peak). MALDI-TOF MS: 1712 [M^+]

2.37: ^{1}H NMR (500 MHz, $CDCl_3$) δ: 8.40 (dd, 8H), 6.84 (m, 4H), 4.73-4.07 (m, 28H), 1.30-1.40 (m, 24H, overlapped with grease peak). MALDI-TOF MS: 1712 [M^+]

References

[1] (a) S. Zhang, D. Dong, L. Gan, Z. Liu, C. Huang, *New J. Chem.*, **2001**, *25*, 606-610; (b) S. Lan Jeon, D. Loveless, W. Yount and S. Craig. *Inorg. Chem.*, **2006**, *45*, 11060-11068.

[2] J-P. Sauvage, J-P. Collin, J-C. Chambron, S. Guillerez and C. Coudret, *Chem. Rev.* **1994**, *94*, 993-1019.

[3] (a) M. Kabešová, B. Boča, M. Melník, D. Valigura and M. Dunaj-Jurčo, *Coord. Chem. Rev.*, **1995**, *140*, 115. (b) J. Ciszek, and J. Tour, *Chem. Mater.* **2005**, *17*, 5684. (c) J. Ciszek, Z. Keane, L. Cheng, M. Stewart, L. Yu, D. Natelson, and J. Tour, *J. Am. Chem. Soc.* **2006**, *128*, 3179-3189.

[4] S. Zhang, O. Lukoyanova, and L. Echegoyen, *Chem. Eur. J*. **2006**, *12*, 2846-2853.

[5] V. M. Ohta and M. Masaki, *Bull. Chem. Soc. Jpn.* **1960**, *33*, 1150-1150.

[6] J. D. Gough, J. M. Gargano, A. E. Donofrio and W. J. Lees, *Biochemistry*, **2003**, *42*, 11787-11797.

[7] M. Maggini G. Scorrano and M. Prato, *J. Am. Chem. Soc.* **1993**, *115*, 9798-9799.

[8] J. C. Love, L. A. Estroff, J. K. Kriebel, R. G. Nuzzo and G. M. Whitesides, *Chem. Rev.*, **2005**, *105*, 1103-1169.

[9] (a) J. W. Ciszek and J. Tour, *Chem. Mater.*, **2005**, *17*, 5684-5690; (b) J. W. Ciszek, Z. K. Keane, L. Cheng, M. P. Stewart, L. H. Yu, D. Natelson and J. Tour, *J. Am. Chem. Soc*., **2006**, *128*, 3179-3189.

[10] R. Schwenninger, T. Müller and B. Kräutler, *J. Am. Chem. Soc*. **1997**, *119*, 9317-9318.

[11] A. Ortiz, D. Riviera, A. Athans and L. Echegoyen, *Eur. J. Org. Chem.*, **2009**, 3396-3403.

[12] L. Pasimeni, A. Hirsch, I. Lamparth, A. Herzog, M. Maggini, M. Prato, C. Corvaja, G. Scorrano, *J. Am. Chem. Soc.* **1997**, *119*, 12896–12901.

[13] A. Hirsch, I. Lamparth, G. Schick, *Liebigs Ann.* **1996**, *11*, 1725–1734.

[14] O. Lukoyanova, Studies of the stability and potential applications of pyrrolidinofullerenes and other fullerene derivatives. PhD Thesis, Clemson University, Clemson, SC, USA. **2007**.

[15] M. S. Rodríguez-Morgade, M. E. Plonska-Brzezinska, A. J. Athans, E. Carbonell, G. de Miguel, D. M. Guldi, L. Echegoyen and T. Torres, *J. Am. Chem. Soc.*, **2009**, *131*, 10484–10496.

[16] L. Cao, S. Chen, D. Wei, Y. Liu, L. Fu, G. Yu, H. Liu, X. Liu and D. Wu, *J. Mater. Chem.*, **2010**, *20*, 2305-2309.

[17] M. N. Chaur, F. Melin, A. L. Ortiz and L. Echegoyen, *Angew. Chem. Int. Ed.*, **2009**, *48*, 7514-7538.

[18] (a) R. D. Bolskar, *Nanomedicine* **2008**, *3*, 201 – 213. (b) V. K. Koltover, Progress in Fullerene Research, Nova Science, Hauppauge, **2007**, p. 199.

[19] (a) R. Kitaura, H. Shinohara, *Jpn. J. Appl. Phys. Part 1* **2007**, *46*, 881 – 891; (b) S. F. Yang, L. Z. Fan, S. H. Yang, *Chem. Phys. Lett.* **2004**, *388*, 253 – 258. (c) J. R. Pinzon, M. E. Plonska-Brzezinska, C. M. Cardona, A. J. Athans, S. S. Gayathri, D. M. Guldi, M. A. Herranz, N. Martin, T. Torres, L. Echegoyen, *Angew. Chem. Int. Ed.* **2008**, *47*, 4173 – 4176. (d) J. Tang, G. Xing, Y. Zhao, L. Jing, H. Yuan, F. Zhao, X. Gao, H.

Qian, R. Su, K. Ibrahim,W. Chu, L. Zhang, K. Tanigaki, *J. Phys. Chem. B* **2007**, *111*, 11929 – 11934.

[20] J. S. Yadav, B. V. S. Reddy, S. Shubashree, K. Sadashiv, *Tetrahed. Lett.*, **2004**, *45*, 2951-2954.

[21] R. M. Valerio, P. F. Alewood, R. Johns, *Synthesis* **1988**, 786-790.

CHAPTER THREE

ELECTROLYTIC RETRO-CYCLOPROPANATION OF PYRROLIDINO-C_{60} ADDUCTS

The Bingel-Hirsch[1] reaction (cyclopropanation reaction) is a versatile reaction that has been used to synthesize a wide range of fullerene derivatives such as donor-acceptor systems,[2] dendrimers,[3] and supramolecules,[4] among others. Even though these methano-fullerene derivatives are stable in air, and under high thermal and oxidative conditions, they can be removed efficiently under reduction conditions (chemically[5-6] and electrochemically[7]). The retro-cyclopropanation of methanofullerenes upon reductive potential by controlled potential electrolysis (CPE) was previously reported.[7a] The retro-Bingel reaction of the (alkoxycarbonyl)methanofullerenes of C_{60}, C_{70}, C_{76} and *ent*-C_{76} at the second reduction potential upon CPE recovered the parent fullerenes in 75-82%, 70% and 5-9% yield, respectively, after the addition of four electrons per molecule.[8]

An important process during the course of retro-cyclopropanation reactions by CPE is the electrochemically induced isomerization of the addends by migration on the C_{60} fullerene surface, known as the "*walk on the sphere*".[9] For instance, a pure *cis*-2-*bis*-malonate-adduct was transformed to the *e* (57%), *trans*-3 (31%), *trans*-4 (8%) and *cis*-3 (4%) isomers after it was subjected to CPE with a charge transfer of one electron per molecule.[9] During the "*walk on the sphere*" of *bis*-adducts the major isomers formed were always the *trans*-2 derivative (40-50%), followed by *e*- (25%) isomer. Their predominance was explained in terms of their inherently higher stability. Another

surprising result was the formation of the *trans*-1-*bis*-adduct with 10% yield,[9] which had been isolated only in 0.8-2% yield from the chemical reaction.[10]

This chapter will discuss the synthesis of *trans-1*- and *trans-2*-adducts from the *hexakis*-adducts reported in Chapter II via CPE, which involves the removal of the four (ethoxycarbonyl)methylene groups. All experiments were carried out using a homemade cell described elsewhere [11] at room temperature. The CPE was performed on each sample under high vacuum in CH_2Cl_2 with 0.1M $TBAF_6P$ as the supporting electrolyte. To determine the potential to be applied, the cyclic voltammograms (CVs) of each compound was recorded at the beginning of each experiment. After electrolysis, the solutions were exhaustively re-oxidized at 0 V before purification and product analysis.

Controlled potential electrolysis of *N*-(4-Thiocyanatophenyl)pyrrolidine-C_{60} derivates

The CPE of 3 mg of compound **3.1** (Figure 3.1) was performed at -1.6 V *vs* a Ag wire pseudo reference electrode separated from the solution using a Vycor tip. Figure 3.2A (black solid line) shows the CV of **3.1** before the CPE, exhibiting two reversible fullerene-based reductions at -1.03 and -1.42 V. After approximately 6 electrons per molecule were transferred, the CV (Figure 3.2A, red solid line) displayed three reversible redox waves, corresponding to the typical redox behavior of pristine C_{60} (-0.84, -1.24 and -1.62 V). C_{60} was obtained in 80% yield (1 mg) after re-oxidation and purification. This (previously reported) control experiment agreed results[12-13] indicative of efficient removal of the four cyclopropane addends by this method.

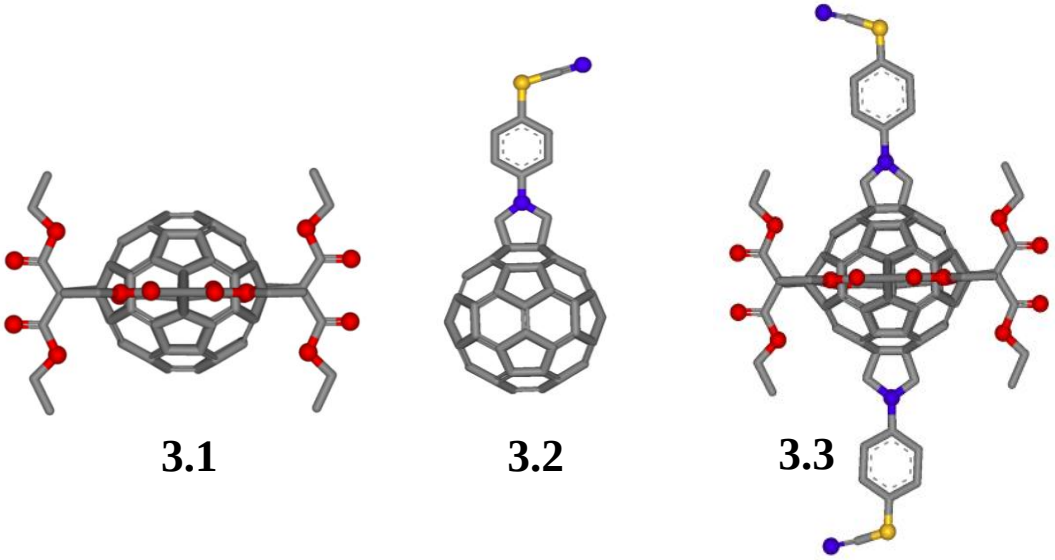

Figure 3.1 Structures of compounds **3.1**, **3.2** and **3.3**.

The CPE of 1.2 mg of compound **3.2** (Scheme 3.1) was carried out at -1.7 V as a second control experiment. After the addition of 5 e^- per molecule the electrolysis was stopped. Following re-oxidation the crude reaction was purified by column chromatography using CS_2 as eluant. Three fractions were recovered (3^{rd} fraction was **3.2**) and pure C_{60} was not found in any of them, which was expected because the Pyrr are stable under reductive conditions.[14] In fact, Pyrr addends can be removed only under chemical[15] or electrochemically oxidative[16] conditions.

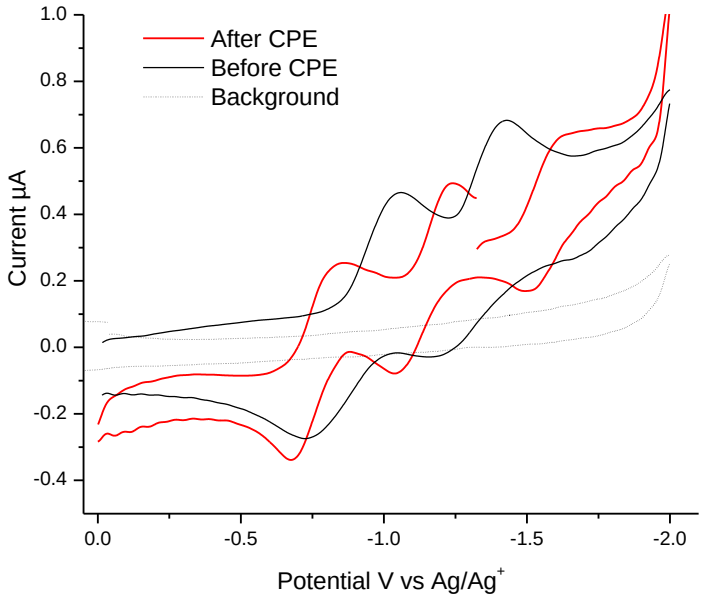

Figure 3.2 Cyclic voltammograms (CV) of compound **3.1** before (−) and after (−) electrolysis. Supporting electrolyte: 0.1 M $TBAPF_6$ in CH_2Cl_2, Scan rate: 0.1 V s^{-1}.

The MALDI-TOF MS of fraction 1 (Figure 3.3) showed the molecular ion peak for *N*-(4-Thiolphenyl)pyrrolidine-C_{60} (PhSH-Pyrr-C_{60}), **3.4**, and the disulfide (C_{60}-Pyrr-PhS−SPh-Pyrr-C_{60}), which indicated that the SCN group can be reduced to SH under CPE.[17] This result was expected based on the work of Hawley and co-workers.[17] They studied the effect of the thiocyanate substituent in the decomposition of nitroaromatic compounds by electrolysis. They reported that the electrochemical reduction of *p*-nitrophenyl thiocyanate **3.5** (Scheme 3.2) formed the anion radical **3.5a** in a one electron process, which was unstable and decomposes slowly with loss of cyanide ion to form the radical, **3.5c**. The neutral radical was immediately reduced (chemically or electrochemically) to give **3.5d**. If the electrochemical reduction of **3.5** was carried out at

the second reduction potential the dianion **3.5b** was formed, which decomposed rapidly to **3.5d** and the cyanide ion. The neutral radicals react by numerous pathways including dimerization, hydrogen atom abstraction and coupling with an anion to form a new more stable anion radical.[17]

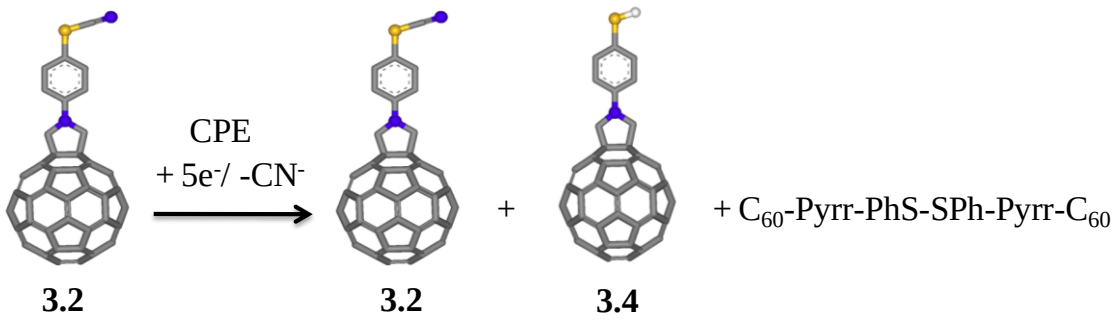

Scheme 3.1 Electrolysis of compound **3.2**.

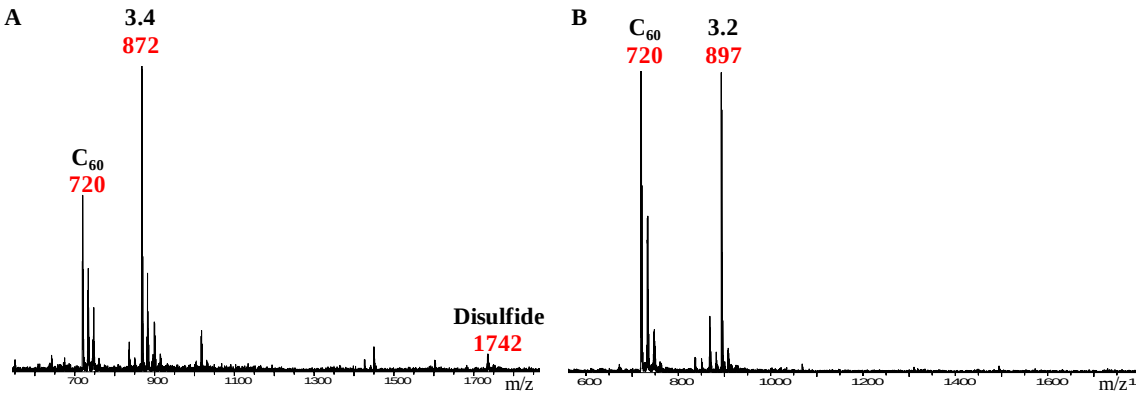

Figure 3.3 MALDI-TOF MS spectrum of the products after CPE of **3.2**: A) fraction one and B) fraction three.

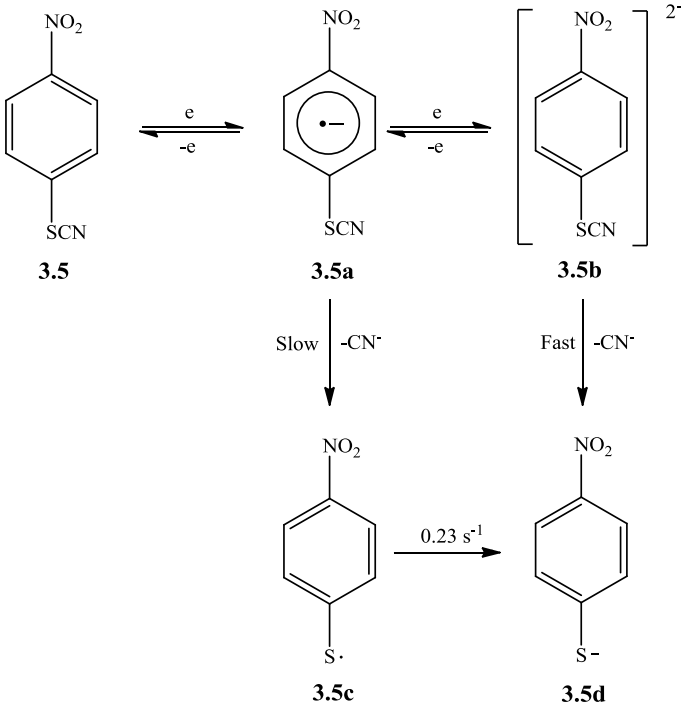

Scheme 3.2. Mechanism of the electrolysis of *p*-nitrophenyl thiocyanate **3.5**. [17].

Finally, the CPE of **3.3** was performed to obtain the *trans-1-bis-N*-(4-Thiocyanatophenyl) pyrrolidine-C_{60} derivative. Figure 3.4 shows the CVs of **3.3** before (black solid line) and after (red solid line) electrolysis. A one-electron irreversible process at -1.34 V *vs* Ag wire was observed before the CPE. This unstable behavior upon reduction indicates that this *hexakis*-adduct is not useful for applications in electronic devices because it will decompose upon electron transfer in the system. The CPE of 3.5 mg of **3.3** was carried out at -1.70 V and stopped after 9 electrons per molecule had been transferred. At this point, the CV (red solid line, Figure 3.4) exhibited three reversible reduction waves at -0.83, -1.04 and -1.20 V indicating that the cyclopropane groups were removed. But, to our surprise C_{60} was recovered in a 67% yield without the presence of

the desired *trans-1* product after purification (Scheme 3.3). The CPE was repeated at lower potential (-1.1 V) and the starting material **3.3** was recovered. This is the first example of removal of a Pyrr ring under reductive conditions. Even though the mechanism of this process is not understood, it was clear that the presence of the cyclopropane rings, CN^- and S^- or $S^{\bullet}$ played an important role on the removal of the Pyrr rings. We know that the mechanism of the retro-Bingel reaction by means of CPE involves the heterolytic opening of the cyclopropane ring, leading to charge formation either in the fullerene core or in the addend.[18] This ring-opened species probably reacts with the species CN^- and S^- or $S^{\bullet -}$ generating the pyrrolidine ring removal.

Although we did not obtain the desired product, this finding can open new avenues for the synthesis of new fullerene derivatives.

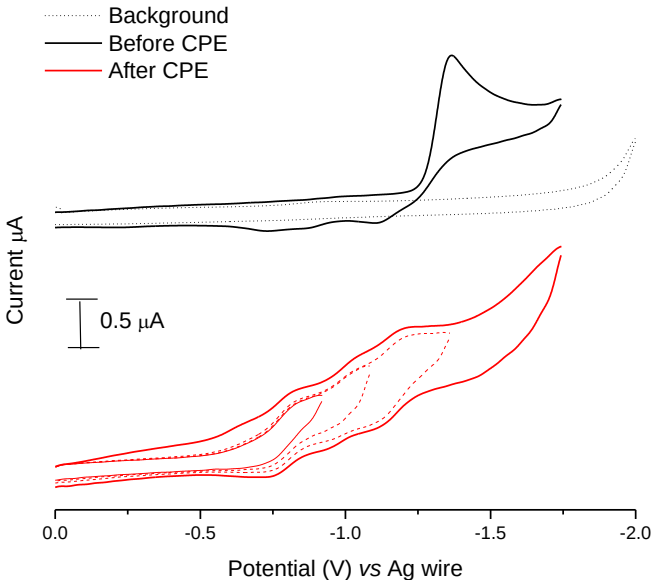

Figure 3.4 Cyclic voltammograms (CV) of compound **3.3** before (−) and after (−) electrolysis. Supporting electrolyte: 0.1 M $TBAPF_6$ in CH_2Cl_2, Scan rate: 0.1 V s^{-1}.

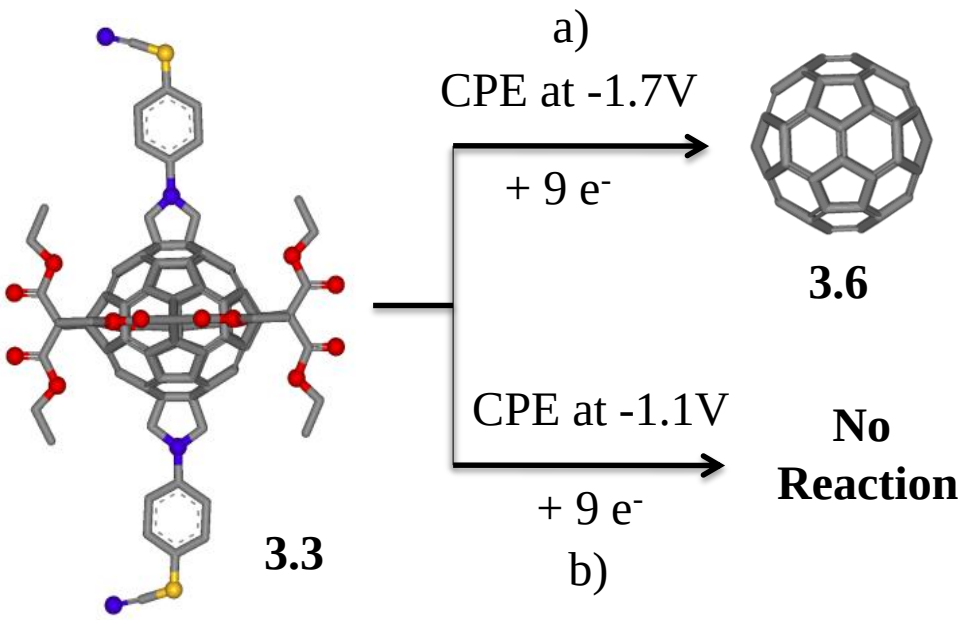

Scheme 3.3. CPE of compound **3.3**: a) addition of 9 electrons at -1.7 V; b) addition of 9 electrons at -1.1 V.

Controlled potential electrolysis of Pyridyl-pyrrolidine-C_{60} derivates

The next compounds to be analyzed were **3.7** and **3.8** (Figure 3.5). CPE of the control compound **3.7** was carried out at -1.7 V and stopped after 7 electrons were transferred. An evident change was observed in the CV of **3.7** after (red solid line, Figure 3.6A) the CPE, from an initial two irreversible peaks (-1.43 and -1.69 V *vs* Ag wire) to two reversible peaks (-1.22 and -1.49 V *vs* Ag wire). The reaction crude was characterized by means of MALDI-TOF after re-oxidation at 0 V, and the spectrum showed the molecular ion peak for the species with three (*m/z* = 1156, Figure 3.6B) and four cyclopropane addends removed (*m/z* = 840, Figure 3.6B). C_{60} was not detected, indicating the stability of the pyridyl pyrrolidine addend under reductive contidions.

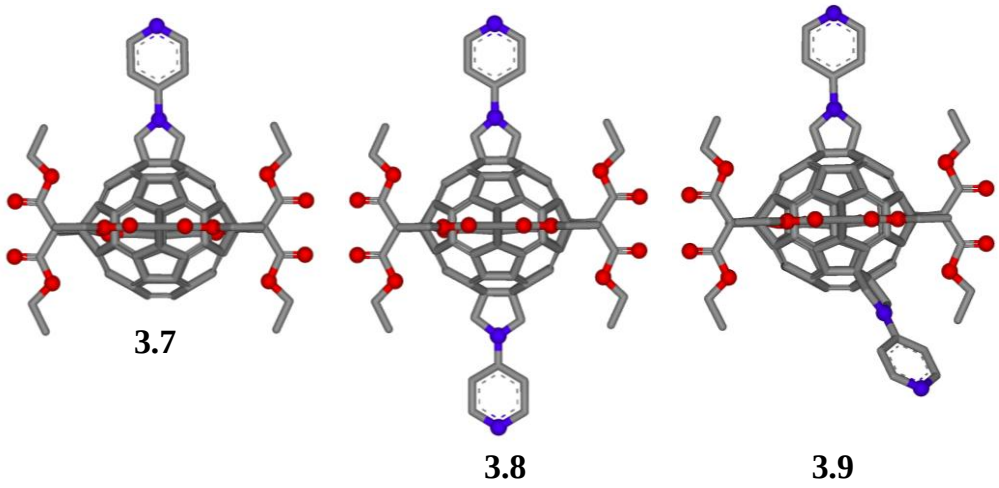

Figure 3.5. Structures compounds **3.7**, **3.8** and **3.9.**

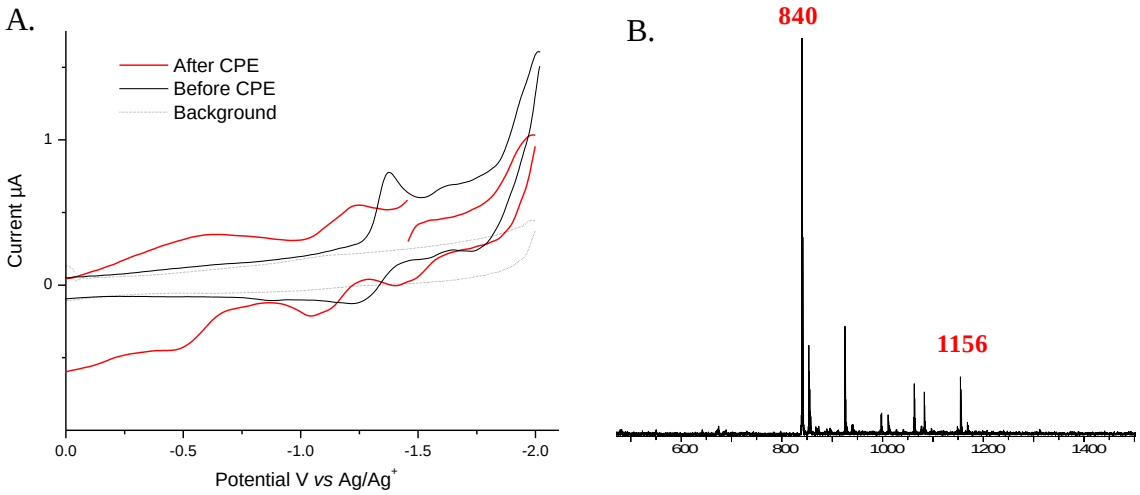

Figure 3.6 A) Cyclic voltammograms (CV) of compound **3.7** before (−) and after (−) electrolysis. Supporting electrolyte: 0.1 M $TBAPF_6$ in CH_2Cl_2, Scan rate: 0.1 $V.s^{-1}$. B) MALDI-TOF spectrum of the reaction crude after CPE of **3.7**: *m/z*: 1156 (without 3 malonate groups) and 840 (without 4 malonate groups).

Figure 3.7 (black solid line) shows the CV of compound **3.8** before CPE, which exhibits irreversible electrochemistry under reductive conditions. The *hexakis*-adduct **3.8** was subjected to CPE and after discharging the equivalent of 6 electrons per molecule, the electrolysis was stopped. At that point the CV (red solid line, Figure 3.7) clearly showed the appearance of two reversible reductive processes at -1.10 and -1.44 V *vs* Ag wire. Three products were detected in the reaction crude by MALDI-TOF corresponding to the removal of: two (**3.10**), three (**3.11**) and four malonate (**3.12**) groups, respectively (Scheme 3.4).[19]

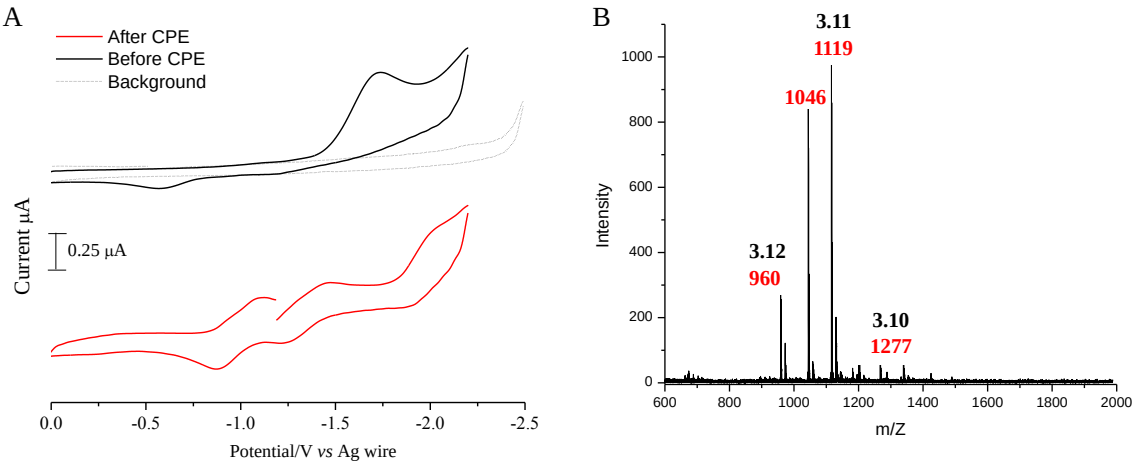

Figure 3.7 A) Cyclic voltammograms (CV) of compound **3.8** before (−) and after (−) electrolysis. Supporting electrolyte: 0.1 M $TBAPF_6$ in CH_2Cl_2, Scan rate: 0.1 $V.s^{-1}$. B) MALDI-TOF spectrum of the reaction crude after CPE of **3.8**: *m/z*: 1277 (without 2 malonate groups); 1119 (without 3 malonate groups) and 960 (without 4 malonate groups).

The *tetrakis*-adduct **3.10** was isolated (18% yield) and fully characterized as a single isomer with a remarkable (*e,e,e,e*)-D_{2h}- symmetry by means of NMR spectroscopy, mass spectrometry, UV-*Vis* and electrochemistry. The ^{1}H-NMR (Figure 3.8A) of compound **3.10** displayed one triplet for the –CH_3 protons at 1.39 ppm (integrating for 12 protons), one quartet for the methylene protons from of the malonate groups (integrating for 8 protons at 4.51 ppm), one singlet for the 8 methylene protons of the pyrrolidine rings at 5.18 ppm; and two doublets for the eight aromatic protons (7.06 and 8.51 ppm, respectively, 4 protons each).

Figure 3.8B shows the ^{13}C-NMR spectrum of **3.10**, one signal for the two carbonyls (δ = 164.30), one for the methyls (δ = 14.21) and one for the methylenes (δ = 66.87 ppm) of the two malonate groups, one peak for the methylenes (δ = 63.21) and three (δ = 110.34, 150.67 and 152.39) for the aromatic carbon atoms of the pyrrolidine rings and two sp^3-C peaks (δ = 60.25 and 69.36) for the fullerene cage indicating that they are magnetically equivalent. Finally, seven signals between δ =141.18 - 152.39 for the sp^2-C atoms of the fullerene cage were observed. The NMR spectra of **3.10** indicated D_{2h} symmetry, in other words all of the addends are located on the equator of the fullerene.[19]

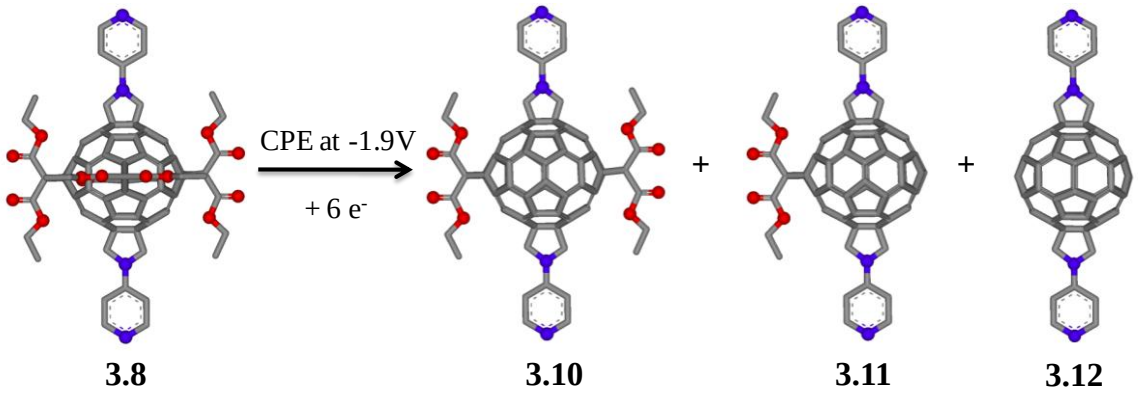

Scheme 3.4 Reduction of compound **3.8** under electrochemical conditions.

This unusual *tetrakis*-adduct **3.10** with a never reported and unique (*e*,*e*,*e*,*e*) architecture with two Pyrr groups (*trans-1* to each other) and two cyclopropane rings (also *trans-1* to each other) could have potential applications in molecular electronics because it exhibits reversible chemical and electrochemical behavior upon reduction conditions (Figure 3.9). The CV of compound **3.10** shows two one electron reversible reduction processes at -0.76 and - 1.15 V *vs* Fc/Fc+ (Fc= ferrocene) (Figure 3.9).[19]

On the other hand, the unexpected exclusive formation of this highly symmetric isomer of compound **3.10** led us to investigate its stability and isomeric preference upon electrochemically induced isomerization ("walk-on-the-sphere" process). The CPE of compound **3.10** at the first reduction potential was performed in CH_2Cl_2 at room temperature, and it did not result in any isomerization or other changes.[19]

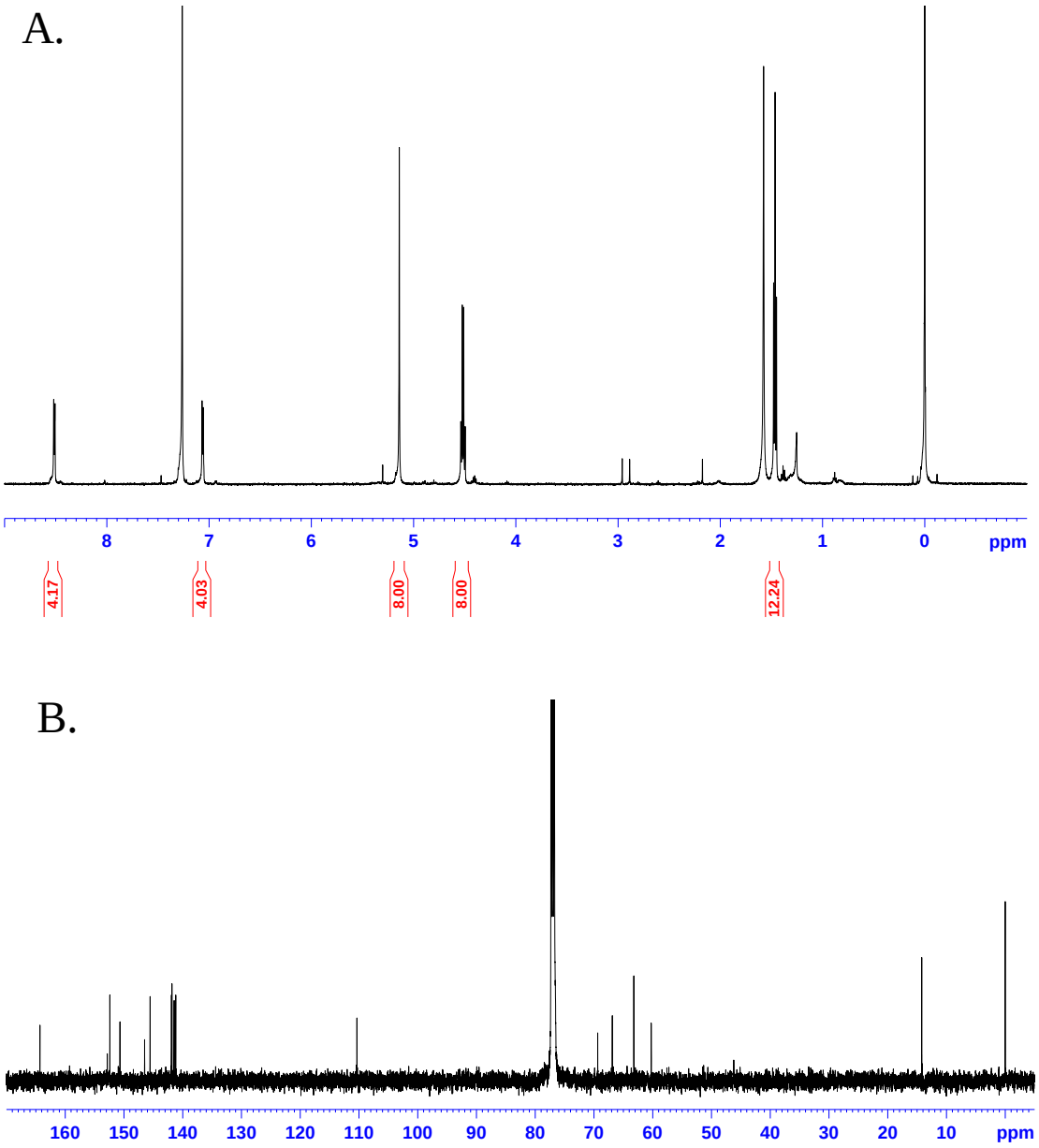

Figure 3.8 A) ^{1}H-NMR spectrum of (*e*,*e*,*e*,*e*)-tetrakis-adducts **3.10**; B) ^{13}C-NMR spectrum of (*e*,*e*,*e*,*e*)-tetrakis-adducts **3.10**. (500 MHz, $CDCl_3$).

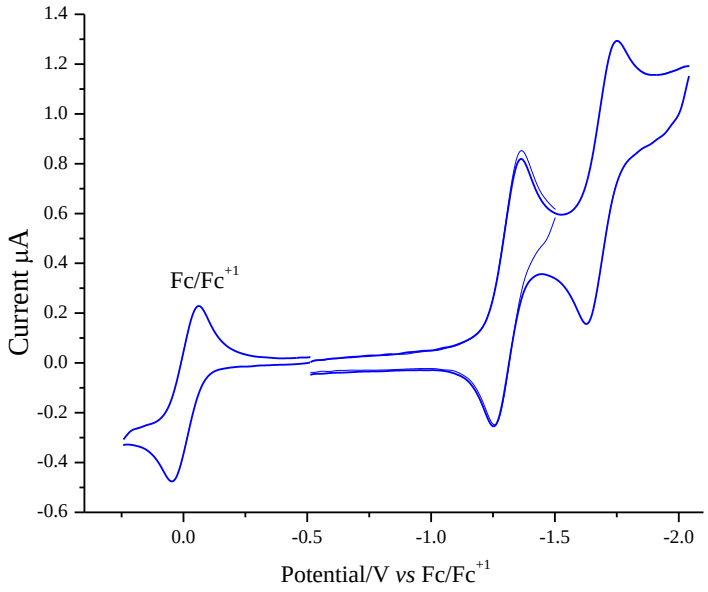

Figure 3.9. Cyclic voltammogram of (*e*,*e*,*e*,*e*)-*tetrakis*-[60]-fullerene adduct **3.10**. Supporting electrolyte: 0.1 M $TBAPF_6$ in CH_2Cl_2, Scan rate: 0.1 V s^{-1}.

The formation of only one isomer out of the two possible (*e*,*e*,*e*,*e*)-D_{2h}-[60]fullerene derivatives (**3.10'** and **3.10''**, Figure 3.10) from the CPE of compound **3.8** is currently not understood. Furthermore, we are currently not even able to identify which of these isomers was obtained since spectroscopic methods are unable to differentiate them. X-ray structural analysis may be the only way to elucidate which isomer is preferentially formed.[19] Based on simple steric arguments **3.10''** would seem to be slightly preference but proof will only be obtained from a diffraction structure.

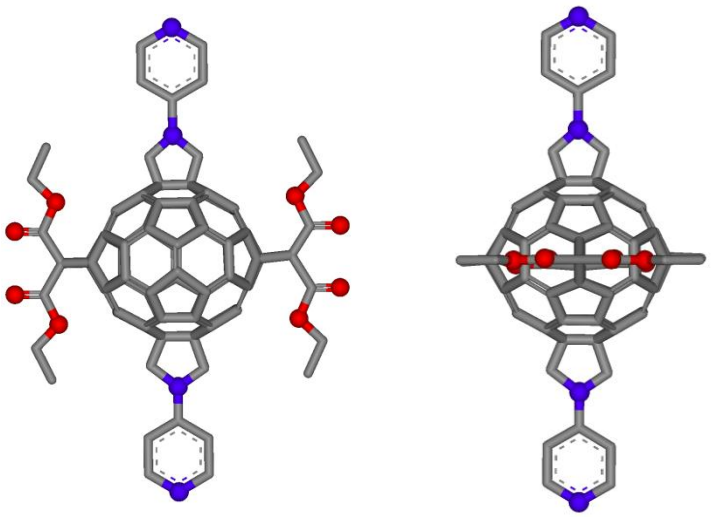

3.10' **3.10"**

Figure 3.10. Possible isomers of compound **3.10** based on the observed NMR symmetry.

Single molecule conductance was performed on **3.10** by Xiulan Li from Professor Tao's group in Arizona State University. The description of the conductivity measurement by the STM break junction method[20] was given in section the "Molecular-based electronic devices" section, Chapter I.

Compound **3.10** was initially self-assembled on a gold substrate and this was loaded onto the STM setup (Figure 3.11A). The STM tip was then approached close to the analyte monolayer (Figure 3.11B) immersed in mesitylene and then the tip was pulled away from the surface. Mesitylene was chosen as a solvent because it minimizes the leakage current between the STM tip and the Au electrodes.

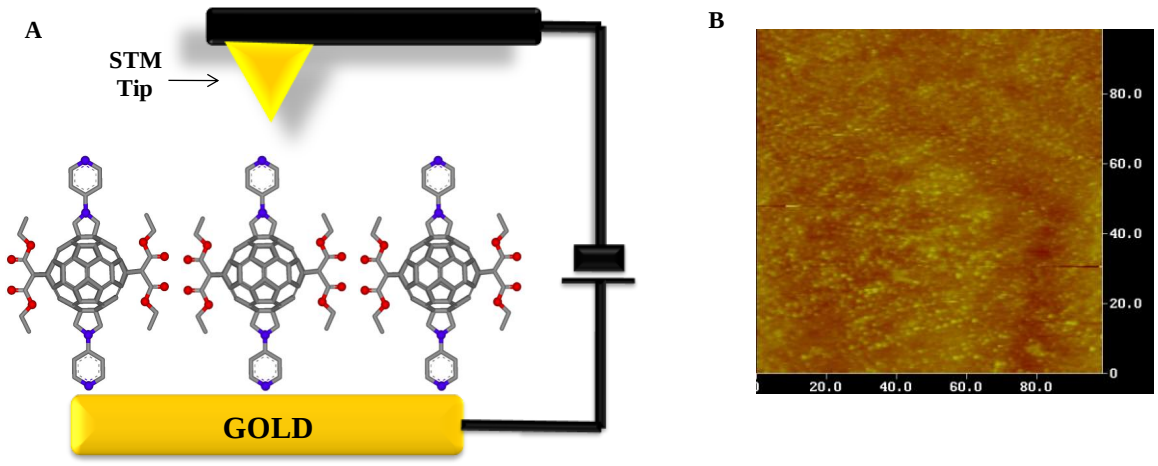

Figure 3.11. A) STM setup of compound **3.10**; B) STM image of Au (111) substrate modified with molecules of compound **3.10**.

Figure 3.12A shows the conductance histogram measured for compound **3.10** and the conductance value was found to be 0.4 G_0, which is very close to the value of 0.7 G_0 measured for C_{60}. The conductance of compound **3.10** was expected to be lower than that of pure C_{60} because of the presence of the addends. A possible interpretation is that the compound is resting on the surface directly through the fullerene core with the addends extended so that the conductance reflects only the value through the fullerene and not through the addends as desired. Use of SH-Pyrr groups instead of pyridyls-Pyrr could help establish the surface orientation of these compounds, along with other techniques, such as reflection absorption infrared spectroscopy (RAIRS). Nevertheless, this preliminary data shows has promising results for fullerene-based single molecular transistors.

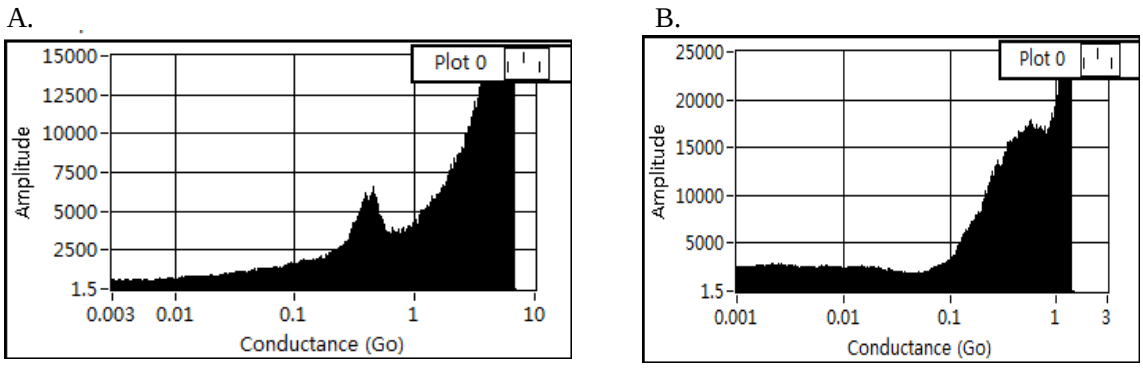

Figure 3.12. A) Conductance histogram of compound **3.10** in mesitylene, 1000nA/V preamplifer, the histogram was built by 982 curves from 1042 individual measurements using auto selection program E_{bias}= 20 mV. B) Conductance histogram of pure C_{60} in mesitylene, 1000nA/V preamplifer, the histogram was built by 1048 curves from 1140 individual measurements using auto selection program E_{bias}= 97 mV.

Finally, the CPE of 7 mg of compound **3.9** was performed at -1.8 V and it was stopped after 6 electrons were transferred. Figure 3.13A shows the CVs of **3.9** before (black solid line) and after (red solid line) electrolysis. One electron irreversible process at -1.62 V was observed in the CV before the CPE and two one electron reversible processes at -0.95 and -1.27 V were observed after the CPE. A brown solid was suspended in the solution reaction after re-oxidation at 0 V, which was separated using a centrifuge and washed several times with CH_2Cl_2. This solid was identified as *trans-2*-bispyridyl-pyrrolidine-C_{60} (2 mg, 50%) derivative **3.13** by means of MALDI-TOF MS (Figure 3.13B).

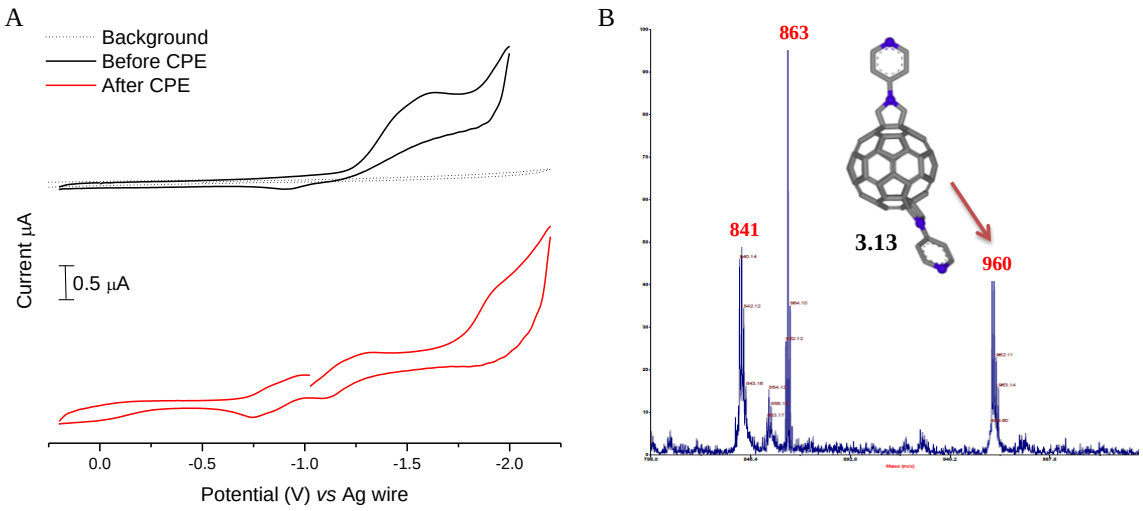

Figure 3.13 A) Cyclic voltammograms (CV) of compound **3.9** before (−) and after (−) electrolysis. Supporting electrolyte: 0.1 M $TBAPF_6$ in CH_2Cl_2, Scan rate: 0.1 V s^{-1}. B) MALDI-TOF spectrum of compound **3.13**: *m/z*: 960.

Conclusions

In this chapter, the reductive controlled potential electrolysis of seven different C_{60} derivatives was discussed. The SCN phenyl pyrrolidine derivatives lost their addends upon CPE, the first examples of pyrrolidine removal by reductive electrolysis. For the derivatives with pyridyl-Pyrr addends, the CPE of an *hexakis*-adduct of C_{60} generated a unique and unusual (*e*,*e*,*e*,*e*) derivative containing two different addends in relative *trans-1* arrangements over the C_{60} core. This compound is highly symmetric and exhibits electrochemically and chemically reversible behavior, thus potentially useful in molecular electronic applications. The preliminary conductance data of the (*e*,*e*,*e*,*e*) derivative showed promising results for fullerene based break junctions. Finally, the *trans-2*-bispyridyl-pyrrolidine-C_{60} derivative was successfully obtained from the electrolysis of a *hexakis*-adduct of C_{60} by CPE.

Experimental Section

General: Reagents were purchased from commercial suppliers and used without further purification. The syntheses of compounds **3.1**[14] and **3.3**[14] were discussed in Chapter II. Syntheses of compounds **3.7**,[21] **3.8** and **3.9**[13, 22] were performed using the same methodology as that used for **3.1**[14] and **3.3**[14] and they were reported by our group previously. NMR spectra were recorded on a Bruker AC 500 MHz spectrometer. Mass spectroscopy was recorded with an Omni Flex MALDI-TOF spectrometer.

Electrochemical measurements: All electrochemical measurements were performed in dry CH_2Cl_2 (degassed with argon) with 0.1 M $TBAPF_6$ as the supporting electrolyte using a BASi Electrochemical Workstation. The tetrabutylammonium hexafluorophosphate ($TBAPF_6$, Fluka, 99%) was recrystallized two times from ethanol and dried under vacuum for 24 hours prior to use. Cyclic voltammetry (CV) was performed under an argon atmosphere at room temperature at a scan rate of 100 mV s^{-1} and pulse rate of 0.05 s with increments of 4 mV and an amplitude of 50 mV. A standard three-electrode setup was used consisting of a glassy carbon working electrode (Cypress, 1.0 mm), a platinum wire auxiliary electrode (Aldrich, 1.0 mm) and a non-aqueous reference electrode $Ag/AgNO_3$ (calibrated externally versus the ferrocene/ferricenium (Fc+/Fc) redox couple). The half-wave potential, $E_{1/2}$, was determined as $(E_{pa} + E_{pc})/2$, where E_{pa} and E_{pc} are the anodic and cathodic peak potentials from the CV.

Bulk electrolysis was performed using a homemade electrochemical cell. A 2–7 mg sample of fullerene derivatives **3.1**, **3.2**, **3.3**, **3.7**, **3.8, 3.9** or **3.10** was used for each experiment. The cell was degassed and pumped to a pressure of 10^{-6} torr. Dry CH_2Cl_2 (18

mL), which had also been degassed and pumped to the same pressure in the presence of calcium hydride, was vapor-transferred directly into the cell. Prior to CPE, cyclic voltammetry was performed by using a glassy carbon electrode (1 mm) to obtain the reduction potential versus a Ag wire pseudoreference electrode. The latter was separated from the bulk solution by a Vycor tip. CPE at 293 K was performed on a Pt-mesh (100 mesh, 6.5 cm^2) working electrode. After reductive electrolysis, the solution was reoxidized at 0 V. Compound **3.9** (1 mg, 0.0010 mmol, 18%) was purified by prep-Alumina TLC using CH_2Cl_2/MeOH 2% as eluant: ^{1}H NMR ($CDCl_3$, 500 MHz) δ 1.48-1.45 (t, 12H), 4.54-4.50 (q, 8H), 5.14 (s, 8H), 7.06 (d, 4H), 8.51 (d, 4H); ^{13}C NMR ($CDCl_3$, 125 MHz) δ 14.21 (CH_3), 46.00, 60.25 (C), 63.21 (CH_2), 66.87 (CH_2), 69.36 (C), 110.34 (Py), 141.18 (C), 141.45 (C), 141.82 (C), 141.91 (C), 145.54 (C), 146.48 (C), 150.67 (Py), 152.39 (C), 152.83 (Py), 164.30 (CO); UV*vis* (CH_2Cl_2): 277, 288, 326 and 478 nm; MS (MALDI): *m/z*: 1277 [M+45]. ***Hexakis*-adduct 3.9:** ^{1}H NMR (500 MHz, $CDCl_3$) δ: 8.40 (br d, 4H), 6.84 (br d, 2H), 6.78 (br d, 2H), 4.68-4.50 (m, 8H), 4.37-4.25 (m, 16H), 1.38-1.29 (m, 24H). ^{13}C NMR (500 MHz, $CDCl_3$) δ: 163.96, 163.86, 163.48, 163.18, 153.65, 153.05, 152.70, 152.56, 152.19, 151.91, 151.46, 151.01, 150.17, 148.67, 147, 85, 146.98, 146.58, 146.30, 146.21, 145.95, 145.69, 145.54, 145.38, 145.26, 144.36, 144.11, 143.41, 143.09, 142.92, 142.50, 142.35, 142.12, 141.83, 141.50, 141.29, 140.89, 140.67, 140.27, 139.70, 138.84, 138.08, 136.77, 136.60, 136.18, 136.05, 130.20, 125.15, 70.39, 70.22, 69.10, 68.91, 67.63, 67.57, 67.25, 66.98, 66.84, 66.01, 63.58, 63.01, 62.92, 62.93, 62.85, 62.60, 61.16, 61.09, 60.43, 60.03, 59.96, 59.60, 45.53, 43.76, 43.49, 42.04, 14.13, 14.09, 14.04. MALDI-TOF MS: 1594 [M^+ + 1]

References

[1] I. Lamparth and A. Hirsch, *J. Chem. Soc., Chem. Commun.* **1994**, *116*, 1727-1728.

[2] S. Gónzalez, N. Martín and D. M. Guldi, *J. Org. Chem*., **2003**, *68*, 779-791.

[3] (a) F. Diederich, C. Dietrich-Buchecker, J-F. Niergartent and J-P. Sauvage, *Chem. Commun.*, **1995**, *7*, 781-782.; (b) M. Brettreich and A. Hirsch, *Tetrahed. Lett*., **1998**, *39*, 2731-2734.

[4] Y. Nakamura, S. Minami, K. Iizuka and J. Nishimura, *Angew. Chem. Int. Ed. Engl.*, **2003**, *42*, 3158-3162.

[5] N. N. P.Moonen, C. Thilgen, L. Echegoyen and F. Diederich, *Chem. Commun.* **2000**, *5*, 335-336.

[6] M. A. Herranz, J. A. Rivera, R. J. Alvarado, N. Martín, C. Thilgen, F. Diederich and L. Echegoyen, *J. Supramol. Chem.* **2001**, *1*, 299-303.; (b) M. A. Herranz, L. Echegoyen, M. W. J. Beulen, J. A. Rivera, N. Martín, B. Illescas and M. C. Díaz, *Proc.-Electrochem. Soc.*, **2002**, *12*, 307-317. (Fullerenes 2002-volume 12: The Exciting World of Nanotubes and Nanocages).

[7] (a) F. Arias, Y. Yang, L. Echegoyen, Q. Lu and S. R. Wilson, *Proc.-Electrochem. Soc.*, **1995**, *10*, 200-212. (Fullerenes 1995-volume 10: The Exciting World of Nanotubes and Nanocages); (b) M. Keshavarz-K., B. Knight, R.C. Haddon and F. Wudl, *Tetrahedron*, **1994**, *52*, 5149-5159.

[8] R. Kessinger, J. Crassous, A. Herrmann, M. Rüttimann, L. Echegoyen and F. Diederich, *Angew. Chem. Int. Ed.* **1998**, *37*, 1919-1922.

[9] R. Kessinger, M. Gómez-López, C. Boudon, J.-P. Gisselbrecht, M. Gross, L. Echegoyen and F. Diederich, *J. Am. Chem. Soc.* **1998**, *120*, 8545-8546.

[10] (a) A. Hirsch, I. Lamparth and H. R. Karfunkel, *Angew. Chem., Int. Ed. Engl.* **1994**, *33*, 437-438. (b) F. Djojo, A. Herzog, I. Lamparth, F. Hampel and A. Hirsch, *Chem. Eur. J.* **1996**, *2*, 1537-1547.

[11] (a) R. Kessinger, J. Crassous, A. Herrmann, M. ROttimann, L. Echegoyen, F. Diederich, *Angew. Chem. Int. Ed.* **1998**, *37*, 1919 – 1922; (b) J. Crassous, J. Rivera, N. S. Fender, L. H. Shu, L. Echegoyen, C. Thilgen, A. Hermann, F. Diederich, *Angew. Chem. Int. Ed.* **1999**, *38*, 1613 –1617; (c) M. A. Herranz, F. Diederich, L. Echegoyen, *Eur. J. Org. Chem.* **2004**, 2299 –2316.

[12] O. Lukoyanova, Studies of the stability and potential applications of pyrrolidinofullerenes and other fullerene derivatives. PhD Thesis, Clemson University, Clemson, SC, USA. **2007**.

[13] S. Zhang, O. Lukoyanova, and L. Echegoyen, *Chem. Eur. J.* **2006**, *12*, 2846-2853.

[14] A. Ortiz, D. Riviera, A. Athans and L. Echegoyen, *Eur. J. Org. Chem.*, **2009**, 3396-3403.

[15] N. Martín, M. Altabe, S. Filippone, A. Martín-Domenech, L. Echegoyen and C. M. Cardona, *Angew. Chem. Int. Ed.*, **2006**, *45*, 110-114.

[16] O. Lukoyanova, C. M. Cardona, M. Altabe, S. Filippone, A. Martín Domenech, N. Martín and L. Echegoyen, *Angew. Chem. Int. Ed.*, **2006**, *45*, 7430-7433.

[17] D. E. Bartak, T. M. Shields and M. D. Hawley, *J. Electroanal. Chem.*, **1971**, *30*, 289-300.

[18] M. A. Herranz, F. Diederich and L. Echegoyen *Eur. J. Org. Chem.* **2004**, 2299-2316.

[19] A. L. Ortiz and L. Echegoyen, *J. Mater. Chem*., DOI:10.1039/C0JM00754D.

[20] B. Xu and N. J. Tao, *Science*, **2003**, *301*, 1221–1223.

[21] F. T. Tat, Z. G. Zhou, S. MacMahon, F. Y. Song, A. L. Rheingold, L. Echegoyen, D. I. Schuster and S. R. Wilson, *J. Org. Chem.*, **2004**, *69*, 4602-4606.

[22] M. S. Rodríguez-Morgade, M. E. Plonska-Brzezinska, A. J. Athans, E. Carbonell, G. de Miguel, D. M. Guldi, L. Echegoyen and T. Torres, *J. Am. Chem. Soc.*, **2009**, *131*, 10484–10496.

CHAPTER FOUR

COMPLEXES (Fe^{II} and Ru^{II}) OF TERPYRIDYL-YRROLIDINO-C_{60} DERIVATIVES

In the previous Chapters we introduced a versatile strategy to synthesize a library of C_{60} derivatives, featuring cyclopropane and pyrrolidine ring addend on the surface of the cage. The cyclopropane addends acted as protecting groups in order to synthesize these compounds, and the pyrrolidine addends gave special characteristics to each derivative.[1] For example, the pyridyl (Py) group can self-assemble on Au, Pd, or Pt,[2] while the terpyridyl (Tpy) group is known to form stable complexes with Ru(II), Co(II), Fe(II), and Os(II)[3] and the SCN group can self-assemble on Au.[4] We also proposed their potential use in molecular electronics as single molecule transistors after removal of the cyclopropane addends. These derivatives are also appealing as building blocks in self-assembled systems because of their three dimensional architecture and ability to form stable complexes. The study of these complexes also support our predictions that they could behave as coordination driven single molecule transistors by surface-controlled self-assembly on solid supports.[5]

The self-assembly of molecules which mimic systems in nature has been the focus of many research groups.[6] This process is driven by the properties and information stored in their units, which can be designed using different functional groups.[7] External factors also play an important role in the assembly of the units such as concentrations, stoichiometries of the components and presence of foreign species.[8]

Different types of interactions are the glue in self-assembled systems such as electrostatic interactions, hydrogen bonds, Van der Waals interactions, π-π interactions, charge-transfer interactions and hydrophobic binding.[6b] We are interested on metal coordination driven self assembly due to the nature of some of the addends in the C_{60} derivatives (e.g. Py-Pyrr and Tpy-Pyrr). Metal-ligand bonds (10-30 kcal/mol) are not as strong as covalent bonds (90-140 kcal/mol) but stronger than electrostatic and π-π stacking interactions.[3] Coordination chemistry provides a useful tool for the elucidation of the self-assembly process itself.[9] Several beautiful examples have been reported using metal-directed synthesis in the last two decades such as "self-sorting systems" or helicates, knots, rotaxanes and catenanes.[6b]

In this Chapter, we will introduce the formation of complexes based on the fullerene derivatives reported in Chapter II. Their characterization will be discussed by means of NMR spectroscopy, electrospray ionization mass spectrometry (ESI MS), MALDI-TOF MS and electrochemistry.

Metal coordination of the *pentakis*-C_{60} adduct bearing a single Tpy group with Fe(II), Ru(II), Os(II) and Co(II)

We studied the coordination of Fe (II), Ru (II), Os (II), and Co (II) with the *pentakis*-adduct **4.1** in order to probe the self-assembly of the C_{60} derivatives by metal-directed synthesis, as follows (Scheme 4.1):

Fe (II) complex **4.2a**: 0.012 mmol of **4.1** and 0.006 mmol of $FeCl_2.4H_2O$ were mixed in 5 mL CH_2Cl_2:methanol 3:2 under argon at room temperature. The initial orange

solution turned purple instantly. The reaction was stirred for 24 hours and protected from light, then 5 mL of 0.1 M KPF_6 in methanol was added. A purple solid was formed and separated using the centrifuge. One product (90% yield) was produced and subjected to full characterization.

Ru (II) complex **4.2b**: A solution of 0.012 mmol of **4.1** and 0.006 mmol of $RuCl_2(Me_2SO)_4$[10] on 5 mL CH_2Cl_2:methanol 3:2 was refluxed under argon during 24 hours, then 5 mL of 0.1 M KPF_6 in methanol was added. An orange solid was formed and separated using the centrifuge. This solid was purified by preparative thin layer chromatography (prep-TLC) with CH_2Cl_2:methanol 92:8 as eluent. Four fractions were isolated and the product **4.2b** (18% yield) was found in the second fraction.

Os (II) complex **4.2c**: 0.012 mmol of **4.1** was mixed with 0.006 mmol of NH_4OsCl_6 in 5 mL CH_2Cl_2:methanol 3:2 and refluxed under argon during 24 hours, then 5 mL of 0.1 M KPF_6 in methanol was added. A brown solid was formed and separated using the centrifuge. This solid was purified by prep-TLC with CH_2Cl_2:methanol 97:3 as eluent. Two fractions were isolated and first one being the expected product.

Co (II) complex **4.2d**: A solution of 0.012 mmol of **4.1** and 0.006 mmol of $CoCl_2.xH_2O$ in 5 mL CH_2Cl_2:methanol 3:2 was refluxed under argon during 24 hours, then 5 mL of 0.1 M KPF_6 in methanol was added. An orange solid was formed and separated using the centrifuge. This solid was purified by prep-TLC with CH_2Cl_2:methanol 97:3 as eluent. Three fractions were obtained.

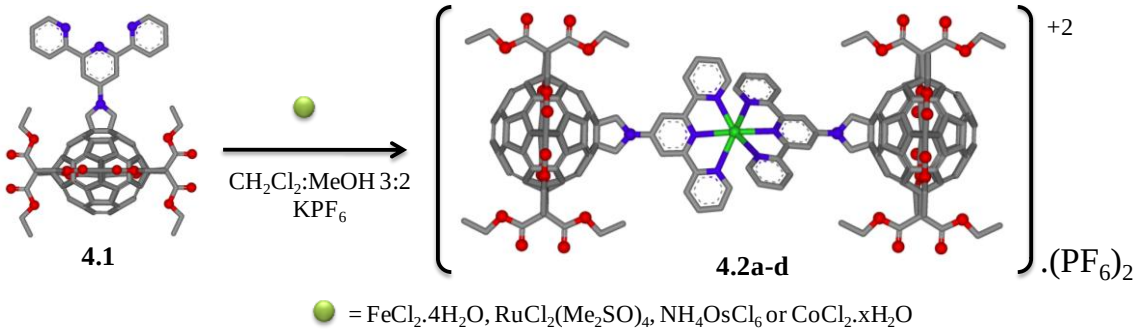

Scheme 4.1. Metal coordination of **4.1** with Fe (II) **4.2a**, Ru (II) **4.2b**, Os (II) **4.2c** and Co (II) **4.2d**.

Figure 4.1 shows the ^{1}H-NMR spectra of compounds **4.1** and **4.2a**. Protons H_5 and H_6 shift downfield from δ = 8.0 and 4.65 to δ = 8.12 and 5.05, respectively. Protons $H_{1\text{-}4}$ were shifted upfield from δ = 8.68, 8.63, 7.85 and 7.35 to δ = 7.28, 8.29, 7.75 and 7.17, respectively. This behavior was expected due to Fe^{2+} coordination with the N's of the terpyridyl group, which shields the protons $H_{1\text{-}4}$ upfield. The ^{1}H-NMR spectrum of compound **4.2a** exhibits high symmetry; only five signals were observed in the aromatic region that corresponded to 20 protons indicating that the two Tpy ligands are equivalent. This suggested that the Fe (II) complex has a D_{2d} symmetry (Tpy-Pyrr addends are in an orthogonal near-plane respect to the Fe).[11]

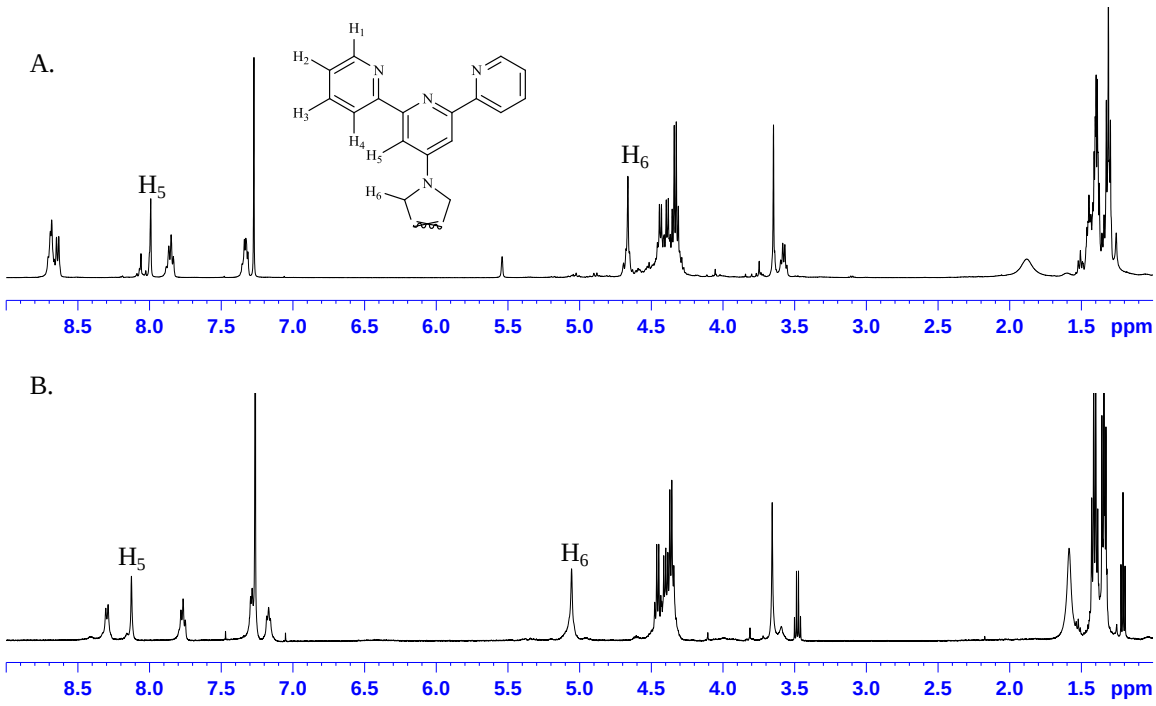

Figure 4.1 ^{1}H-NMR spectra of: (A) compound **4.1** and (B) compound **4.2a**. (500 MHz and $CDCl_3$).

Figure 4.2 shows the ESI MS spectra of compound **4.2a** and the corresponding simulation, confirming the structure of the complex. Figure 4.3 shows the ^{1}H NMR spectra of compounds **4.1** and **4.2b**. Complex **4.2b** shows that the aromatic protons shift upfield, the pyrrolidine protons (H_6) are not equivalent and shifted downfield from δ = 4.65 to δ = 4.79 and 4.97. This was attributed to the coordination of the Tpy-Pyrr groups with the metal ion Ru (II). The number of total signals was double relative to **4.1**; for example, eight signals for aromatic protons were observed. This indicates a different NMR environment for the two **4.1** units on complex **4.2b** and that the symmetry of complex was not D_{2d} as **4.2a**.

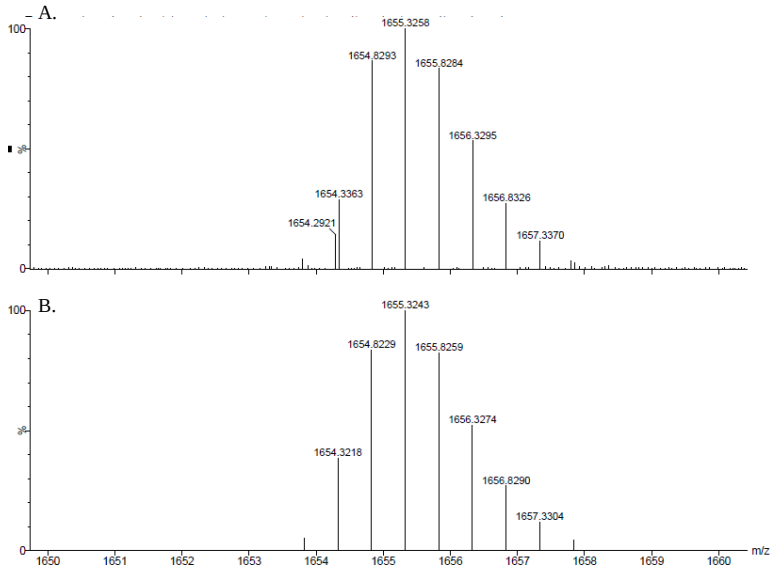

Figure 4.2. ESI MS spectra of: (A) compound **4.2a** and (B) simulation of compound **4.2a**.

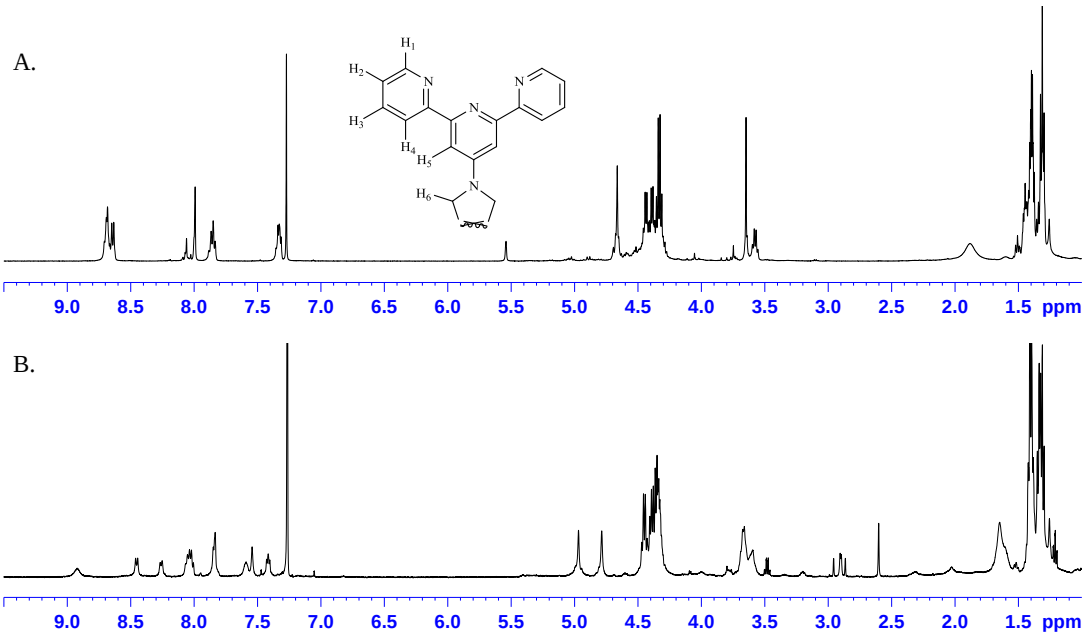

Figure 4.3. ^{1}H-NMR spectra of: (A) compound **4.1** and (B) compound **4.2b**. (500 MHz and $CDCl_3$).

The electrochemical behavior of complexes **4.2a** and **4.2b** was studied by means of cyclic voltammetry (CV) and Osteryoung Square Wave Voltammetry (OSWV) in a 3-electrode cell, using CH_2Cl_2 as solvent and $TBAPF_6$ as electrolyte. The CV of complex **4.2a** exhibited two one electron irreversible reduction processes (-1.57 and -1.93 V *vs* Fc/Fc^{+1}) and a one electron reversible oxidation process (0.35 V *vs* Fc/Fc^{+1}), Figure 4.4A. This reversible oxidation process is assigned to the Fe^{2+}/Fe^{3+} couple. The CV of complex **4.2b** only showed two one electron irreversible reduction processes (-1.62 and -2.06 V *vs* Fc/Fc^{+1}), Figure 4.4B. The redox couple Ru^{2+}/Ru^{3+} was not observed in this potential window.

Figure 4.5 shows the OSWV reduction scan of *tetrakis*-(ethoxycarbonyl)methano-C_{60} derivative (Curve A), compound **4.1** (Curve B), complex **4.2b** (Curve C) and complex **4.2a** (Curve D), respectively. The two peaks at -1.21 and -1.57 V *vs* Fc/Fc^{+1} in Curve A are fullerene based, therefore the peak at -1.56 V *vs* Fc/Fc^{+1} in Curve B is attributed to the Tpy ligand and the peaks at -1.41 and -1.77 V *vs* Fc/Fc^{+1} are fullerene based. The 20 mV cathodic shift of the peaks of Curve B with respect to Curve A is a typical for the addition of a new group on the sphere,[12] because it increases the LUMO energy level thus making it more difficult to reduce.[13] Curve C exhibits two fullerene based peaks at -1.62 and -2.06 V *vs* Fc/Fc^{+1} and no electrochemical response of the Tpy, which must mean that it was cathodically shifted out side of the potential window. Finally, Curve D shows two fullerene based peaks at -1.57 and -1.93 V *vs* Fc/Fc^{+1} and one peak at -2.20 V *vs* Fc/Fc^{+1} associated with the Tpy ligand. The peak of

the Tpy group was shifted by 64 mV compared to Curve B. Hence, the Ru(II) metal ion has a stronger effect on the Tpy groups compared to Fe(II).

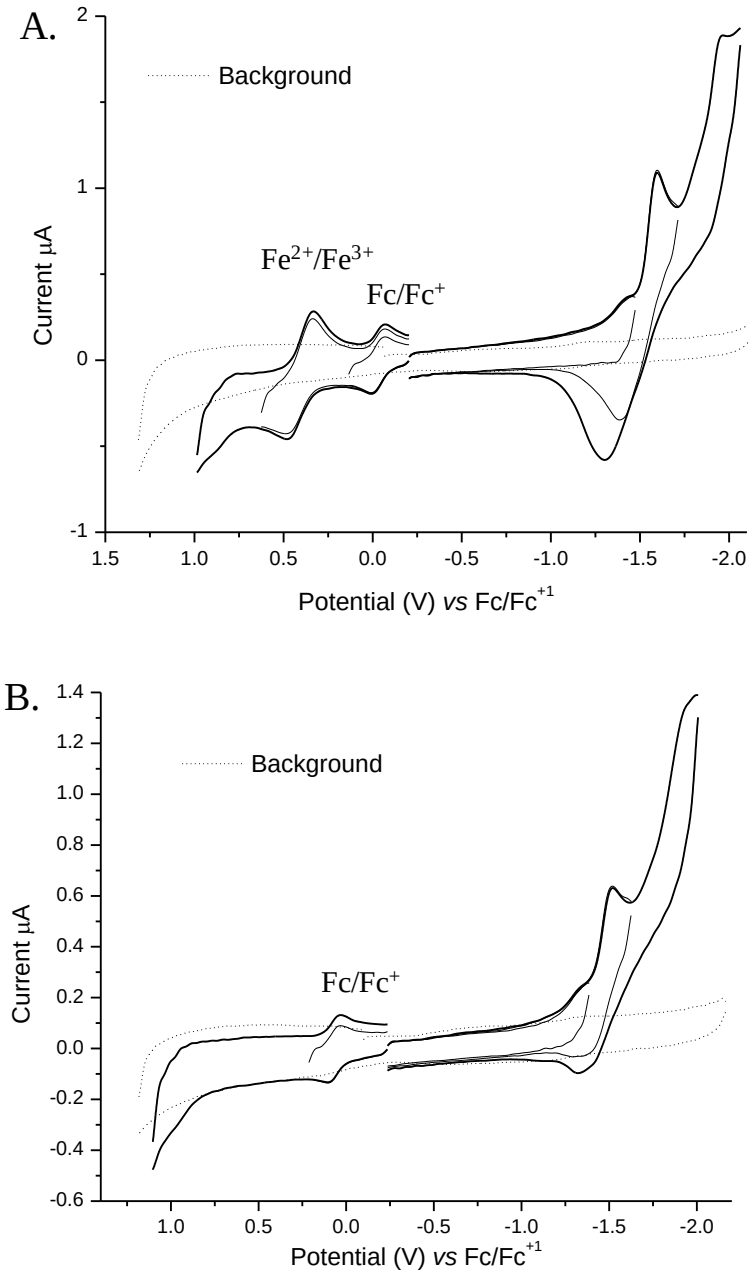

Figure 4.4. (A) Cyclic voltammogram (CV) of compound **4.2a** and (B) CV of compound **4.2b**. Supporting electrolyte: 0.1 M $TBAPF_6$ in CH_2Cl_2, Scan rate: 0.1 V s^{-1}.

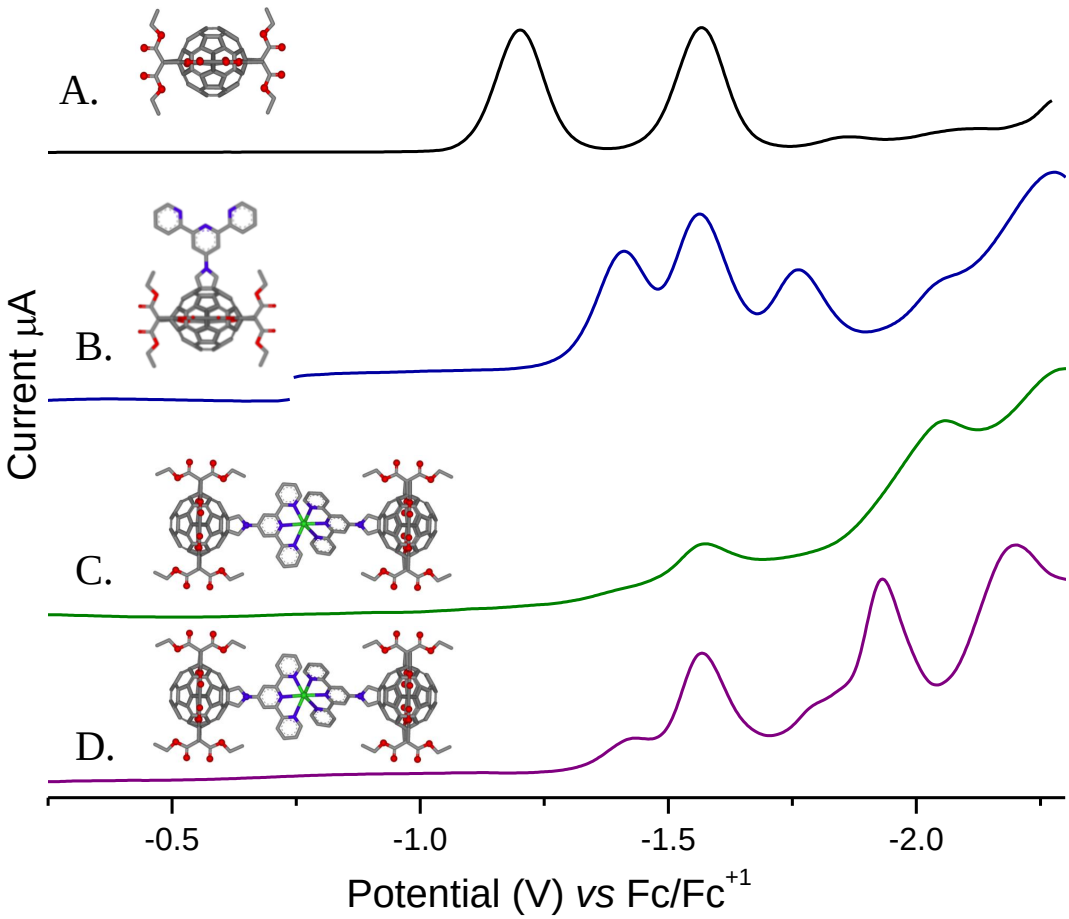

Figure 4.5. Osteryoung Square Wave Voltammetry (OSWV) in dichloromethane containing $TBAPF_6$ (0.1 M) for: (A) *tetrakis*-(ethoxycarbonyl)methano-C_{60} derivative; (B) compound **4.1**; (C) complex **4.2b** and (D) complex **4.2a**. Parameters: Step E 4 mV, S.W. amplitude 25 mV, S.W. frequency 15 Hz and quiet time 2 sec.

Compounds **4.2c** and **4.2d** were not isolated and characterized. Our purpose was to find the best metal to react with the derivatives, therefore the results from **4.2a** and **4.2b** were satisfactory enough to proceed to investigate larger systems, and these are discussed in the next section.

Fe(II) complexes of the *hexakis*-C_{60} adducts bearing Tpy and Py groups

Since Fe (II) worked best, the *hexakis*-adducts **4.3** (Scheme 4.3) and **4.4** (Scheme 4.4) were coordinated with Fe (II).

Fe (II) complex **4.3a**: 0.0046 mmol of **4.3** and 0.0023 mmol of $FeCl_2.4H_2O$ were mixed in 5 mL CH_2Cl_2:methanol 3:2 under argon at room temperature. The initial orange solution turned purple instantly. The reaction was stirred for 24 hours and protected from light, then 5 mL of 0.1 M KPF_6 in methanol was added. A purple solid was formed and separated using a centrifuge. Only one product (92%) was produced and fully characterized.

Fe (II) complex **4.4a**: 0.0057 mmol of **4.4** was mixed with 0.0029 mmol of $FeCl_2.4H_2O$ in 5 mL CH_2Cl_2:methanol 3:2 under argon at room temperature for 24 hours. The initial orange solution turned purple instantly. Then 5 mL of 0.1 M KPF_6 in methanol was added. A purple solid was formed and separated using the centrifuge. Only one product (90%) was formed and fully characterized.

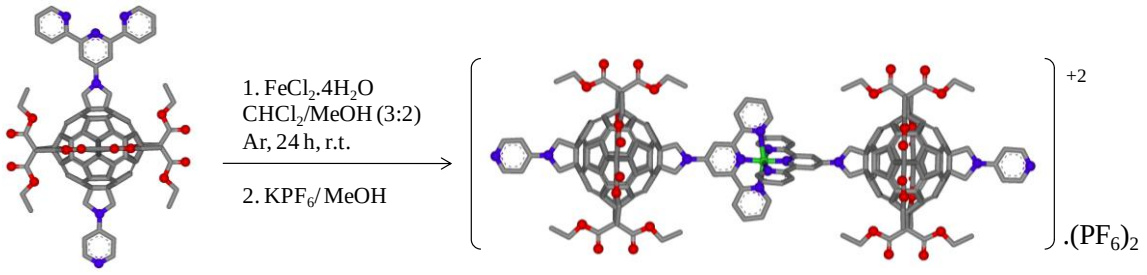

4.3 **4.3a**

Scheme 4.2 Synthesis of Fe (II)- complex **4.3a**.

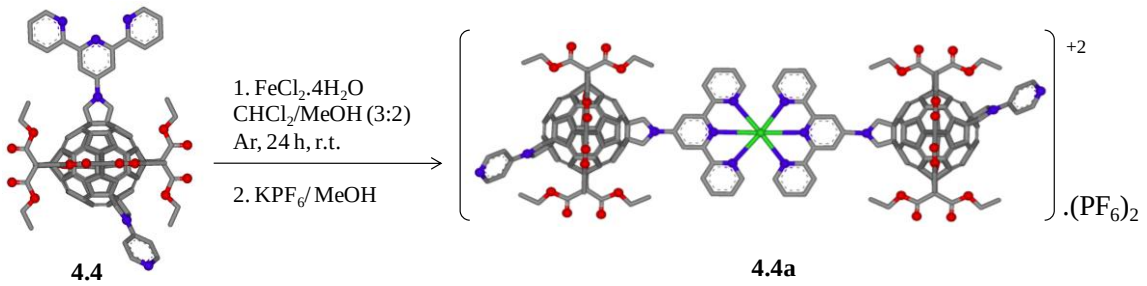

Scheme 4.3 Synthesis of Fe (II) complex **4.4a**.

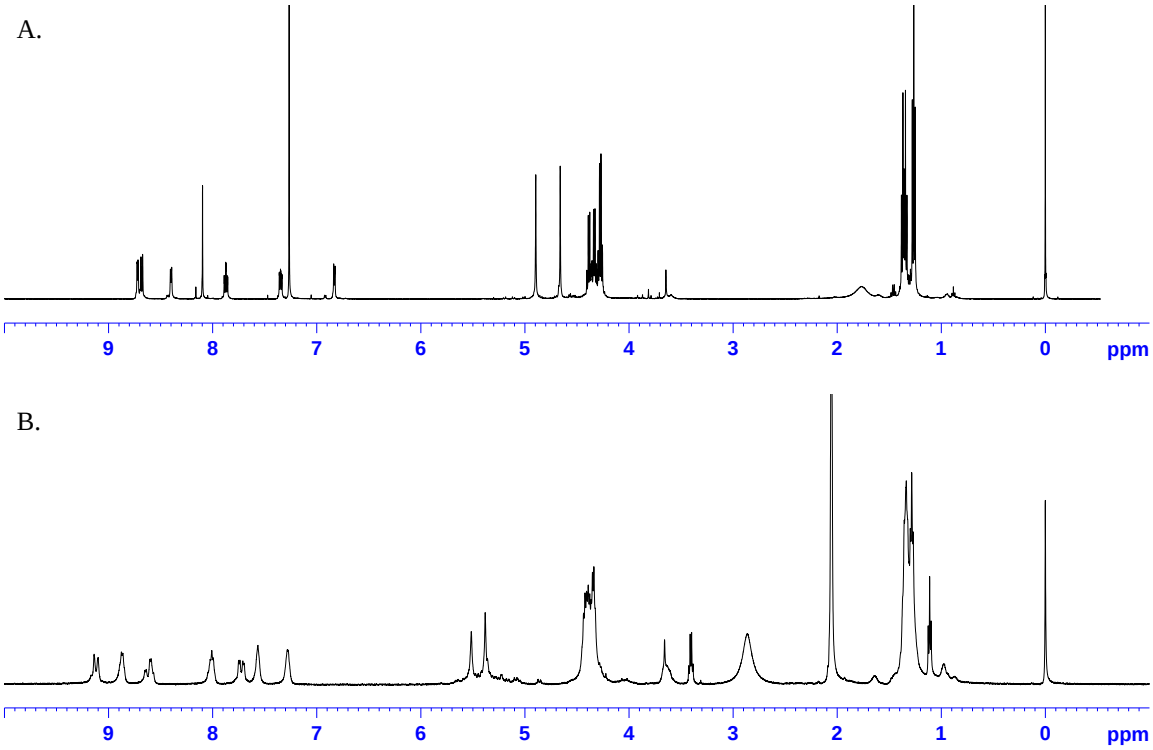

Figure 4.6. ^{1}H-NMR spectra of: (A) compound **4.3** (500 MHz and $CDCl_3$) and (B) compound **4.3a** (500 MHz and Acetone-d_6).

Figure 4.6 shows the ^{1}H-NMR spectra of compound **4.3** and complex **4.3a**. The D_{2h} symmetry of compound **4.3** was assigned by NMR spectroscopy. The ^{1}H-NMR spectrum (Figure 4.6A) displays three sets of triplets for CH_3 protons and three sets of quartets for -CH_2- protons of the malonate groups (with integration ratios of 6:6:12) between δ = 1.24 - 1.39 and δ = 4.25 - 4.40, respectively. One singlet for the methylene protons of the pyrrolidine ring of the Py-Pyrr addend and one singlet for the methylene protons of the pyrrolidine ring of the Tpy-Pyrr addend were observed at δ = 4.66 and 4.89, respectively. The aromatic region shows seven signals, two doublets for the pyridyl protons (δ = 6.83 and 8.40, respectively), four multiplets and one singlet corresponding to the terpyridyl protons (δ = 7.34, 7.87, 8.68, 8.72 and 8.09, respectively).

Even though the ^{1}H-NMR spectrum of **4.3a** (Figure 4.6B) was obtained in a different deuterated solvent than that used with **4.3** due to different solubilities, they were compared. The signals of the protons from the CH_3 and -CH_2- of the malonate groups appeared as multiplets between δ = 1.23 - 1.40 (integration 48) and δ = 4.32 - 4.47 (integration 32), respectively. The singlets at δ = 5.34 and 5.52 were assigned to the methylene protons of the pyrrolidine ring of the Py-Pyrr and Tpy-Pyrr addends, respectively. The seven signals of the aromatic region were assigned: two broad signals for the pyridyl protons (δ = 7.73 and 8.58, respectively) and five broad signals for the terpyridyl protons (δ = 7.29, 7.57, 8.02, 8.58 and 9.13, respectively). The same high symmetry and number of signals observed for **4.3** were observed for **4.3a,** indicating the same symmetry.

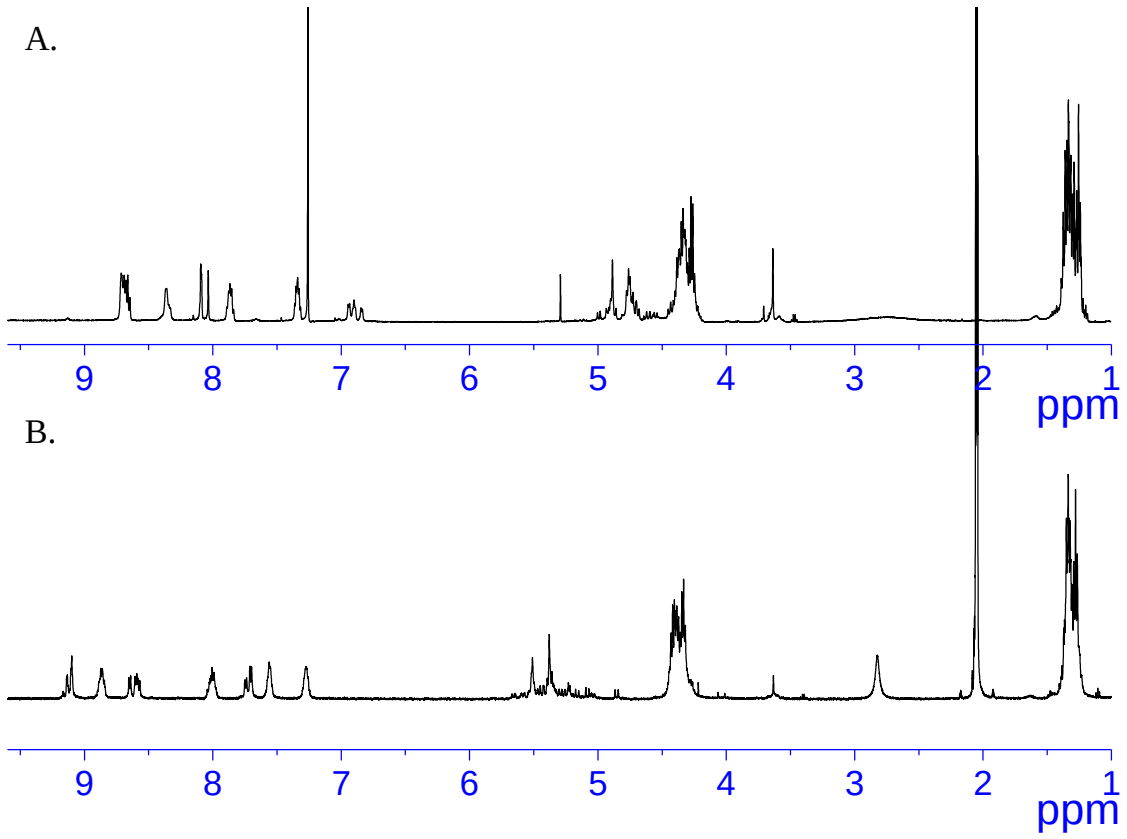

Figure 4.7. ^{1}H-NMR spectra of: (A) compound **4.4** (500 MHz and $CDCl_3$) and (B) compound **4.4a** (500 MHz and Acetone-d_6).

Complex **4.4a** was characterized by means of ^{1}H-NMR spectroscopy (Figure 4.7B) and compared with compound **4.4** (Figure 4.7A) even though they were analyzed in different deuterated solvents due to different solubilities. The ^{1}H-NMR spectrum of compound **4.4** shows two multiplets between δ = 1.24 - 1.38 and δ = 4.26 - 4.35 assigned to the methyl and methylene protons of the malonate groups, respectively. Two multiplets between δ = 4.73 - 4.78 and δ = 4.87 - 4.90 corresponding to the methylene protons of the pyrrolidine ring of the Py-Pyrr addend and the Tpy-Pyrr addends were observed, respectively. The aromatic region illustrates nine signals, three multiplets and two singlet signals

corresponding to the terpyridyl protons (δ = 7.34, 7.87, 8.66, 8.70, 8.04 and 8.10, respectively).

The signals from the ^{1}H-NMR spectrum of **4.4a** (Figure 4.7B) were broader, but they retain the same symmetry, which was expected for the coordination of **4.4** with Fe(II). It shows two multiplets between δ = 1.27 - 1.36 and δ = 4.32 - 4.42 assigned to the methyl and methylene protons from the malonate groups, respectively. Multiplet signals between δ = 5.05 to 5.67 were assigned to the methylene protons of the pyrrolidine ring of the Py-Pyrr and Tpy-Pyrr addends. Ten signals were displayed in the aromatic region, four doublets for the pyridyl protons (δ = 7.70, 7.74, 8.60 and 8.65, respectively) and six broad signals for the terpyridyl protons (δ = 7.27, 7.56, 8.00, 8.86, 9.10 and 9.13, respectively).

Finally, the molecular weight of complex **4.4a** was confirmed by MALDI-TOF MS (Figure 4.8). The electrochemistry of the complexes **4.4a** was also studied and will be discussed in the next section.

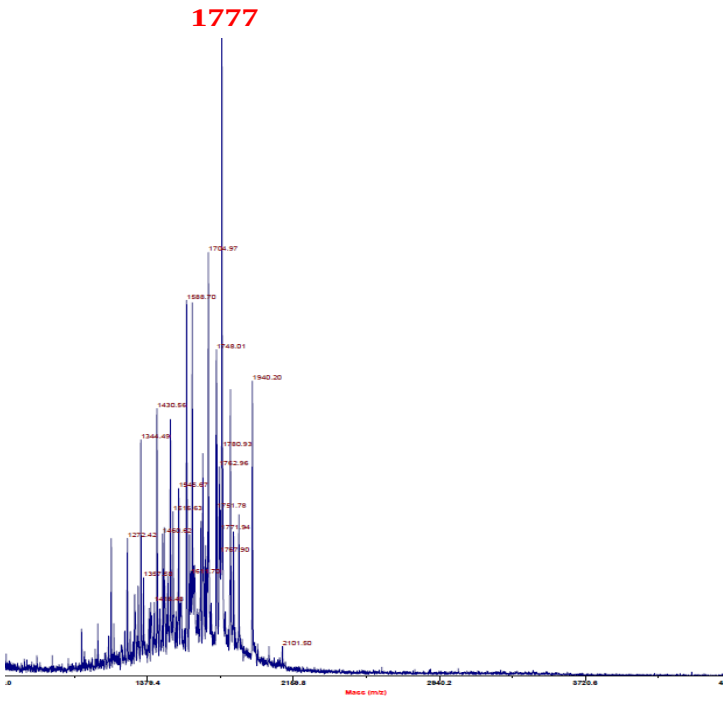

Figure 4.8. MALDI-TOF MS spectrum of complex **4.4a**.

Controlled potential electrolysis of complexes 4.2a and 4.4a

In Chapter III, we introduced the controlled potential electrolysis (CPE) process as a useful tool to remove the malonate addends. So, we explored the electrochemical behavior of complexes **4.2a** and **4.4a** upon electrolysis. All experiments were carried out using a homemade cell, previously described, under high vacuum with 0.1M $TBAPF_6$ as the supporting electrolyte.[14]

Electrolysis of complex **4.2a**: It was already mentioned that **4.2a** exhibits two one-electron irreversible reduction processes (Figure 4.19A) and a one-electron reversible oxidation process. The complex has eight malonate groups, therefore it was expected to require 16 electrons to remove all the addends. Electrolysis of 5 mg of **4.2a** was carried out in a solution of 0.1 M $TBAPF_6$ in CH_2Cl_2 under vacuum and the CV showed two

reversible processes after 10 electrons had been discharged through the solution at -1.7 V (Figure 4.9B). The addition of 10 electrons per molecule probably removes ~ 5 addends and leads to a compound exhibiting a reversible electrochemistry. After 16 electrons per molecule had been discharged at -1.85 V the CV still showed reversible reduction processes (Figure 4.9C). The *mono*-terpyridylpyrrolidino-C_{60} derivative (Figure 4.10) was identified from the crude reaction by means of MALDI-TOF MS spectrometry (Figure 4.10), after performing an exhaustive re-oxidation at 0 V.

These results clearly indicate that electrolysis removed the eight malonate groups of the complex but somehow also the ion metal Fe (II) was lost during the electrolytic process to form *mono*-terpyridylpyrrolidino-C_{60} derivative (Figure 4.10).

Electrolysis of complex **4.4a**: The CV of complex **4.4a** exhibited two one electron irreversible processes at -1.50 and -1.84 V and a one electron reversible process assigned to the couple Fe^{2+}/Fe^{3+}at 0.66 V, Figure 4.11. Electrolysis was conducted at different potentials (-1.80, -1.90 and -2.0 V, respectively), but the retro-cyclopropanation did not proceed under these conditions.

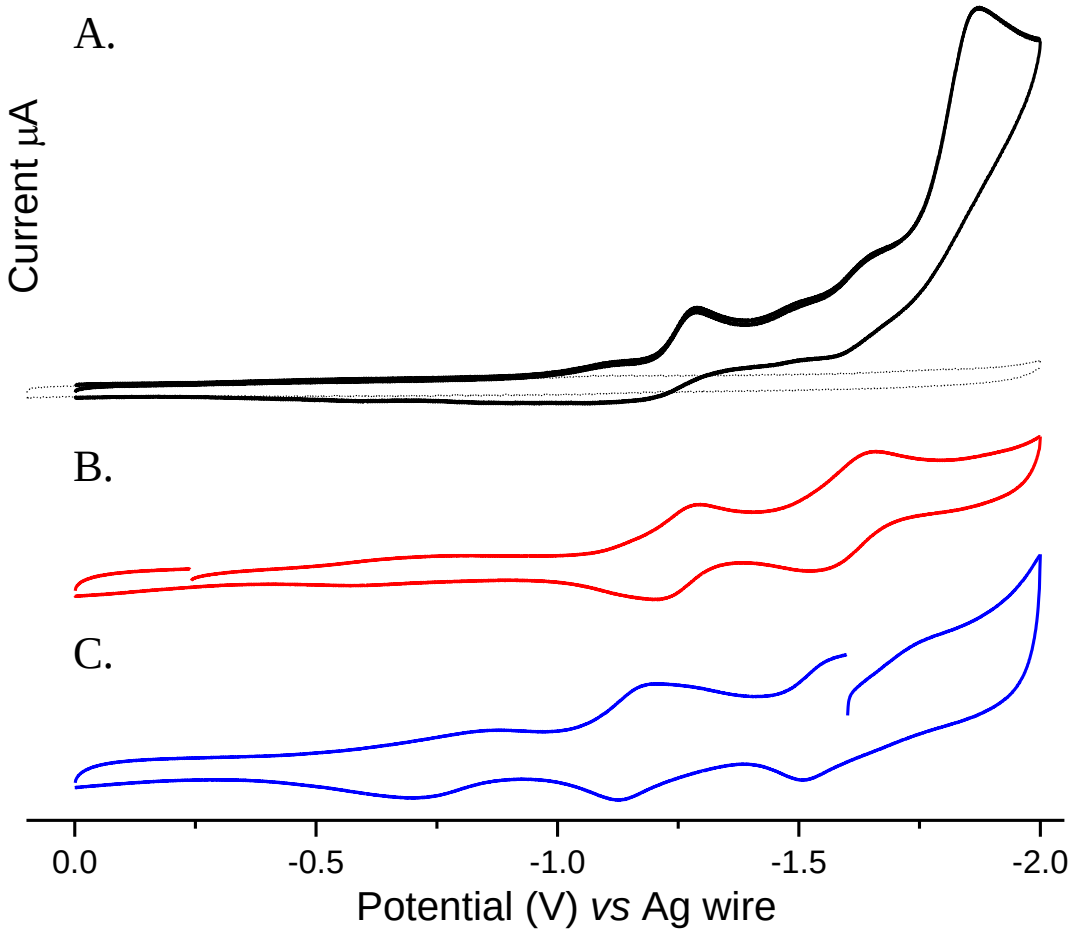

Figure 4.9. Electrolysis of compound **4.2a**: (A) Cyclic voltammogram (CV) of compound **4.2a** before electrolysis; (B) CV of **4.2a** after the discharge of 10 electrons and (C) CV of **4.2a** after the discharge of 16 electrons. Supporting electrolyte: 0.1 M $TBAPF_6$ in CH_2Cl_2, Scan rate: 0.1 V s^{-1}.

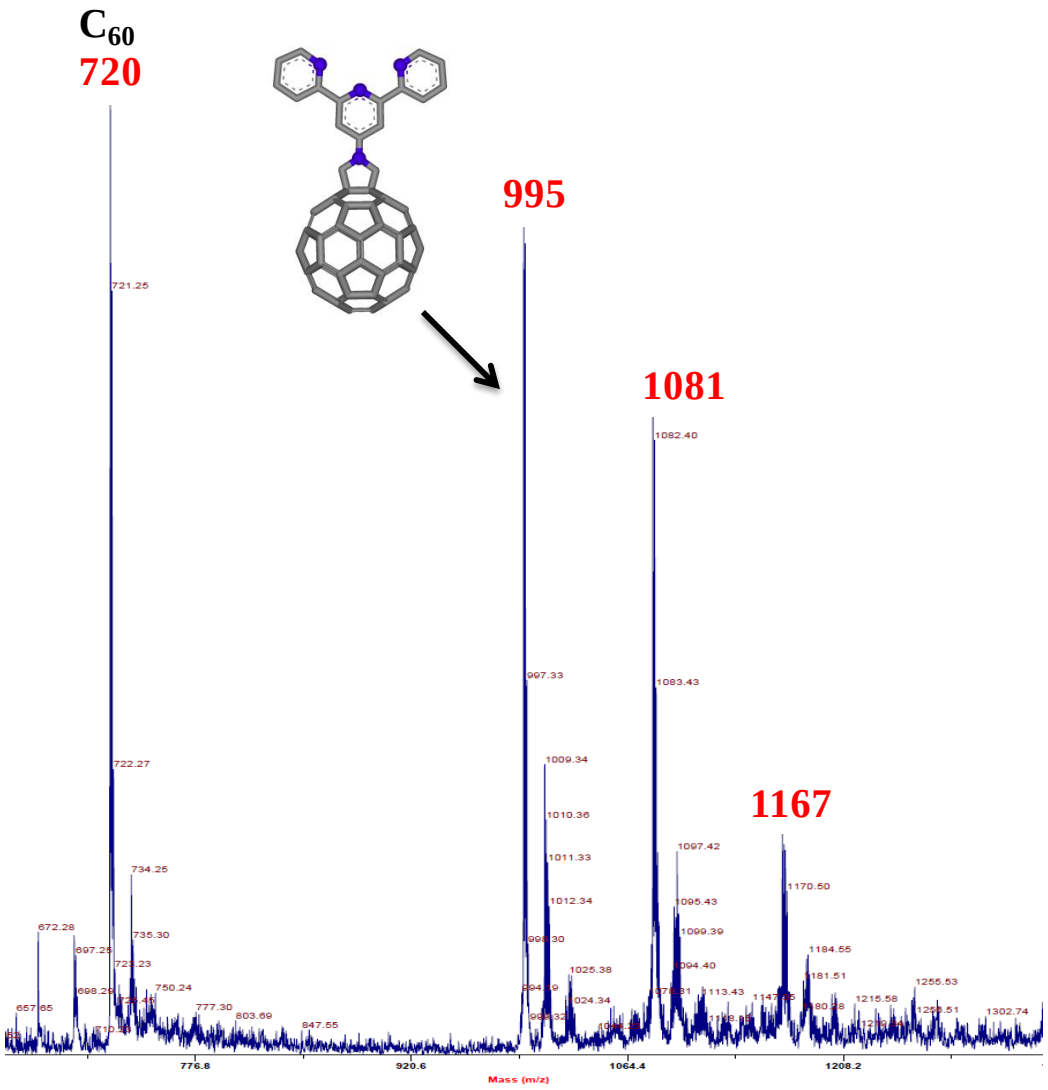

Figure 4.10. MALDI-TOF spectrum of the crude reaction of the electrolysis of **4.2a**.

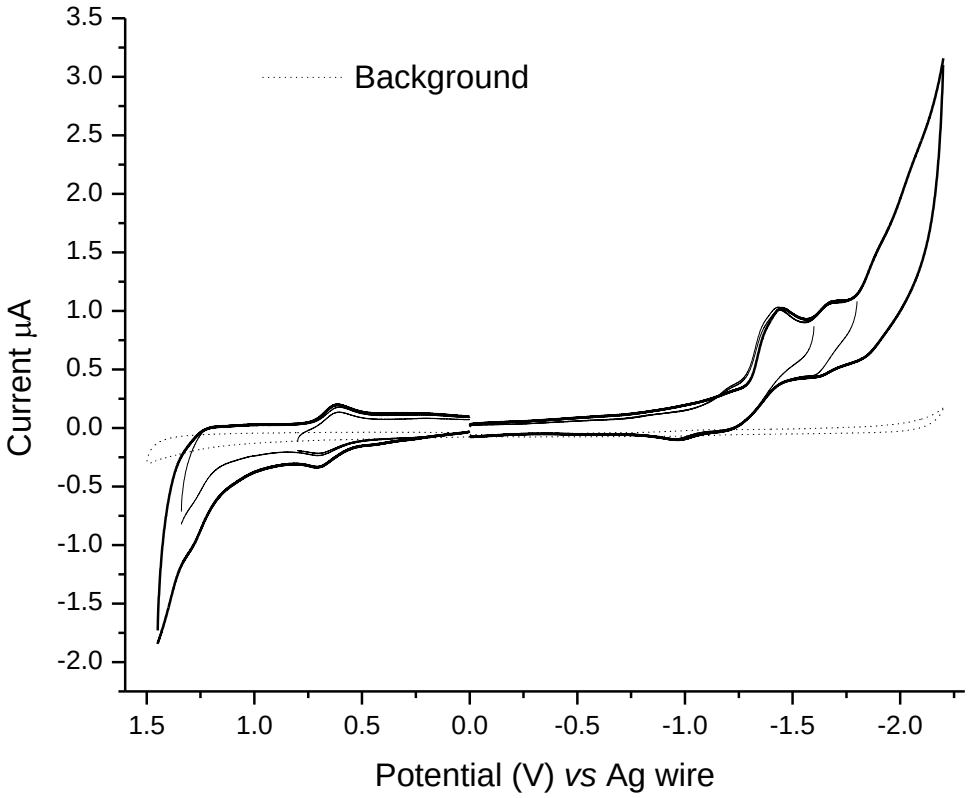

Figure 4.11. Cyclic voltammograms (CV) of complex **4.4a** under vacuum. Supporting electrolyte: 0.1 M $TBAPF_6$ in CH_2Cl_2, Scan rate: 0.1 V s^{-1}.

In order to increase the potential window, the CPE was performed in ACN at -1.9 V. The electrolysis was stopped after the addition of 12 electrons per molecule and re-oxidized at 0 V. Figure 4.13 shows the CV recorded immediately after CPE. It shows the reversible processes indicative of to cyclopropane addend removal and the *trans-2*-pyridylpyrrolidino-terpyridylpyrrolidino-C_{60} derivative was detected in the crude reaction by MALDI-TOF MS (*m/z*= 1114, Figure 4.13). The peaks at *m/z* = 995 and 720 were assigned to *mono*-terpyridylpyrrolidino-C_{60} derivative and C_{60}, respectively.

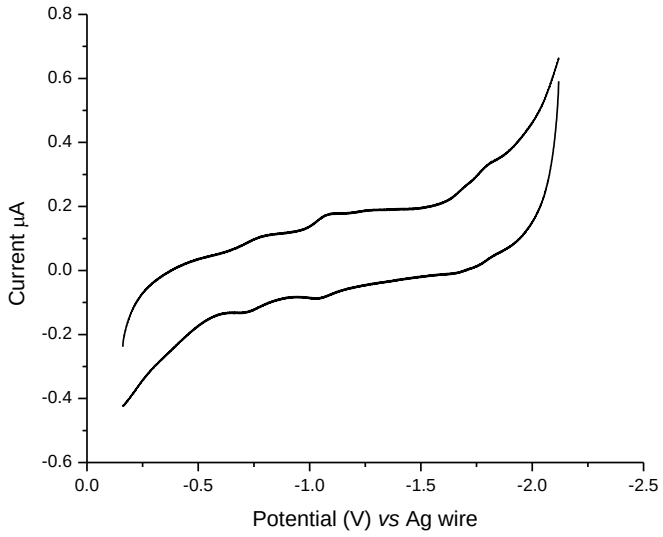

Figure 4.12. Electrolysis of compound **4.4a**: Cyclic voltammogram of compound **4.4a** after the discharge of 12 electrons per molecule. Supporting electrolyte: 0.1 M $TBAPF_6$ in CH_3CN, Scan rate: 0.1 V s^{-1}.

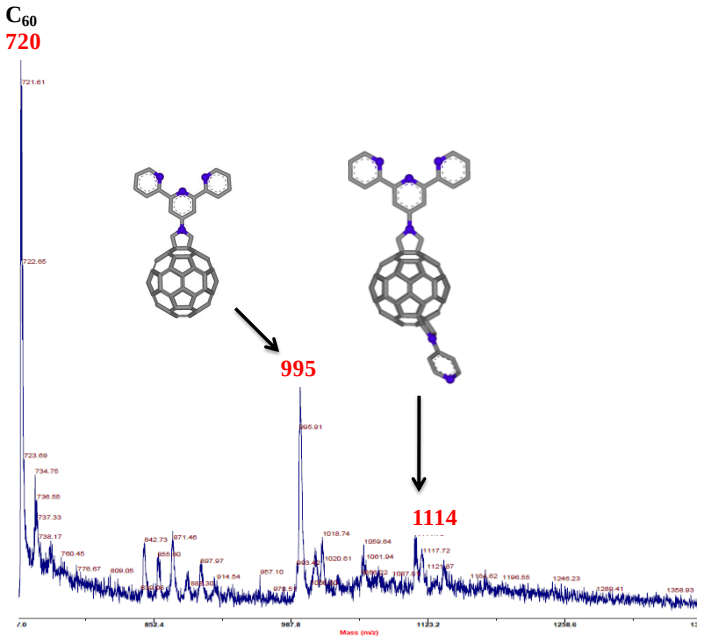

Figure 4.13. MALDI-TOF spectrum of the crude reaction of the electrolysis of **4.4a**.

It can be concluded that the CPE of the complexes **4.2a** and **4.4a** led to successful removal of the cyclopropane addends and the loss of the Fe (II). Hence, it can be used as an alternative route for the synthesis of the *bis*- and *tris*-adducts proposed in Chapter I.

Conclusions

Chapter IV described the formation of metal complexes of some of the C_{60} derivatives with a Tpy-Pyrr addend from the compound library describe in Chapter II. The metals Fe (II) and Ru (II) were used for the metal-directed self assembly process being Fe (II) metal the most suitable. Fe(II)-C_{60} derivative complexes with a D_{2d} symmetry (Tpy-Pyrr addends were in an orthogonal near-plane respect to the Fe) were obtained in high yields (>90%) and full characterized.

Also, they were stable at room temperature, air, light and oxidative conditions but unstable under reductive conditions. Removal of the cyclopropane addends and loss of the Fe (II) ion metal was achieved upon reduction conditions using CPE.

References

[1] A. Ortiz, D. Riviera, A. Athans and L. Echegoyen, *Eur. J. Org. Chem.*, **2009**, 3396-3403.

[2] (a) S. Zhang, D. Dong, L. Gan, Z. Liu, C. Huang, *New J. Chem.*, **2001**, *25*, 606-610; (b) S. Lan Jeon, D. Loveless, W. Yount and S. Craig. *Inorg. Chem.*, **2006**, *45*, 11060-11068.

[3] J-P. Sauvage, J-P. Collin, J-C. Chambron, S. Guillerez and C. Coudret, *Chem. Rev*. **1994**, *94*, 993-1019.

[4] (a) M. Kabešová, B. Boča, M. Melník, D. Valigura and M. Dunaj-Jurčo, *Coord. Chem. Rev.*, **1995**, *140*, 115. (b) J. Ciszek, and J. Tour, *Chem. Mater.* **2005**, *17*, 5684. (c) J. Ciszek, Z. Keane, L. Cheng, M. Stewart, L. Yu, D. Natelson, and J. Tour, *J. Am. Chem. Soc.* **2006**, *128*, 3179-3189.

[5] L. Pirondini, F. Bertolini, B. Cantadori, F. Ugozzoli, C. Massera and E. Dalcanale, *Proc. Natl. Acad. Sci.* **2002**, *99*, 4911-4915.

[6] (a) S. Zhang, , *Nature Nanotechnology*, **2006**, *1*, 169 – 170; (b) L. Lindoy and Atkinson. Self-Assembly in supramolecular Systems. Cambridge:R.S.C. **2000**, 117-184; (c) R. Krámer, J-M. Lehn and A. Marquis-Rigault, *Proc. Natl. Acad. Sci.* **1993**, *90*, 5394 -5398.

[7] S. Leininger, B. Olenyuk and P. J. Stang, *Chem. Rev.*, **2000**, *100*, 853-908.

[8] J-M. Lehn, *Science*, **2000**, *295*, 2400-2403.

[9] G .F. Swiegers and T. J. Malefetse, *Chem. Rev.* **2000,** *100*, 3483-3537.

[10] I. P. Evans, A. Spencer and G. Wilkinson, *J. Chem. Soc., Dalton Trans*, **1973**, 204-209.

[11] E. C. Constable, *Chem. Soc. Rev.*, **2007**, *36*, 246–253

[12] L. Echegoyen and L. E. Echegoyen, *Acc. Chem. Res.*, **1998**, *31*, 593–601.

[13] S. Zhang, O. Lukoyanova, and L. Echegoyen, *Chem. Eur. J*. **2006**, *12*, 2846-2853.

[14] a) R. Kessinger, J. Crassous, A. Herrmann, M. Rottimann, L. Echegoyen and F. Diederich, *Angew. Chem. Int. Ed.* **1998**, *37*, 1919–1922; b) J. Crassous, J. Rivera, N. S. Fender, L. H. Shu, L. Echegoyen, C. Thilgen, A. Hermann and F. Diederich, *Angew. Chem. Int. Ed.* **1999**, *38*, 1613–617; c) M. A. Herranz, F. Diederich and L. Echegoyen, *Eur. J. Org. Chem*. **2004**, 2299–316.

CHAPTER FIVE

ELECTROCHEMICAL PROPERTIES OF SUPRAMOLECULES: PHTHALOCYANINE AND PORPHYRIN DERIVATIVES

In this Chapter, the electrochemical behavior of some phthalocyanines and porphyrins derivatives under electroreductive and oxidative conditions are discussed in detail, as well as the experimental techniques used to conduct these studies. Phthalocyanine compounds were provided by Fernando Fernandez-Lazaro at Universidad Miguel Hernández de Elche, Spain and porphyrin compounds were provided by David Schuster group at New York University, New York City, USA.

Electrochemistry of silicon phthalocyanine azobenzene derivatives

Phthalocyanines (Pc) are planar aromatic macrocycles that have been used as building blocks for the preparation of a wide variety of materials with outstanding electronic and optical properties, ranging from nonlinear optical applications to photoconductors.[1] These properties depend on the type of central atom and/or the substituents present. For example, silicon-phthalocyanine (SiPcs) derivatives have been shown to possess antitumor activity under photodynamic conditions.[2] The SiPcs are also of great interest because of the possibility of axial substitution that enhances their solubility.[3] For instance, azobenzene-SiPc-azobenzene (Azo-SiPc-Azo) is a photoswitchable derivative, where the axially coordinated azoarene forms an on-off (E-Z states) fluorescence signal that can help to modulate the emission properties of Azo-SiPc-Azo.[3] In this section, we report the effect of different axial substituents on the electrochemical properties of SiPc (Figure 5.1). Compounds **5.1** – **5.5** and **5.1'** – **5.5'**

were received in pure form from the research group of Professor Fernando Fernandez-Lazaro at Universidad Miguel Hernández de Elche, Spain.

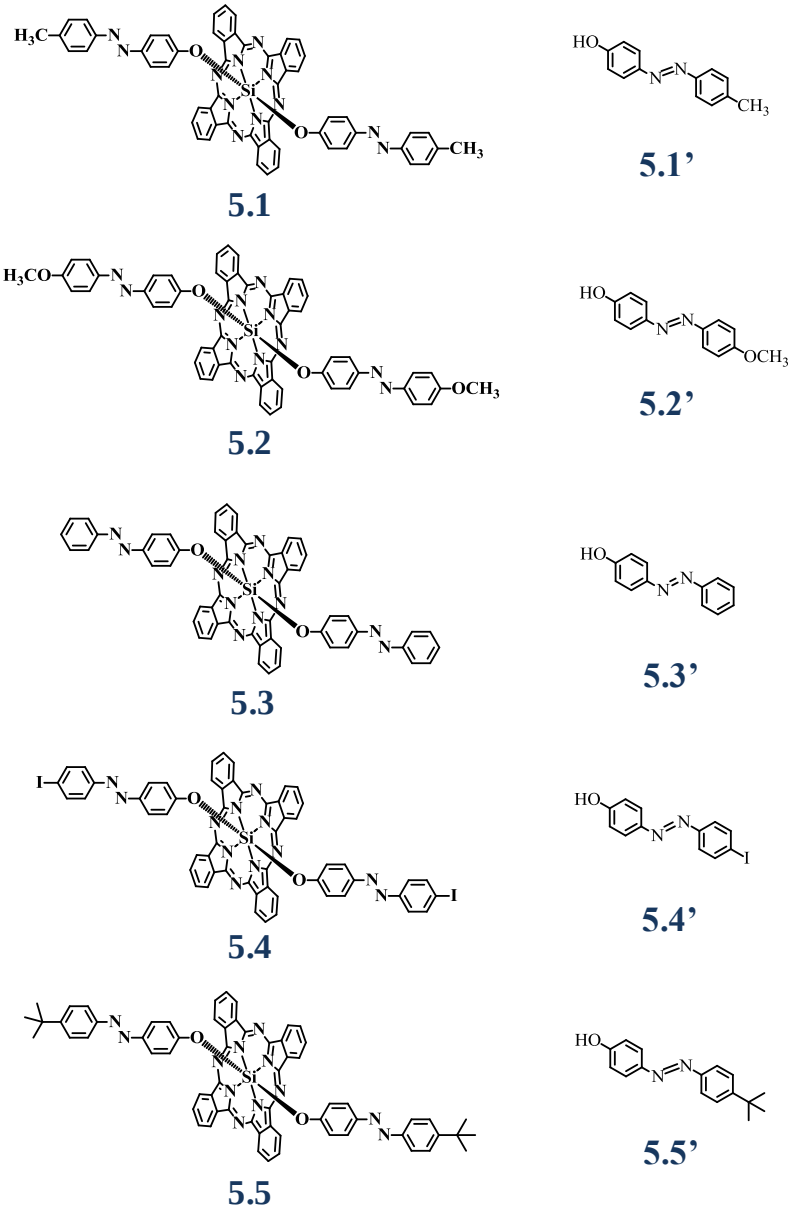

Figure 5.1. Azobenzene-phthalocyanine-azobenzene compounds (**5.1**-**5.5**) and their respective azobenzene compound reference (**5.1'**-**5.5'**).

Figure 5.2 shows the CV of: (A) azo-SiPc-azo compounds (**5.1**-**5.5**) and (B) azoarene reference compounds (**5.1'**-**5.5'**). Each azo-SiPc-azo shows two reversible one-electron reduction processes coming from the Pc and at least two irreversible reduction peaks above -1.7 V *vs* Fc/Fc^{+} that correspond to reduction processes of the azoarene group. This is the typical electrochemical behavior of these macrocycles compounds: two reversible one-electron reduction processes and generally one reversible one-electron oxidation process.[4]

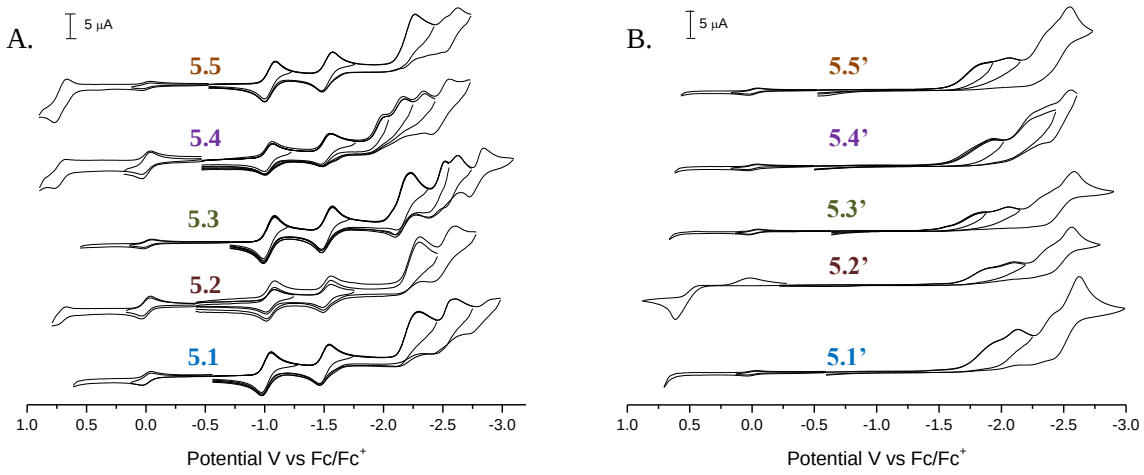

Figure 5.2. Cyclic voltammograms (CV) in THF containing $TBAPF_6$ (0.1 M) for: (A) Azo-SiPc-Azo compounds **5.1**-**5.5**; (B) Azobenzene reference compounds **5.1'**-**5.5'.** Sweep rate was 100 mV s^{-1}.

The electrochemical potentials are summarized in Table 5.1. Comparing the third reduction potential of azo-SiPc-azo with of its azoarene groups **5.1'-5.5'** the following can be concluded: Compounds **5.1**, **5.3** and **5.4** had a cathodic shift about 10 mV and compounds **5.2** and **5.5** had a cathodic shift about 30 mV. This indicated that the azo-SiPc-azo is more difficult to reduce than the azoarene group, which is likely due to charge transfer between the donors (SiPc) and the acceptor (azobenzenes addends).

Table 5.1. Electrochemical potentials E/V *vs* Fc/Fc^{+} measured in THF containing (0.1 M) as supporting electrolyte.

Compound	**Reduction Potentials (V)**						**Oxidation Potentials (V)**
	E^1	**E^2**	**E^3**	**E^4**	**E^5**	**E^6**	**E^1**
5.1	-1.02[a]	-1.51[a]	-2.31[b]	-2.54[b]	-2.97[b]	--	--
5.1'	--	--	-2.12[b]	-2.51[b]	-2.66[b]	--	--
5.2	-1.05[a]	-1.53[a]	-2.31[b]	-2.60[b]	--	--	0.83[b]
5.2'	--	-1.37[b]	-2.04[b]	-2.47[b]	--	--	0.71[b]
5.3	-1.03[a]	-1.50[a]	-2.16[b]	-2.46[b]	-2.56[b]	-2.73[a]	--
5.3'	--	--	-2.04[b]	-2.54[b]	--	--	--
5.4	-1.04[a]	-1.51[a]	-1.99[b]	-2.17[b]	-2.35[b]	-2.58[b]	0.78[b]
5.4'	--	--	-1.88[b]	-2.17[b]	--	-2.47[b]	0.73[b]
5.5	-1.05[a]	-1.53[a]	-2.27[b]	-2.63[b]	-2.85[b]	--	0.73[a]
5.5'	--	-1.79[b]	-2.01[b]	-2.45[b]	--	--	--

[a] Denotes $E_{1/2}$ potentials. Range 60-92 mV of anodic-to-cathodic peak separation.
[b] Denotes a peak potential for an electrochemically irreversible wave.

As seen from the CV illustrated in Figure 5.2, the oxidation process was not measured because the potential was close to the end of the available solvent potential window. Therefore, all the experiments were carried out in dichloromethane in order to find the first oxidation peak and thus measure the HOMO-LUMO energy gap of each azo-SiPc-azo compound. Figure 5.3 shows the OSWV for compounds **5.1**-**5.5** and **5.1'**-**5.5'** obtained in dichloromethane. The same cathodic shift of the third reduction potential in the range of 20–55 mV was observed for the azo-SiPc-azo **5.1**-**5.5** compounds. Their electrochemical potentials and HOMO-LUMO energy gaps are summarized in Table 5.2.

Figure 5.4 represents the two energy gaps of each azo-SiPc-azo compound as follows: **(a)** difference between 1st oxidation potential and 1st reduction potential of each azo-SiPc-azo compound and **(b)** difference between 1st oxidation potential and 3rd reduction potential (the 3rd process is assigned to the reduction of the azobenzene ligand) of each azo-SiPc-azo compound.

Each azo-SiPc-azo compound has a similar HOMO-LUMO^{b} gap in the range 1.67 - 1.70 V *vs* Fc/Fc^{+} (Figure 5.4, curve a, Table 5.2 HOMO-LUMO^{b}). In the case of HOMO-LUMO^{c} compounds **5.1**, **5.2**, **5.3** and **5.5** have similar energy gaps in the range 2.83 - 2.90 V *vs* Fc/Fc^{+}, but for compound **5.4** the energy gap is smaller 2.67 V (Figure 5.4, curve b, Table 5.2 HOMO-LUMO^{c}). This effect was expected base on the difference in electron donating ability between I and the other substituent.

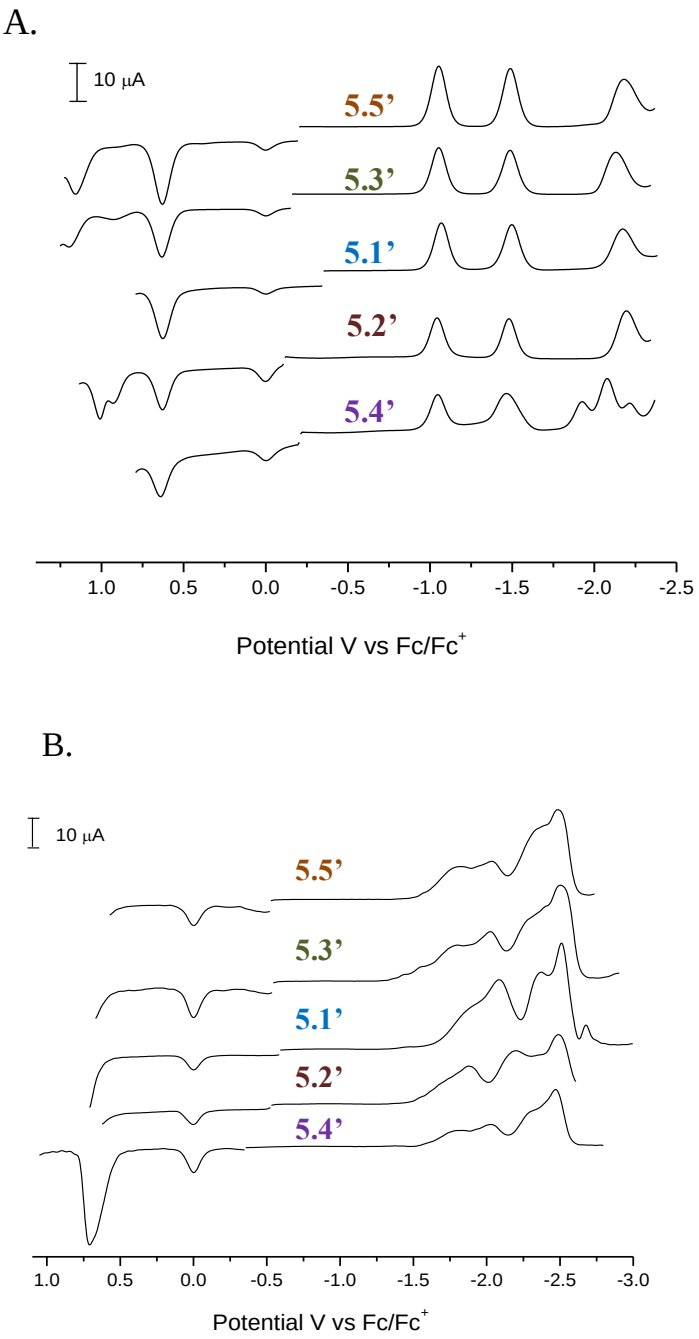

Figure 5.3. Osteryoung square wave voltammetry (OSWV) in dichloromethane containing $TBAPF_6$ (0.1 M) for: (A) Azo-SiPc-Azo compounds **5.1-5.5**; (B) Azobenzene reference compounds **5.1'-5.5'.** Parameters: Step E 4 mV, S.W. amplitude 25 mV, S.W. frequency 15 Hz and quiet time 2 sec.

Table 5.2. Electrochemical potentials E/V *vs* Fc/Fc^+ measured in dichloromethane containing $TBAPF_6$ (0.1 M) as supporting electrolyte.

Compound	Reduction Potentials (V)					Oxidation Potentials		HOMO LUMO[c]	HOMO LUMO[d]
	E^1	E^2	E^3	E^4	E^5	E^1	E^2	ΔE (V)	ΔE (V)
5.1	-1.07[a]	-1.50[a]	-2.22[b]	--	--	0.62[a]	--	1.69	2.84
5.1'	--	--	-1.67[b]	--	--	--	--		
5.2	-1.04[a]	-1.49[a]	-2.26[b]	--	--	0.63[a]	1.04[b]	1.67	2.89
5.2'	--	-1.58[b]	-1.89[b]	--	--	0.72[b]	--		
5.3	-1.06[a]	-1.49[a]	-2.20[b]	--	--	0.63[a]	1.21[b]	1.69	2.83
5.3'	--	--	-1.89[b]	--	--	--	--		
5.4	-1.06[a]	-1.47[a]	-2.03[b]	-2.12[b]	-2.26[b]	0.64[b]		1.70	2.67
5.4'	--	--	-1.83[b]	--	--	--	--		
5.5	-1.05[a]	-1.49[a]	-2.27[b]	--	--	0.63[a]		1.68	2.90
5.5'	--	--	-1.84[b]	--	--	--	--		

[a] Denote $E_{1/2}$ potentials. Range 60-92 mV of anodic-to-cathodic peak separation.
[b] Denotes a peak potential for an electrochemically irreversible wave.
[c] HOMO-LUMO: $\Delta E = E_{oxi\text{-}1st} - E_{red\text{-}1st}$
[d] HOMO-LUMO: $\Delta E = E_{oxi\text{-}1st} - E_{red\text{-}3rd}$

Conclusion: The azo-SiPc-azo compounds exhibit cathodic shifts of more than 10 mV for the 3rd reduction process. This third reduction is assigned to the first reduction process of the azobenzene group. Thus these dyads compounds are harder to reduce than the reference compound due to charge transfer between the donor (phthalocyanine) and the acceptor (azobenzenes). The HOMO-LUMO[c] of the phthalocyanine compounds is not affected by the azobenzene substituents and the HOMO-LUMO[d] of the phthalocyanine compounds does not exhibit any special behavior or trend.

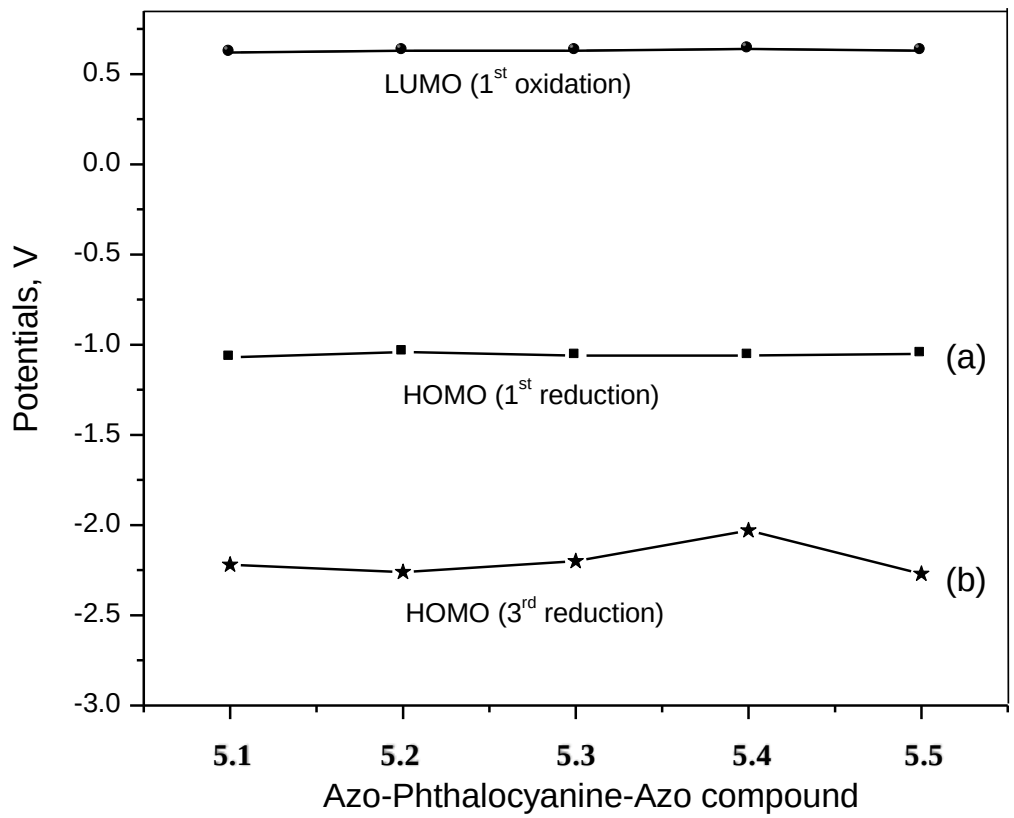

Figure 5.4. Electrochemically measured HOMO and LUMO energy levels of each Azobenzene-SiPc-Azobenzene **5.1-5.5**: **curve a:** HOMO from 1st reduction potential, **curve b:** HOMO from 3rd reduction potential and **curve c:** LUMO from 1st oxidation potential.

Electrochemistry of Triazole-Linked Porphyrin-Fullerene Dyads

Electron-transfer (ET) processes and long-lived charge separated states (CS) of Porphyrin-fullerene dyads have been studied because of implications of in optoelectronic applications. C_{60} is a good electron acceptor and the porphyrin compounds are good electron donors,[5] so one of the principal targets has been the synthesis of different bridges that can act as efficient and unsymmetric electronic coupling agents between the donor-acceptor groups. Therefore, characteristics such as the length conjugation and angle of the bridge have been modified and reported.[6] Here we report the electrochemical study of a series of triazole-linked porphyrin-fullerene dyads (Figure 5.5) and their triazole bridge units (Figure 5.6) by means of CV and differential pulse voltammetry (DPV).

Figure 5.7a shows the CVs of porphyrin compounds **5.6'**, **5.8'**, **5.10** and Figure 5.7b shows the CVs of **5.7'**, **5.9'** and **5.11**, bridge units. Except for **5.8'** each CV shows two reversible one-electron oxidation processes, one reversible one-electron reduction process and one irreversible one-electron reduction process, similar to previously reported results.[7] **5.8'** is an exception and exhibits one reversible and two irreversible one-electron reduction processes.

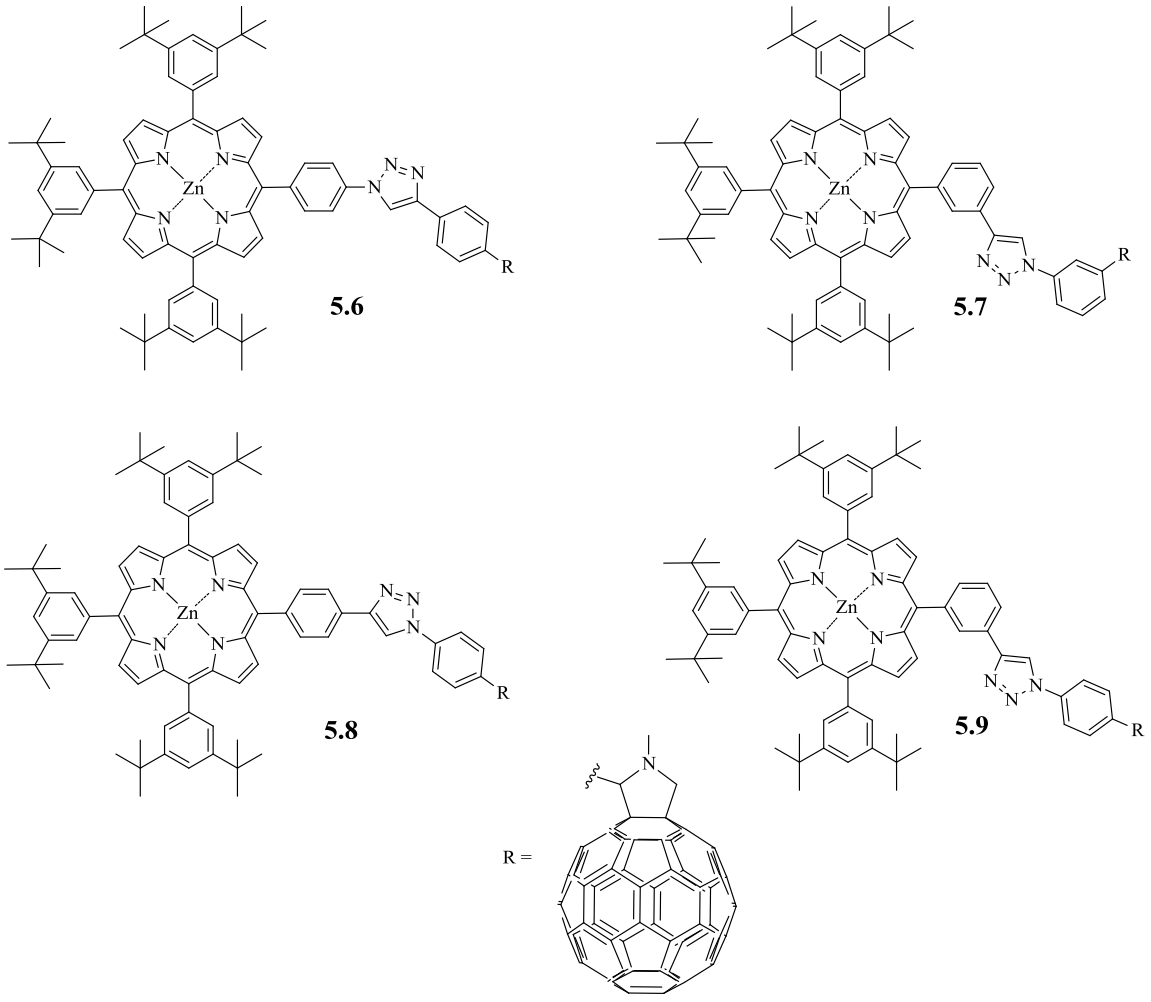

Figure 5.5 Triazole-linked porphyrin-fullerene dyads **5.6**-**5.9**.

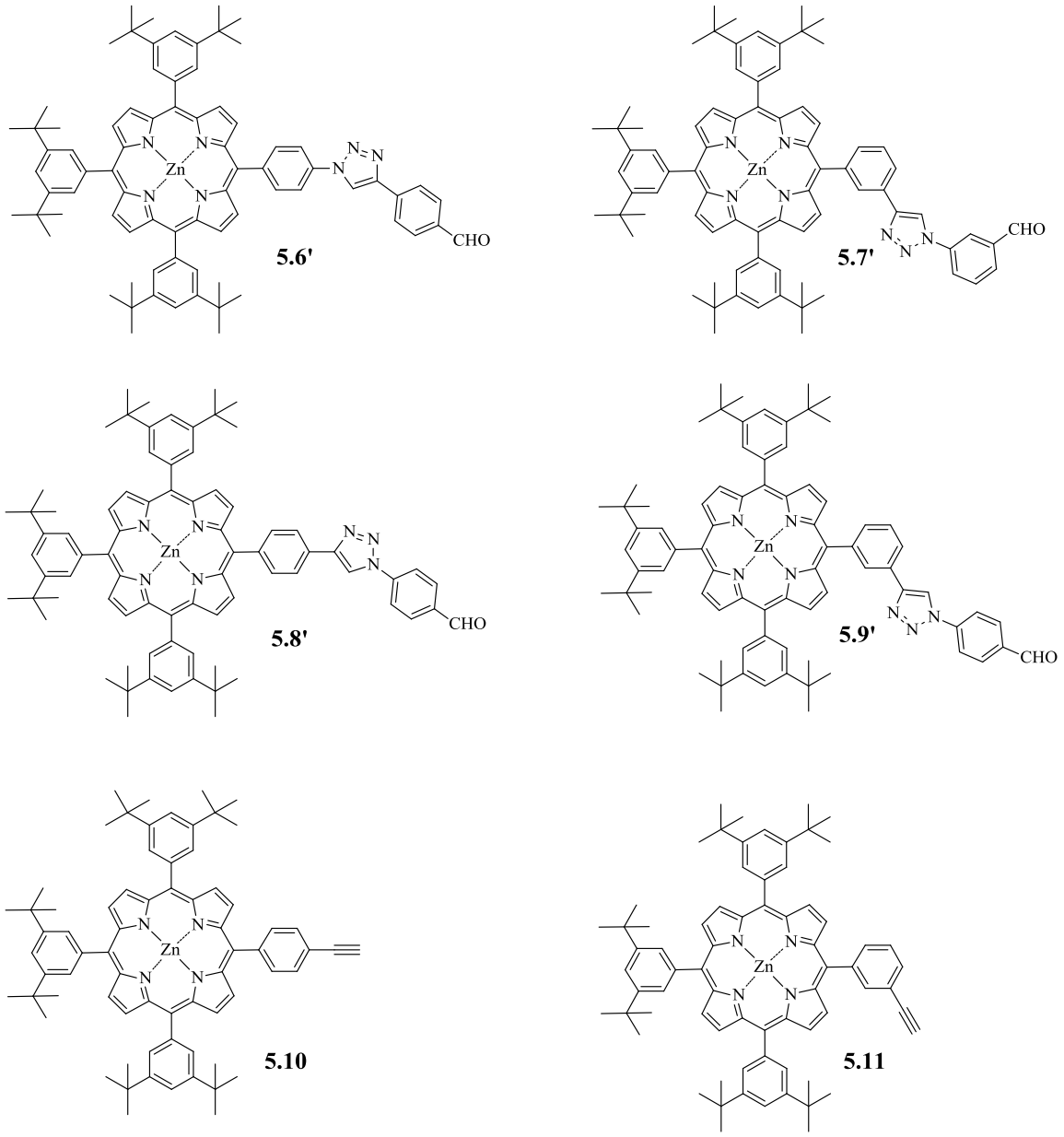

Figure 5.6. Porphyrin dyads **5.6'-5.9'** and **5.10-5.11**.

From the CV (Figure 5.7) as well as from the DPV (Figure 5.8) of **5.6'** and **5.8'**, it can be seen that the first reduction and oxidation potentials are shifted anodically by 20-100 mV compared to **5.10**. Thus, they are easier to reduce and harder to oxidize relative to the parent compound, **5.10**. This was attributed to the stronger electron-withdrawing effect of the triazole group.[8] In the case of the **5.7'** and **5.9'**, an anodic shift is observed when compared to **5.11** for the first reduction potential (20 mV) and a cathodic shift for the first oxidation potential (20 mV). This last effect could be attributed to the *meta* connection of the triazole group, which makes it easier to reduce and to oxidize.

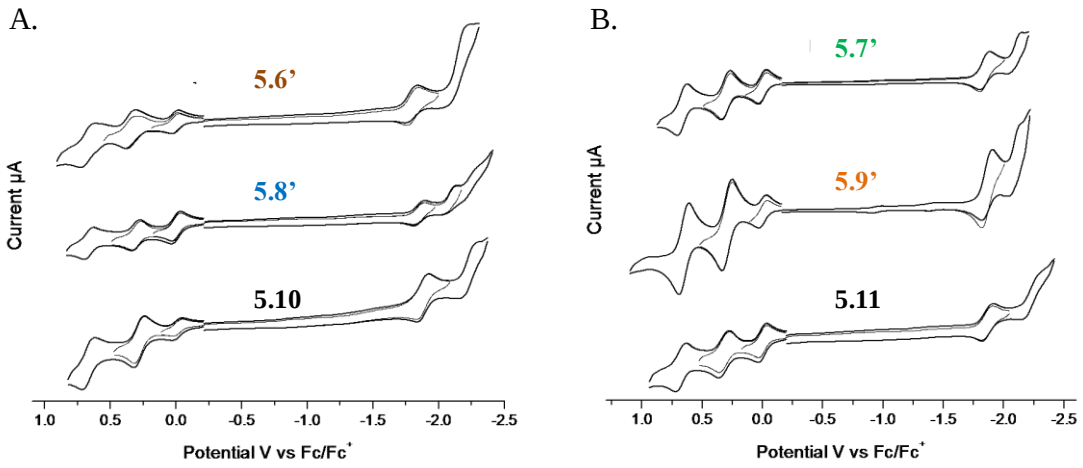

Figure 5.7. Cyclic voltammograms (CV) in CH_2Cl_2 containing $TBAPF_6$ (0.1 M) for: (A) **5.6'**-triazole, **5.8'**-triazole, **5.10** compounds and (B) **5.7'**-triazole, **5.9'**-triazole and **5.11** reference compounds. Sweep rate was 100 mV s^{-1}.

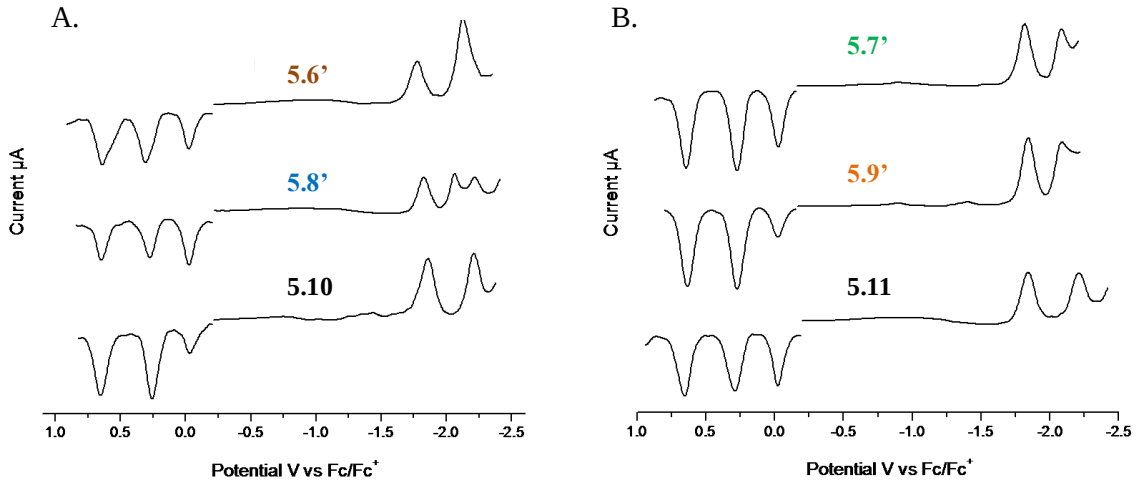

Figure 5.8. Differential pulse voltammetry (DPV) in CH_2Cl_2 containing $TBAPF_6$ (0.1 M) for: (A) **5.6'**-triazole, **5.8'**-triazole, **5.10** compounds and (B) **5.7'**-triazole, **5.9'**-triazole and **5.11** reference compounds.Sweep rate was 100 mV s^{-1}.

Figure 5.9A shows the CV of **5.6**, **5.7**, **5.8**, and **5.9**. These compounds show two oxidation and at least four reduction processes. The first oxidation peak is attributed to the triazole group (**5.6'-5.9'**), which was shifted cathodically (30, 10, 40 and 20 mV for compounds **5.7**, **5.9**, **5.6** and **5.8**, respectively). The first and the second reductions correspond to the fulleropyrrolidine unit, while the third appears to be centered on the porphyrin, based on the values obtained for the reference compounds (**5.6'-5.9'**, Figure 5.10). The first reduction peak of the dyads **5.6**, **5.8**, **5.9** and **5.7**, is shifted cathodically (60, 30, 50 and 90 mV, respectively) compared to the first reduction potential (-1.07 V) of N-methyl-2-pyridylfulleropyrrolidine (**5.12**, Figure 5.11), reported previously.[8]

The third reduction peak of **5.7**, **5.9**, **5.6** and **5.8** shift cathodically (50, 30, 100 and 10 mV, respectively) with respect to the corresponding reference triazole porphyrin compound (**5.7'**, **5.9'**, **5.6'** and **5.8'**, respectively). This indicates that the dyads **5.6**-**5.9**

are harder to reduce compared to the triazole reference compounds **5.6'-5.9'** and **5.12**, which is a result of the charge transfer between the donors (porphyrin) and the acceptor (fullerene moiety). The two extra reduction peaks in the DPV of **5.6** (Figure 5.9b) are not currently assigned. They may result from contamination with pristine C_{60}.

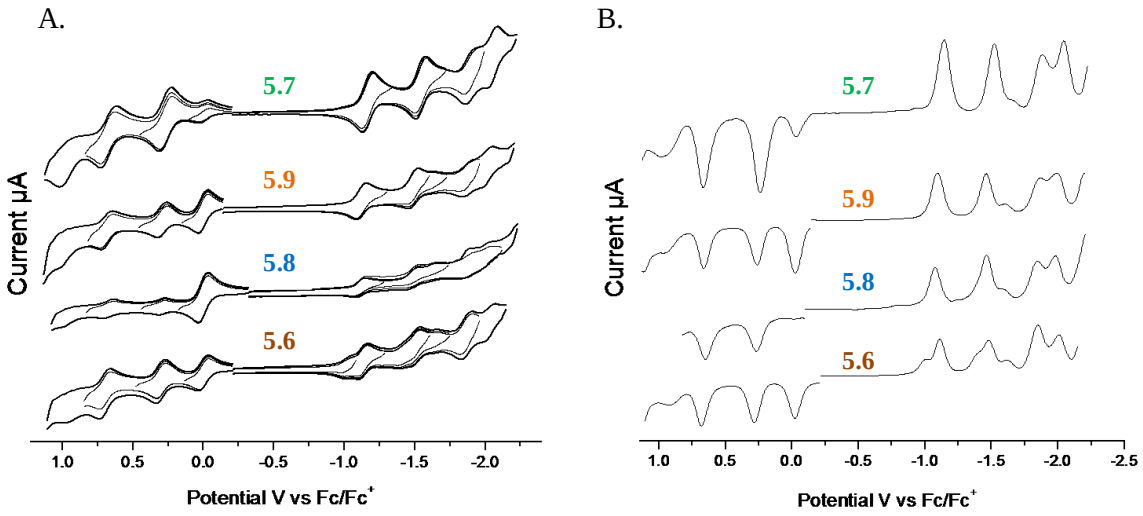

Figure 5.9. (A) Cyclic voltammograms (CV) in CH_2Cl_2 containing $TBAPF_6$ (0.1 M) for **5.6**, **5.8**, **5.9**, and **5.7**; (B) Differential pulse voltammetry (DPV) in CH_2Cl_2 containing $TBAPF_6$ (0.1 M) for **5.6**, **5.8**, **5.9**, and **5.7**. Sweep rate was 100 mV s^{-1}.

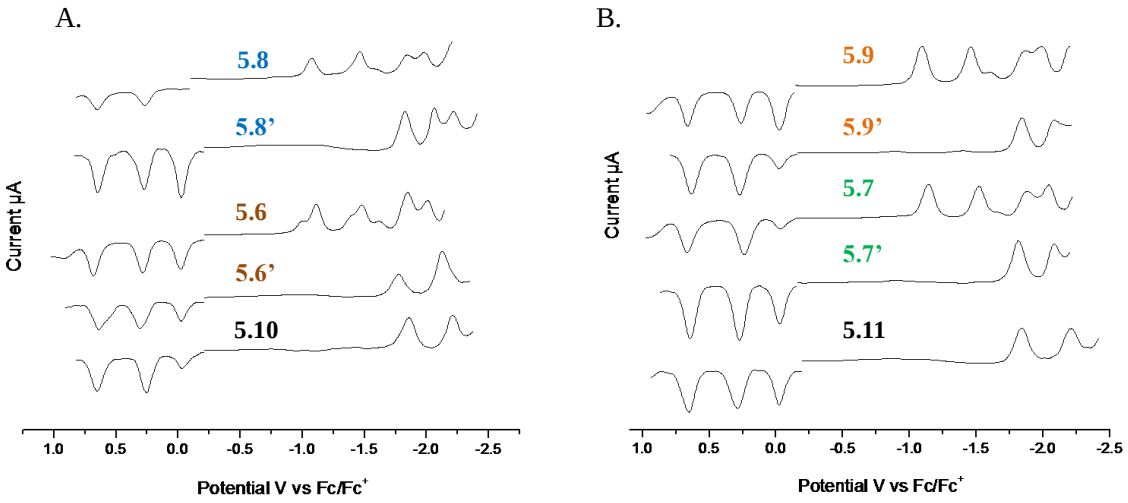

Figure 5.10. (A) Differential pulse voltammetry (DPV) in CH_2Cl_2 containing $TBAPF_6$ (0.1 M) for **5.10**, **5.6'**, **5.6**, **5.8'** and **5.8**; (B) Differential pulse voltammetry (DPV) in CH_2Cl_2 containing $TBAPF_6$ (0.1 M) for **5.11**, **5.7'**, **5.7**, **5.9'** and **5.9**.

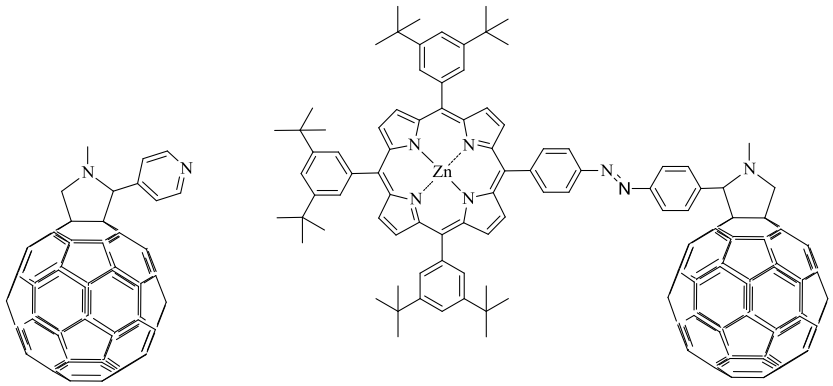

5.12 **5.13**

Figure 5.11. (A) N-methyl-2-pyridylfulleropyrrolidine (2-NMFP).[8] (B) Azobenzene-linked porphyrin-fullerene dyad.[9]

Table 5.3 reports all the electrochemical potentials of these series of dyads and their respective reference compounds. Two energy gaps are calculated for each dyad: **a)** HOMO-LUMO[c] difference between the 1st oxidation potential and the 1st reduction potential of the dyads **5.6-5.9** and **b)** HOMO-LUMO[d] difference between the 1st oxidation potential and the 3rd reduction potential (the 3rd process is assigned to the reduction of the porphyrin ligand) of the dyads **5.6-5.9**. Every dyad has a similar HOMO-LUMO[c] and HOMO-LUMO[d] gap (139-143 mV) and (215-218 mV), respectively. Also, the HOMO-LUMO[c,d] gaps were similar to that of compound **5.13** (Figure 5.11) as previously reported.[9] No strong influence is observed due to the presence of the triazole group.

Conclusion: The CV and DPV of the dyads **5.6-5.9** closely correspond to the sum of the independent electrochemical features of the fullerene and porphyrin moieties. Their third reduction potential was assigned to the first reduction process of the triazole porphyrin compounds **5.6'-5.9'**, which showed cathodic shifts of more than 10 mV. This cathodic shift can be assigned to the electronic coupling between the fullerene and the porphyrin. The HOMO-LUMO gap of the dyads does not show any unusual behavior or trend.

Table 5.3. Electrochemical potentials E/V *vs* Fc/Fc^+ measured in dichloromethane containing $TBAPF_6$ (0.1 M) as supporting electrolyte.

Compound	Reduction Potentials (V)							Oxidation Potentials (V)		HOMO LUMO[c]	HOMO LUMO[d]
	E^1	E^2	E^3	E^4	E^5	E^6	E^7	E^1	E^2	ΔE (V)	ΔE (V)
5.6	-1.02[b]	-1.13[a]	-1.54[b]	-1.67[b]	-1.87[a]	-2.01[b]	--	0.30[a]	0.70[a]	1.43	2.17
5.8	--	-1.10[a]	-1.49[a]	-1.67[b]	-1.86[b]	-2.01[b]	--	0.29[a]	0.68[a]	1.39	2.15
5.7	--	-1.16[a]	-1.54[a]	--	-1.89[b]	-2.05[b]	--	0.27[a]	0.67[a]	1.43	2.16
5.9	--	-1.12[a]	-1.49[a]	--	-1.89[b]	-2.02[b]	--	0.29[a]	0.69[a]	1.41	2.18
5.6'	--	--	--	--	-1.77[a]	-2.13[b]	--	0.34[a]	0.69[a]	2.11	--
5.8'	--	--	--	--	-1.85[a]	-2.09[b]	-2.24[b]	0.31[a]	0.67[a]	2.16	--
5.10	--	--	--	--	-1.87[a]	--	-2.22[b]	0.29[a]	0.69[a]	2.16	--
5.7'	--	--	--	--	-1.84[a]	-2.10[b]	--	0.30[a]	0.67[a]	2.14	--
5.9'	--	--	--	--	-1.86[a]	-2.10[b]	--	0.30[a]	0.65[a]	2.16	--
5.11	--	--	--	--	-1.86[a]	--	-2.22[b]	0.32[a]	0.68[a]	2.18	--
5.12[e]	--	-1.07[a]	-1.45[a]	--	-1.98[a]	--	--	--	--	--	--
5.13	--	-1.07[a]	-1.45[a]	--	-1.82[a]	-1.99[b]	--	0.34[a]	0.69[a]	1.41	2.16

[a] Denote $E_{1/2}$ potentials. Range 60-92 mV of anodic-to-cathodic peak separation.
[b] Denotes a peak potential for an electrochemically irreversible wave.
[c] HOMO-LUMO: $\Delta E = E_{oxi\text{-}1st} - E_{red\text{-}1st}$
[d] HOMO-LUMO: $\Delta E = E_{oxi\text{-}1st} - E_{red\text{-}3rd}$
[e] N-methyl-2-pyridylfulleropyrrolidine[7]

Experimental Section

The electrochemical studies of compounds **5.1-5.10** and **5.1'-5.9'** were performed in oxygen-free anhydrous dichloromethane (DCM, Sigma-Aldrich, anhydrous, 99.8%) and distilled tetrahydrofuran (THF, Sigma-Aldrich, anhydrous, 99.9%). Tetrabutylammonium hexafluorophosphate ($TBAPF_6$, Fluka, 99%) was added as a supporting electrolyte. It was recrystallized two times from ethanol and was dried under vacuum for 24 hours prior to use. The CV, OSWV, and DPV experiments were performed with either a Model CHI440A (CH Instruments Electrochemical Workstation) or potentiostat/galvanostat BAS100B (Bioanalytical Systems Inc.) (potentiostat/galvanostat). A standard three-electrode configuration was used with a glassy carbon working electrode (Cypress, 1.0 mm), a platinum wire as the auxiliary electrode (Aldrich, 1.0 mm) and a non-aqueous reference electrode (Ag/Ag^+). The redox couple Fc/Fc^+ was used as internal standard. The experiments were performed at room temperature and protected from light. The half-wave potential, $E_{1/2}$, was determined as $(E_{pa} + E_{pc})/2$, where E_{pa} and E_{pc} are the anodic and cathodic peak potentials from the CV. Additionally, $E_{1/2}$, was checked by DPV experiments using the equation: $E_{max(DPV)} = E_{1/2} - (\Delta E/2)$, where ΔE is the pulse amplitude (50 mV).[10]

References

[1] (a) N. B. McKeown, *Adv. Mater*., **1999**, *11*, 67-69; (b) J. Silver, J. L. Sosa-Sánchez and C. S. Frampton, *Inorg. Chem*., **1998**, *37*, 411-417; (c) C. Farren, C. A. Christensen, S. FitzGerald, M. R. Bryce and A. Beeby, *J. Org. Chem.*, **2002**, *67*, 9130-9139; (d) G. Kodis, C. Herrero, R. Palacios, E. Mariño-Ochoa, S. Gould, L. de la Garza, R. van Grondelle, D. Gust, T. A. Moore, A. L. Moore and J. T. M. Kennis, *J. Phys. Chem. B*, **2004**, *108*, 414-425; (e) P.-C. Lo, S. Wang, A. Zeug, M. Meyer, B. Röder and D. K.P. Ng, *Tetrahedron Lett.*, **2003**, *44*, 1967-1970.

[2] (a) C. M. Whitacre, D. K. Feyes, T. Satoh, J. Grossmann, J. W. Mulvihill, H. Mukhtar and N. L. Oleinick, *Clin. Cancer Res.* **2000**, *6*, 2021-2027; (b) D. Wohrle, S. Muller, M. Shopova, V. Mantareva, G. Spassova, F. vietri, F. Ricchelli and G. Jori, *J. Photochem. Photobiol., B* **1999**, *50*, 124-128; (c) N. Ahmad, S. Gupta and H. Mukhtar, *Oncogene* **1999**, *18*, 1891-1896.

[3] R. Rodríguez-Redondo, A. Sastre-Santos, F. Fernández-Lázaro, D. Soares, G. Azzellini, B. Elliott and L. Echegoyen, *Chem. Commun*., **2006,** 1265-1267.

[4] J. Silver, C. Frampton, G. Fern, D. Davies, J. Miller and J.L. Sosa-Sanchez, *J. Inorg. Chem.* **2001**, *40*, 5434-5439.

[5] (a) D. M. Guldi, *Chem. Soc. Rev.* **2002**, *31*, 22-36. (b) P. J. Bracher, D. I. Schuster, *Fullerenes: From Synthesis to Optoelectronic Properties*; D. M. Guldi, N. Martin, Eds.; Kluwer Academic Publishers: Dordrecht, **2002**, 163-212.

[6] H. Imahori, K. Hagiwara, M. Aoki, T. Akiyama, S. Taniguchi, T. Okada, M. Shirakawa, Y. Sakata, *J. Am. Chem. Soc.* **1996**, *118*, 11771-11782.

[7] S. A. Vail, P. J. Krawczuk, D. M. Guldi, A. Palkar, L. Echegoyen, J. P. C. Tomé, M. A. Fazio, D. I. Schuster, *Chem. Eur. J.* **2005**, *11*, 3375 – 3388.

[8] T. Mochida, H. Shimizu, S. Suzuki and T. Akasaka, *J. Organomet. Chem*., **2006**, *691*, 4882–4889.

[9] D. I. Schuster, K. Li, D. M. Guldi, A. Palkar, L. Echegoyen, C. Stanisky, R. J. Cross, M. Niemi, N. V. Tkachenko, and H. Lemmetyinen , *J. Am. Chem. Soc*.., **2007**, *129*, 15973-15982.

[10] A. J. Bard, L. R. Faulkner, *Electrochemical Methods: Fundamentals and Applications*, 2nd ed., Wiley, New York, **2001**.